KTH VETENSKAP OCH KONST

KTH Architecture and
the Built Environment

Essential modelling details in dynamic FE-analyses of railway bridges

MAHIR ÜLKER-KAUSTELL

Doctoral Thesis
Stockholm, Sweden 2013

TRITA-BKN. Bulletin 120, 2013
ISSN 1103-4270
ISRN KTH/BKN/B–120–SE

KTH School of ABE
SE-100 44 Stockholm
Sweden

Akademisk avhandling som med tillstånd av Kungliga Tekniska högskolan framlägges till offentlig granskning för avläggande av teknologie doktorsexamen i brobyggnad fredagen den 1 november 2013 klockan 13:00 i sal Kol, Kungliga Tekniska högskolan, Brinellvägen 8, Stockholm.

Tryck: Universitetsservice US-AB

Summary

The increased need to reduce the use of fossil fuels imposes higher demands on the efficiency of rail transportation. Therefore, an improved knowledge regarding the dynamic properties of railway bridges and infrastructure for railway traffic in general is required. Typically, increased train speed, longer trains and increased axle loads increase the dynamic response in railway bridges. Modelling details for bridge structures such as the flexibility of the foundations, radiation damping in the subsoil and the embankments as well as hysteretic effects in bridge bearings and the track superstructure are typically neglected. The reason for this is that suitable models which consider the influence of such effects in engineering calculations have not yet been implemented in the effectual design codes. This thesis is mainly based on a case study of a ballasted, simply supported steel-concrete composite bridge, which shows a considerable variation in the natural frequencies and damping ratios depending on the amplitude of vibration. Furthermore, the natural frequencies were found to increase significantly during the winter. It is well known that the dynamic properties of typical civil engineering structures are dependent on the amplitude of vibration. However, the fact that certain railway bridges exhibit such non-linear behaviour also for very small amplitudes of vibration has been shown only during later years. This has been verified by means of measurements of the free vibrations after train passages on three typical Swedish beam bridges for railway traffic. Possible sources to this amplitude dependency have been identified primarily in the bridge bearings and the track superstructure. Models of these structural components, based on the so called Bouc-Wen model, have been implemented in a commercial finite element program and was used in a preliminary study. The results indicate that roller bearings and pot bearings can give rise to a non-linear mode of vibration, characterised by two different states. At very small amplitudes of vibration ($\lesssim 0.1\,\mathrm{m/s^2}$), no movement over such bearings occur (state 1) since their initial resistance to motion is not overcome. Depending on parameters such as the longitudinal stiffness of the foundations and substructures, the beam height over the supports as well as the bearing type, there is an amplitude of vibration at which the initial resistance to motion is completely overcome (state 2). The bearings are then free to move, with a resistance characterised by the kinematic friction (pot bearings) or the rolling resistance (roller bearings). During the transition from state 1 to state 2, the frequency decreases continuously towards an asymptotic value and the damping initially grows considerably, from a value which corresponds quite well to the recommendations of the Eurocodes and then returns to a value similar to that in state 1. The preliminary study indicates that it is possible to design certain bridges so that this increase in damping is optimal over the relevant range of amplitudes of vibration.

Sammanfattning

Det ökade behovet att minska användandet av fossila bränslen ställer högre krav på effektiviteten hos spårbunden trafik. Därför krävs en ökad kunskap om de dynamiska egenskaperna hos järnvägsbroar och infrastruktur för järnvägstrafik i allmänhet. Ökade tåghastigheter, längre tåg och ökade axellaster leder typiskt till en ökning av den dynamiska responsen hos järnvägsbroar. Modelleringsdetaljer för broar som till exempel grundläggningskonstruktioners eftergivlighet, strålningsdämpning i undergrund och banker samt hysteretiska effekter från brolager och banöverbyggnad försummas regelmässigt. Detta beror av att lämpliga modeller som tar hänsyn till dylika effekter i ingenjörsmässiga beräkningsmetoder ännu ej implementerats i gällande beräkningsnormer. Denna avhandling bygger i huvudsak på en fallstudie av en fritt upplagd, ballasterad samverkansbro som visar en betydande variation i egenfrekvens och dämpkvot, beroende på svängningsamplitud. Vidare befanns egenfrekvenserna öka betydligt under vintern. Att de dynamiska egenskaperna hos typiska anläggningskonstruktioner är amplitudberoende har länge varit väl känt. Att vissa typer av järnvägsbroar uppvisar ett sådant beteende även under mycket små svängningsamplituder har dock inte kunnat påvisas förrän under senare år. Detta har verifierats genom mätningar av de fria svängningarna efter tågpassager på tre typiska svenska järnvägsbroar av balktyp. Tänkbara orsaker till detta amplitudberoende har identifierats i främst brolager och banöverbyggnaden. Modeller av dessa delsystem, baserade på den så kallade Bouc-Wen modellen, har implementerats i ett kommersiellt finita element program och använts i en preliminär studie. Resultatet antyder att rullager och pottlager kan ge upphov till en olinjär svängningsmod, karaktäriserad av två olika tillstånd. Vid mycket små svängningsamplituder ($\lesssim 0.1\,\mathrm{m/s^2}$), förhindras rörelsen över lagren (tillstånd 1) eftersom dess initiala rörelsemotstånd då ej övervinns. Beroende på parameterar som den longitudinella styvheten hos grundläggningskonstruktioner och underbyggnader, konstruktionshöjd över stöd och lagertyp finns en svängningsamplitud vid vilken det initiala rörelsemotståndet övervinns helt (tillstånd 2). Lagren fungerar då som rörliga lager, med ett rörelsemotstånd karaktäriserat av kinematisk friktion (pottlager) eller rullningsmotstånd (rullager). Vid en övergång från tillstånd 1 till tillstånd 2, avtar frekvensen kontinuerligt mot ett asymptotiskt värde och dämpningen växer först betydande från ett värde som tycks svara ganska väl mot de av Eurokoderna rekommenderade dämpkvoterna, för att sedan avta och återgå mot ett värde liknande det i tillstånd 1. Den preliminära studien antyder att man kan utforma vissa broar så att denna dämpningstillväxt sker på ett optimalt sätt över det relevanta spannet av svängningsamplituder.

Preface

This research project was financed by the Swedish Transport Administration (Trafikverket), the KTH Railway Group and Tyréns AB. It was supervised by Professor Raid Karoumi and co-supervised by Professor Costin Pacoste, to whom I am highly grateful. I would also like to express my gratitude towards Professor Håkan Sunquist, who gave me the chance to take on this challenging task. Pär Färnlöf at Trafikverket has given his best efforts to support the project in its early stages and this has been highly appreciated.

Many others have influenced my developments both as a Ph.D. student and as a person. Among these, Anders Bodare played a central role in introducing me to soil dynamics and dynamic soil-structure interaction. Jean-Marc Battini has helped me in many ways and also reviewed this thesis and provided many helpful comments. Claes Kullberg and Stefan Trillkott are mentioned for being such nice guys, who have taught me much about field work and the practical aspects of experimental work.

I also wish to thank all the Ph.D. students at the division of Structural Engineering and Bridges (KTH) who have patiently listened to my presentations at our meetings and provided support and comments which have been really helpful. I am especially grateful for the detailed questioning of my assertions and assumptions given by Ignacio Gonzales, Andreas Andersson and Christoffer Johansson.

The staff at the department of Civil and Architectural Engineering (KTH) is a wonderful mix of different professionals and personalities, to whom I owe the greatest gratitude for providing an enjoyable work environment.

The staff at Tyréns bridge department should also be mentioned here, not only for creating an enjoyable work environment, but also for giving me an insight in the daily life of structural engineers while working with this thesis.

Finally, my parents, friends and my family; Sassa, Mika and Kim have given me the support, motivation and inspiration without which this thesis would never have been finalised.

Stockholm, November 2013

Mahir Ülker-Kaustell

List of Publications

This thesis is based on four journal papers, labeled paper I–IV. All the papers present studies of various aspects of the dynamic properties of a single span, ballasted steel-concrete composite bridge.

Paper I M. Ülker-Kaustell and R. Karoumi. Application of the continuous wavelet transform on the free vibrations of a steel-concrete composite railway bridge. *Engineering Structures*, 33:911–919, 2011.

Paper II M. Ülker-Kaustell and R. Karoumi. Influence of non-linear stiffness and damping on the train-bridge resonance of a simply supported railway bridge. *Engineering Structures*, 41:350–355, 2012.

Paper III I. Gonzales, M. Ülker-Kaustell and R. Karoumi. Seasonal effects on the stiffness properties of a ballasted railway bridge. *To appear in Engineering Structures.*

Paper IV M. Ülker-Kaustell and R. Karoumi. Influence of rate-independent hysteresis on the dynamic response of a railway bridge. *To appear in the International Journal of Rail Transportation*, DOI:10.1080/23248378.2013.835129.

Papers I, II and IV were planned, implemented and written by the first author. In paper III, the contribution of the second author consisted mainly in finite element modelling of the bridge and the writing of the paper, while the first author mainly performed the model updating and the analysis of the experimental data. However, the development of the model and the analysis procedures was performed in close collaboration between the first and the second author. The experimental work was performed by Claes Kullberg and Stefan Trillkott.

In addition to the above mentioned papers, the author has also been involved in the following publications:

- M. Ülker-Kaustell. Influence of vibration amplitude on the response of a ballasted railway bridge. *Proceedings of the First International Conference on Railway Technology: Research, Development and Maintenance*, 2012.

- J-M. Battini and M. Ülker-Kaustell. A simple finite element to consider the non-linear influence of the ballast on vibrations of railway bridges. *Engineering Structures*, 33:2597–2602, 2011.

- M. Ülker-Kaustell, R. Karoumi and C. Pacoste. Simplified analysis of the dynamic soil-structure interaction of a portal frame railway bridge. *Engineering Structures*, 32:3692–3698, 2010.

- C. Johansson, A. Andersson, J. Wiberg, M. Ülker-Kaustell, C. Pacoste and R. Karoumi. Höghastighetsprojekt - Bro : Delrapport I: Befintliga krav och erfarenheter samt parameterstudier avseende dimensionering av järnvägsbroar för farter över 200 km/h (in Swedish). Royal Institute of Technology (KTH), Structural Design and Bridges, 2010.

- M. Ülker-Kaustell. Some aspects of the dynamic soil-structure interaction of a portal frame railway bridge. TRITA-BKN, Licentiate Thesis 102, Royal Institute of Technology (KTH), 2009.

- M. Ülker-Kaustell. The dynamic properties of two concrete railway bridges during the testing of Gröna Tåget. TRITA-BKN, Report 117, Royal Institute of Technology (KTH), 2007.

- M. Ülker. Övervakning av accelerationer i broar vid passage av Gröna Tåget (in Swedish). Technical Report 11, Royal Institute of Technology (KTH), Structural Design and Bridges, 2006.

Contents

Summary **i**

Sammanfattning **iii**

Preface **v**

List of Publications **vii**

1 Introduction **1**

1.1 Background 1

1.2 Aims and scope 5

1.3 Outline of the thesis 6

1.4 Scientific contribution 6

2 Hysteretic macro elements **9**

2.1 The Bouc-Wen model 10

2.2 Simple BW-models in Matlab 13

2.3 A BW-element in ABAQUS 15

3 Modelling details **19**

3.1 Modelling of damping 20

3.2 Soil-structure interaction 25

3.3 Track-structure interaction 27

3.4 Bridge bearings 29

4 Analysis of non-stationary signals **33**

4.1 Analytic signals and the Hilbert transform 33

4.2 The instantaneous damping ratio 37

4.3 Estimates of the instantaneous quantities 38

5 Case studies **41**

5.1 Wavelet versus Hilbert 41

5.2 Case 2 - Ullbrobäcken 41

5.3 Case 3 - Sagån 43

5.4 Influence of bearings - all cases 44

5.5 Parameter variations - case 3 47

6 Discussion **51**

6.1 Conclusions 52

6.2 Further research 53

References **55**

Paper I **59**

Paper II **71**

Paper III **79**

Paper IV **95**

Chapter 1

Introduction

1.1 Background

Railway bridge dynamics is a multi-disciplinary mechanical problem ranging over structural, geotechnical and mechanical engineering. Here, the dynamic interaction between a railway bridge and a passing train is our primary concern. More specifically, the repetitive nature of the load induced by a passing train can cause a state of train-bridge resonance. In the simplest case, only one mode of vibration is involved in the train-bridge resonance which will occur at different critical train speeds v_{cr}, depending on the natural frequency f of the mode of vibration and some characteristic length (such as the axle or bogie distance) of the train L

$$v_{\mathrm{cr}} = fL \tag{1.1}$$

Several modes of vibration can also interact in resonance states. Although there can be a significant contribution to the traffic load from the dynamic interaction between a railway bridge and a passing train, the main issue in railway bridge dynamics is comfort and safety against train derailment. The structural integrity of the bridge is typically not at risk in a state of train-bridge resonance and therefore, the design for bridge deck acceleration is treated as a serviceability limit state.

There are a number of factors which are often neglected in dynamic analyses of railway bridges for high-speed traffic based on the finite element method (FEM). One important example is the modelling of damping. Typically, viscous damping is used to model the dissipation of energy from the structure. The damping ratios used are based on tests on existing bridges. The damping matrix can then be constructed in many ways. If modal analysis is used to solve the equations of motion, the modal damping ratios can be specified directly. If instead, direct integration of the equations of motion is needed for some reason, a modal damping matrix can be formed by means of the spectral decomposition of the undamped system, but more commonly, Rayleigh damping is used to compute the viscous damping matrix. Rayleigh damping can be defined in at least two ways: in a global sense by using the global mass and stiffness matrices or in a local (element) sense by assigning Rayleigh damping coefficients corresponding to different materials/elements in the model. However,

Table 1.1: The damping ratios recommended by Eurocode [11] for dynamic analysis of railway bridges for high-speed traffic.

	ξ Lower bound of critical damping [%]	
Bridge type	Span length $L \leq 20\,\mathrm{m}$	Span length $L > 20\,\mathrm{m}$
Steel and composite	$\xi = 0.5 + 0.125(20 - L)$	$\xi = 0.5$
Prestressed concrete	$\xi = 1.0 + 0.070(20 - L)$	$\xi = 1.0$
Filler beam and reinforced concrete	$\xi = 1.5 + 0.070(20 - L)$	$\xi = 1.5$

not only material damping is present in a general railway bridge. Many different sources contribute to the total damping of a given bridge. These sources include the track superstructure, friction in bearings, friction in joints and dynamic soil-structure interaction (SSI). Naturally, the damping capacity of a structure plays an important role in its dynamic behaviour, especially at resonance. Therefore, from a safety perspective, it is important that it is not overestimated, while from an economical perspective, it is essential that it is not underestimated. The damping ratios recommended by the Eurocode [11] for dynamic analysis of railway bridges for high-speed traffic are given in table 1.1. Clearly, they never exceed 2.2 % for the most damped type of bridges, i.e. reinforced concrete bridges with very short spans. These values are based on tests performed by the European Rail Research Institute (ERRI) [5]. The extensive tests accounted for in that report were all based on free vibrations after passing trains and a lower bound of those tests formed the basis for the recommendations of the Eurocode. However, it has long been speculated that in a state of resonance, the damping ratio could increase due to non-linear effects such as those mentioned above. To the author's knowledge, there are no reports in the literature of measurements of the response of a railway bridge in a state of global train-bridge resonance, so there is no scientific support for that hypothesis. Nevertheless, Swedish experiences with design calculations and assessments of existing structures based on the Eurocode recommendations, indicate that many otherwise economical designs cannot be verified to meet the criteria for the dynamic response given by the Eurocode. Thus, there is a great need to improve our understanding of the dynamic properties of railway bridges, with emphasis on resonant responses.

There is a natural cause for the negligence of modelling details such as those mentioned above. The complexity of the calculations increases rapidly due to non-linear effects and the frequency dependency of the impedance of the soil-structure interface. In assessments of existing structures, the inclusion of such details can be motivated, since measurements of the dynamic response of the structure in question can then be obtained. However, such measurements are rather costly, and inevitably include effects from all the mechanisms and physical phenomena which govern the response of the structure. Therefore, an increased knowledge of those mechanisms is valuable both from an academic and a practical engineering perspective.

Experimental techniques for existing structures can be roughly divided in two groups; Experimental modal analysis (EMA) and operational modal analysis (OMA). EMA is based on known input and OMA is based on the assumption that the input can be characterised by white or coloured noise. Generally, the structural system is assumed to be time-invariant or stationary and linear, i.e. its properties do not vary with time and is independent of the response. In applications of EMA, we need an exciter which is powerful enough to excite large and heavy structures. This can become highly impractical considering that we are standing in the forrest on a rainy day with a 30 minutes long gap between each train and that the exciter weighs several hundred kilograms. For this reason, and similar reasons in other civil engineering applications, OMA has been given a considerable amount of attention, as in this case, the background noise caused by ground induced vibrations, wind loads and perhaps also traffic loads on the structure itself, is used as the source of excitation. However, many of our railway bridges are situated far away from roads and their natural frequencies are often much higher than the frequency content of the wind loads. Therefore, extremely sensitive sensors are often needed to obtain robust estimates of the modal properties from such tests. Also, it cannot be guaranteed that all modes of vibration within a certain frequency range have been identified by OMA. This can be guaranteed with EMA, and one can also vary the amplitude of vibration to capture non-linear effects. Both approaches can be used to obtain estimates of the mode shapes, which are highly tractable in inverse problems, or model updating problems as they are often denoted by in the civil engineering context.

Model updating is a very attractive tool both in research applications and in dynamical assessments of existing structures. Friswell and Mottershead [24] describe many of the aspects of model updating and stress the fact that the measurements we wish to use in our model updating algorithm will include all the significant physical phenomena and mechanisms in the real structure. Consequently, in order for a model updating algorithm to succeed in finding a realistic set of parameters which makes the theoretical modes of vibration match the measured ones, the theoretical model must also reflect all the significant physical phenomena and mechanisms. Thus, one aim of this project was to learn more about the factors which are essential to the dynamic response of a given structure. Another important aspect of model updating of linearised structural models is that the spectral matrix of the undamped system is not necessarily unique. This means that if only natural frequencies are used in a model updating algorithm, one could end up with matching frequencies, but non-matching mode shapes. Therefore, it is recommended that the objective function which is used in the optimisation part of the model updating scheme is based on both mode shapes and natural frequencies.

Clearly, the costs involved in EMA and OMA are quite large as they involve many sensors, an exciter in the case of EMA and large quantities of data. In practical applications, for dynamical assessments of bridges along an existing railway line, such techniques could become too expensive and time consuming, especially if many bridges need to be assessed. Instead, it would be desirable to use a simple instrumentation with a minimum of sensors and use passing trains as excitation. For this

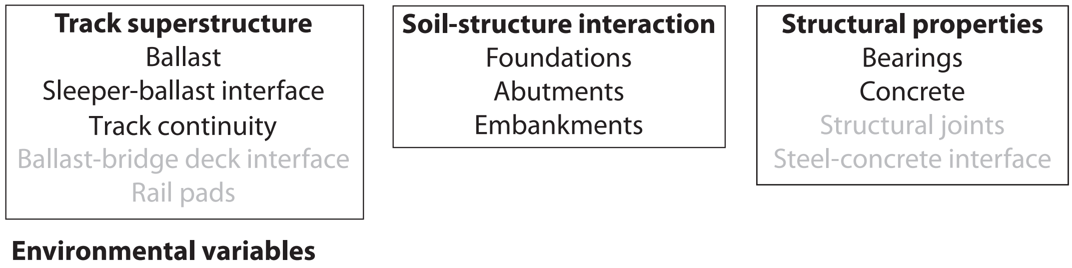

Figure 1.1: An overview of factors which may influence the dynamic response of railway bridges. Factors which have not been considered at all in the thesis are grey.

reason, the research within the project was aimed towards an improved analysis of free vibration data from train passages.

At the beginning of this research project, a list of factors and parameters which may influence the dynamic response of railway bridges was identified. This list is summarised in figure 1.1, excluding train-bridge interaction which is outside the scope of the thesis.

It was decided to start looking at SSI and this was the topic of the licentiate thesis [47] and the journal paper [39] written by the author. In a general context, SSI is a complicated matter, even in a linearly elastic setting. This complexity lies in the infinite extent of the surrounding soil, the non-linear constitutive relations of soil materials, large uncertainties in the soil material properties and their spatial distribution and the frequency dependency in the stiffness and damping characteristics of the soil-structure interface. In the licentiate thesis, a portal frame bridge was studied, and it was concluded that three-dimensional effects must be included and that the typical geotechnical survey may not be sufficient for a correct estimation of the dynamic stiffness functions of the soil-structure interface. Furthermore, the interaction with the embankments needs to be further studied. Geotechnical issues began to dominate the theoretical developments within the project and the financial support needed to take a scientific approach to the general SSI problem in railway bridge dynamics, were simply not available.

However, in parallel with this work, the author initiated and supervised a master thesis [35], much inspired by the work of Rebelo et al. [42]. Rebelo et al. used something similar to the short time Fourier transform (i.e. Fourier transforms of windowed portions of a signal) to show that the natural frequency of certain single span concrete bridges decreased with the amplitude of vibration. Lorieux [35] used a similar technique and found that for our test bridge (case 1, see chapter 5), the frequency decreased, but the damping increased substantially with increasing amplitude of vibration. This provided some motivation to start looking at other factors in the list shown in figure 1.1, however, the first step was to validate the results obtained by Lorieux. This was provided in paper I by an implementation of the continuous wavelet transform (CWT). The implications of the findings in paper

I were discussed in paper II. Paper III provided some insights regarding the possible sources of the non-linear behaviour reported in paper I by the implementation and application of a model updating scheme based on Bayes theorem. Finally, paper IV suggested the longitudinal track resistance and the pre-rolling resistance of the roller bearings as the most likely sources of this non-linear behaviour.

1.2 Aims and scope

The aim of this research project was to use measurements and theoretical models to improve our understanding of the modelling details which should be included in dynamic analyses of railway bridges.

As described in section 1.1, from a bridge engineer point of view, the train-bridge resonance is a serviceability limit state. Therefore the analysis can be based on the linear theory of elasticity, assuming small deformations, small displacements and that no significant effects of material non-linearities will appear in the bridge sub- and/or superstructure. Furthermore, the frequency dependency of the linear stiffness and damping of the foundations was neglected as motivated in the thesis.

Only free vibrations after the passage of a train were used to study the dynamic properties of the bridges. Therefore, only the first few modes of vibration were available and the case studies were essentially limited to the fundamental modes of vibration of the studied bridges.

Three levels of model complexity were used:

1. Single degree of freedom models based on the generalised coordinate of the fundamental mode of vibration.
2. Two dimensional beam models limited to the fundamental mode of vibration.
3. A three dimensional model of the case 1 bridge.

Single degree of freedom models were used mainly for development and benchmarking. The two dimensional models were used to study the non-linear mechanisms in simulations of free vibrations. The three dimensional model was based on linear theories and used in a sensitivity analysis with the purpose of determining the most relevant parameters and mechanisms and to study the seasonal effects on the stiffness of the case 1 bridge.

The Swedish climate is cold and therefore, the dynamic properties of railway bridges can vary significantly over the seasons. This is shown in paper III, but the theoretical analysis performed within the project (paper IV) was limited to the warm season. This choice was made because

1. The variability in the dynamic properties of the case 1 bridge was found to be much higher during the cold season than during the warm season. This

variation appears to be related to the formation of ice within the ballast, but this has not been confirmed.

2. The dynamic properties of the case 1 bridge appears to be more conservative during the warm season.

1.3 Outline of the thesis

Chapter 2 gives a more detailed background to the Bouc-Wen model which was used to model various hysteretic effects in paper IV. In chapter 3, more general motivation for the assumptions made in paper IV is presented in relation to the studied modelling details. The analysis of non-stationary signals formed a basis for the presented research and also played a central role in the analysis of the theoretical models. Therefore, chapter 4 explains the basic features of such signals and the methods used to estimate the dynamic properties of the non-linear modes of vibration. These three chapters form the theoretical background to the performed research.

In chapter 5, three case studies are presented. Most of the results from case 1 have been presented in papers I–IV, but two more bridges have been used in preliminary case studies to illustrate the influence of the modelling details studied on the case 1 bridge in a more general sense. Finally, chapter 6 is devoted to a general discussion of the results, a summary of the main conclusions and suggestions for future research within this field.

1.4 Scientific contribution

This research project has contributed scientifically by verifying that the dynamic properties of certain bridges are dependent on the amplitude of vibration. The most likely sources of these non-linear effects were found in the movable bearings and the longitudinal track resistance. It was shown that, during the warm season of the year, the bearings constitute the main source of the amplitude dependency and that the track superstructure has a considerable, though much smaller effect.

The results of the research within this project have led to the formulation of a hypothesis which can be stated in the following way: "*The non-linear mechanisms of movable bearings give rise to an amplitude dependent mode of vibration which varies between two states wherein (1) all movable bearings are fixed and (2) all movable bearings are free to move. The natural frequency of the mode decreases monotonically and the modal damping ratio is a uni-modal function of the amplitude of vibration during the transition from state 1 to state 2*".

Preliminary case studies performed within the project indicate that it is possible to design railway bridges so that the damping caused by movable bearings is optimised.

It was shown that the total structural damping can be separated into at least four different sources (material damping, radiation damping, and friction-like damping in bearings and the longitudinal track resistance).

Chapter 2

Hysteretic macro elements

The term ”hysteresis” often appears when reading about damping in various contexts. Some authors, especially within the geotechnical community, use the term ”hysteretic damping” for the type of frequency independent damping obtained by using the complex modulus

$$E^* = (1 + i\eta)E \tag{2.1}$$

where E is the modulus of elasticity, $\eta = 2\xi$ is the loss factor and i is the imaginary unit. Clearly, this form of damping only makes sense for linear systems in the frequency domain and a transformation of such solutions to the time domain gives rise to non-causal response [37]. In the commercial finite element package ABAQUS[1], this damping model is referred to as ”structural damping”, which is a more appropriate term. The term hysteresis originates from the ancient Greek and according to Visintin [49], it means ”to lag behind”. In the theory of plasticity, the term is often used with the meaning that a stress-strain or force-displacement relation follows different paths upon loading and unloading. In this sense, all the damping models used in structural dynamics are hysteretic and this is how this term will be used within this thesis. Furthermore, a distinction is made between rate-independent and rate-dependent hysteresis. The Kelvin-Voigt model (i.e. an elastic spring and a viscous damper in parallel) is a typical example of a rate-dependent hysteretic system while friction and plastic mechanisms are examples of rate-independent hysteretic systems.

The concept of macro elements is highly useful in many applications. In some cases, complicated three dimensional mechanical systems can be reduced to spring elements with three translational degrees of freedom and three rotational degrees of freedom. A simple example of such an element is the dynamic stiffness function of foundations used extensively in applications of SSI. This macro element consists of springs and dashpots which may be coupled and are functions of frequency. This very simple, linearly elastic model can be extended to consider non-linear material behaviour and contact mechanics. Such developments have been conducted by many authors, see paper IV and the references therein. In the present context, two new fields of application of macro elements have been introduced: longitudinal track resistance

[1] http://www.3ds.com/products-services/simulia/portfolio/abaqus/latest-release/

and bearing mechanisms.

The main draw-back of condensing mechanisms and substructures into macro elements is that a lumping of parameters is inevitable when both geometrical detail and constitutive relations are merged into force-displacement relations. If a theoretical model cannot be easily constructed in order to validate the macro element, one has to use measurements to calibrate the macro element model parameters. Mechanical systems such as bridge bearings can be studied in laboratory conditions but this is not the case with foundations and abutments. Since their properties are so highly dependent on the in-situ conditions, full scale tests seem to be the most promising approach. However, if one would measure the dynamic stiffness functions during the construction of a bridge, one would have to compensate for the weight of the sub- and superstructure and the initial settlement of the surrounding soil. After the construction of the substructure, it is much more difficult to excite the foundation plate. Also, after the construction of the superstructure, the dynamic stiffness function is no longer that of the foundation alone.

2.1 The Bouc-Wen model

In this section, the Bouc-Wen model (BW-model) will be defined and its model parameters studied. In order to do so, some basic notions regarding hysteresis in mechanical systems will be discussed. As mentioned in the introduction to this chapter, there is a distinction between hysteresis and rate-independent hysteresis. The following discussion will focus on rate-independent hysteresis, as modelled by the Bouc-Wen model, see figure 2.1. Linear rate-dependent mechanisms can be included in a straightforward manner, simply by adding a viscous dashpot in the parallel system shown in figure 2.1.

In 1971, Bouc published the paper [9] which is often cited as the origin of this type of models. However, in the same year, Valanis published a paper [48] in which he defined a theory of plasticity which has become known as the endochronic theory of plasticity. The title of Valanis 1971 paper, "*A theory of viscoplasticity without a yield surface*", speaks for itself and the general framework of plasticity derived by Valanis has, in the authors opinion, not been given the attention it deserves. Actually, Valanis was able to derive several of the classical plasticity models from his framework. The main idea in Valanis work is that the path dependence of the plastic deformations can be controlled by introducing an "intrinsic" time scale, which only depends on the history of deformation. The term appears to have been used because this intrinsic time and the physical, "wall-clock" time share the property that they are both monotonically increasing. Much later, in 2004, Erlicher and Point [21] proved the thermodynamic admissibility of the BW-model and used the concept of intrinsic time in the same way as Valanis did for his continuum models. The BW-models are therefore sometimes referred to as endochronic models or univariate endochronic models. However, the BW-model has also been generalised to constitutive models in a continuum setting. The classical BW-model has a few flaws, which have been shortly described in paper IV, with reference to the work of Charalampakis and

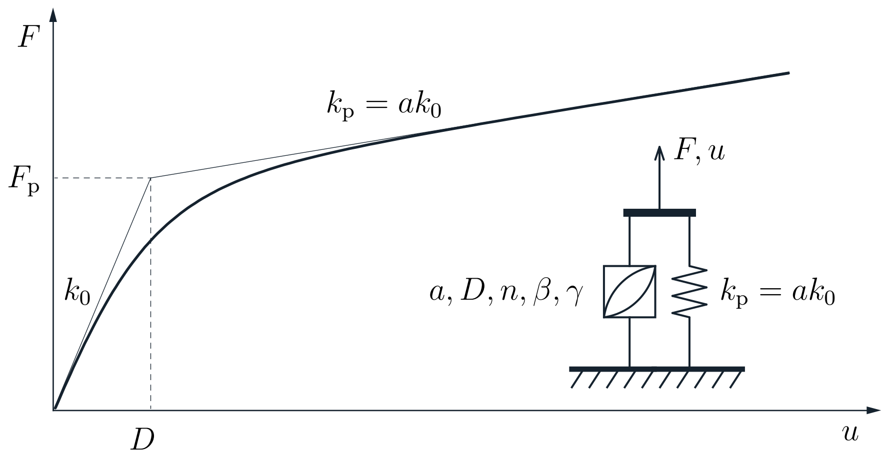

Figure 2.1: The classical Bouc-Wen model.

Koumouosis [15], who used their solution [14] of the differential equation governing the BW-model to remedy these flaws. However, for reasons described in paper IV, this flaws do not influence the type of response studied here. Nevertheless, among the sources studied by the author, Charalampakis and Koumousis [14] provided the most comprehensible description of the BW-model.

The restoring force in the classical univariate Bouc-Wen model is given by

$$F(t) = ak_0u + (1-a)k_0Dz \tag{2.2}$$

where u is the displacement, a is the ratio of the plastic ($k_{\rm p}$) and initial stiffness, k_0 is the initial stiffness, D is the plastic deformation limit and z is an internal variable, responsible for the hysteretic behaviour of the model. The internal variable is governed by an ordinary differential equation, the form of which can be derived by means of the endochronic theory of plasticity as will be briefly described.

The classical, univariate Bouc-Wen model describes the hysteretic behaviour by means of an internal variable z, governed by the non-linear ODE

$$\dot{z} = \frac{\dot{u}}{D}\left[1 - (\beta + \operatorname{sgn}(\dot{u}z)\gamma)|z|^n\right] \tag{2.3}$$

where β,γ and n are model parameters. The sign function $\operatorname{sgn}(x)$ is defined as

$$\operatorname{sgn}(x) = \begin{cases} -1, & x < 0 \\ 0, & x = 0 \\ 1, & x > 0 \end{cases} \tag{2.4}$$

β and γ govern the shape of the hysteresis loops, see figure 2 in paper IV. n governs the length of the transition from the elastic to the plastic part of the backbone curve. When $n \to \infty$, the BW-model tends towards an ideal elasto-plastic model.

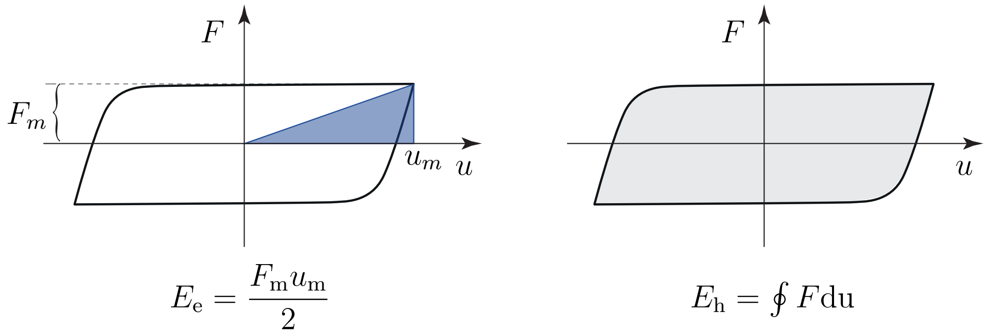

Figure 2.2: The maximum stored elastic energy E_{e} and the hysteretic energy E_{h} (the shaded area), given by the area of the hysteresis loop.

However, the typical issues with non-smooth functions in numerical methods occur when $n \gtrsim 20$ and convergence problems arise.

The book by Ikhouane and Rodellar [30] describes a thorough analysis of many of the mathematical properties of the Bouc-Wen model. However, in the present context, we are much interested in the variation of the damping of a given hysteretic system of the classical Bouc-Wen type. Charalampakis and Koumousis [14] derived analytical solutions, though expressed in terms of special functions which have to be evaluated numerically, for some particular parameter combinations, and outlined a numerical procedure for arbitrary combinations, in the governing equations (2.2) and (2.3).

The variation of the damping ratio with respect the parameter a is of particular interest. The damping ratio for a hysteretic system in a steady state can be defined in terms of the hysteretic energy, which is given by the line integral around the hysteresis loop

$$E_{\mathrm{h}} = \oint F \mathrm{du} \tag{2.5}$$

and the maximum elastic energy stored during the loop

$$E_{\mathrm{e}} = \frac{F_{\mathrm{m}} u_{\mathrm{m}}}{2} \tag{2.6}$$

These notions are illustrated in figure 2.2. Then, the damping ratio is given by (see for example [32])

$$\xi = \frac{E_{\mathrm{h}}}{4\pi E_{\mathrm{e}}} \tag{2.7}$$

As shown in figure 2.3, the ratio between the hysteretic and elastic energies is much affected by the value of a. One can immediately identify two categories of hysteretic systems; for small values of a the damping is dominated by the hysteretic energy and for values of a tending towards one, the damping is increasingly being dominated by the elastic energy. In the proceeding analysis, the hysteretic subsystems, i.e. foundations, bearings and longitudinal track resistance, all fall within the first category, whilst the structural modes of vibration are of the second category. For the track superstructure and the foundations, the plastic stiffness corresponds to

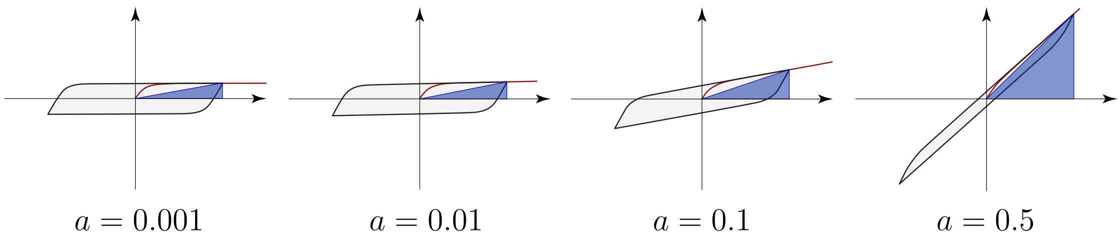

Figure 2.3: The influence of the parameter a on the relation between the hysteretic energy E_{h} and the maximum elastic energy E_{el} of a load cycle.

failure and for the bearings it is presumably zero in reality, corresponding to sliding or rolling where the resistance is constant. Due to their very low plastic stiffness, they represent unstable mechanisms when the load exceeds a certain value.

In a structural system such as a bridge, global structural stability relies on structural elements which constrain the rigid body modes of the structure, i.e. fixed bearings at certain locations. Thus, in the serviceability limit state, we expect a stable global structural behaviour with modes of vibration varying between two states, qualitatively defined by

1. All movable bearings fixed.
2. All movable bearings free.

Naturally, other mechanisms such as the track superstructure may influence the quantitative behaviour, but they cannot violate the demands imposed by the global stability of the structure. Figure 2.4 shows the damping ratios corresponding to the different BW-models shown in figure 2.3, as functions of the amplitude of vibration. These results were computed using the single degree of freedom model described in section 2.2. However, a displacement controlled analysis was used instead of the force controlled analysis described there. It is clear that for sufficiently small values of a, the damping ratio can increase indefinitely with the amplitude of vibration. One can also see that there exists a limit value of a at which the qualitative behaviour changes so that the damping ratio increases, but asymptotically, towards a bounded value. A further increase in a leads to a behaviour where the damping first increases and then decreases, asymptotically, forming a damping "bump".

2.2 Simple BW-models in Matlab

In order to better understand the BW-model, single and two degree of freedom (DOF) systems were studied in Matlab. There, a fourth-order Runge-Kutta scheme was used to solve the equations of motion, although a 2D FEM implementation was also developed. However, the computational efficiency of the FEM implementation

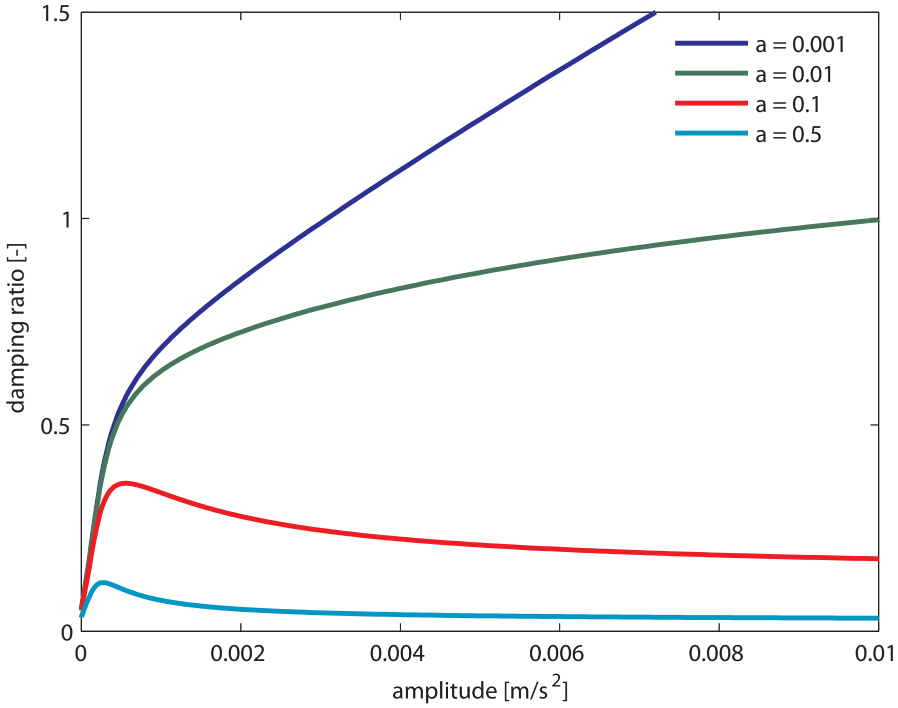

Figure 2.4: The influence of the parameter a on the hysteretic damping.

in Matlab was not much greater than the implementation in ABAQUS (see section 2.3) and it will therefore not be further described here.

The single degree of freedom system is based on the equation of motion

$$m\ddot{x}(t) + c\dot{x}(t) + ak_0x(t) + (1-a)Dk_0z(t) = f(t) \tag{2.8}$$

where z is governed by the non-linear ODE given by equation (2.3). These equations define a state-space system with three degrees of freedom

$$\mathbf{w} = (x, \dot{x}, z)^{\mathrm{T}} \tag{2.9}$$

and we then wish to solve the equation

$$\dot{\mathbf{w}} = \mathbf{f} - \mathbf{B}\mathbf{w} - \mathbf{g}(\mathbf{w}) \tag{2.10}$$

where

$$\mathbf{f} = (0, f(t)/m, 0)^{\mathrm{T}} \tag{2.11}$$

$$\mathbf{B} = \begin{bmatrix} 0 & -1 & 0 \\ ak_0/m & c/m & (1-a)Dk_0/m \\ 0 & 0 & 0 \end{bmatrix} \tag{2.12}$$

and $\mathbf{g}(\mathbf{w})$ is a vector holding the non-linear function from equation (2.3)

$$\mathbf{g}(\mathbf{w}) = \left(0, 0, \frac{\dot{u}}{D}\left[1 - (\beta + \mathrm{sgn}(\dot{u}z)\gamma)|z|^n\right]\right)^{\mathrm{T}} \tag{2.13}$$

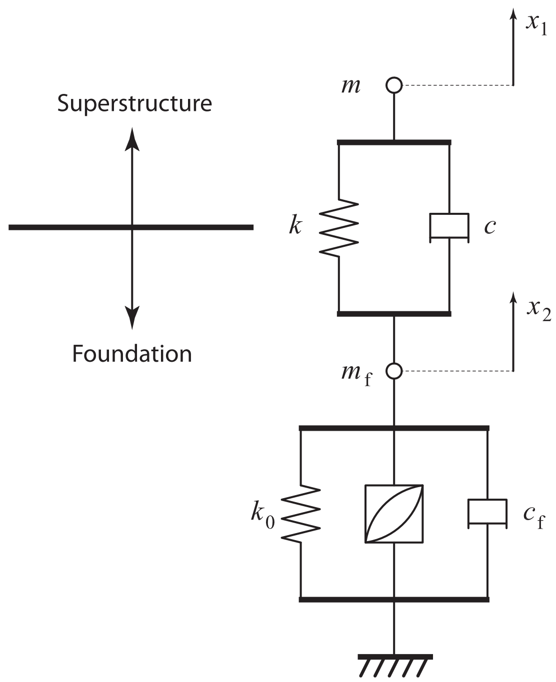

Figure 2.5: The 2-DOF model used to study the influence of non-linear SSI and as a benchmark for the ABAQUS BW-element.

This solution procedure typically gave stable solutions with time steps $\Delta t < 10^{-4}$. This is satisfactory for very small systems of equations, but can be prohibitive in general FE-models.

The 2-DOF BW-model is simply an extension of the 1-DOF model, where the first DOF has a BW-element in parallel with a viscous dashpot and the second DOF is linearly elastic (see figure 2.5). This type of models extend the model used in paper II by separating the motion of the foundations and the generalised coordinate of the first vertical bending mode of the bridge. This feature was used to study the influence of the soil material non-linearity on the response of this mode and as a benchmark for the ABAQUS BW-element (see section 2.3).

2.3 A BW-element in ABAQUS

ABAQUS [19] is a general commercial FE-code which is widely used in many fields of engineering. ABAQUS allows user-defined elements to be defined by writing a FORTRAN subroutine which is then compiled and linked together with the FE-modelling features defined by the standard libraries of ABAQUS. All the computational procedures available in ABAQUS, can be accounted for, i.e. static problems, eigenvalue problems, steady-state dynamics and so on. However, the implementation used within this project is limited to transient dynamics and since we are studying sources of damping which are quite unknown, the trapezoidal rule with-

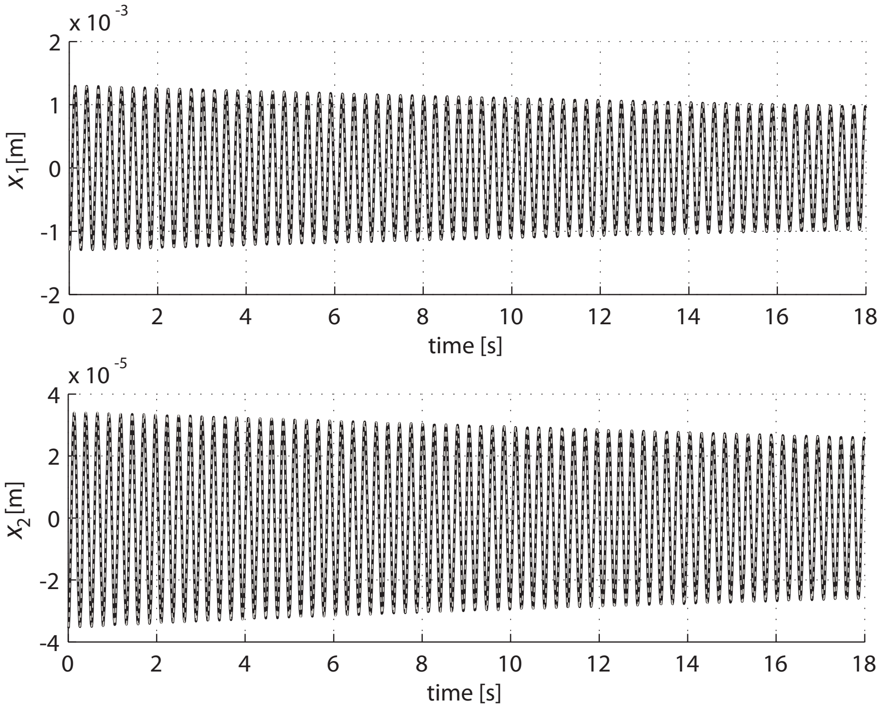

Figure 2.6: Displacements from the benchmark test, Matlab (black, solid lines) and ABAQUS (grey, dashed lines).

out numerical dissipation was used to solve the equations of motion. The global equations of motion are solved using Newton's method and therefore, the tangent stiffness matrix of the user element must be provided. The solution of the hysteretic variables must also be provided and both an implicit (Newton's method) and an explicit Backward Euler method was tested. However, since the internal variables of the BW-element are uncoupled, these two methods were equally efficient although more than 10 iterations were often needed in Newton's method.

In order to compute the tangent stiffness matrix of the BW-element, the derivative

$$\frac{\partial \dot{z}}{\partial z} = -\frac{n}{D}\left(\beta \dot{u}\,\mathrm{sgn}\, z + \gamma |\dot{u}|\right) |z|^{n-1} \tag{2.14}$$

is needed. However, in the form stated above, it is not well defined if $n < 1$. Overflow may occur when $z \to 0$. In order to avoid this problem, z was restricted to $|z| > z_{\mathrm{min}} = 1 \cdot 10^{-14}$. The implementation of the BW-element was benchmarked using the 2-DOF system described in the previous section. The model parameters used in the benchmark test are summarised in table 2.1 and the result of the benchmark test is shown in figure 2.6. Clearly, the two solutions are indistinguishable from each other.

Issues with singularities arose in cases where a very small value was assigned to the parameter a, i.e. the ratio between the plastic and initial stiffness. When the stiffness tends towards zero, extremely small time steps were needed to obtain converged results. This could be slightly improved by assigning a larger value to

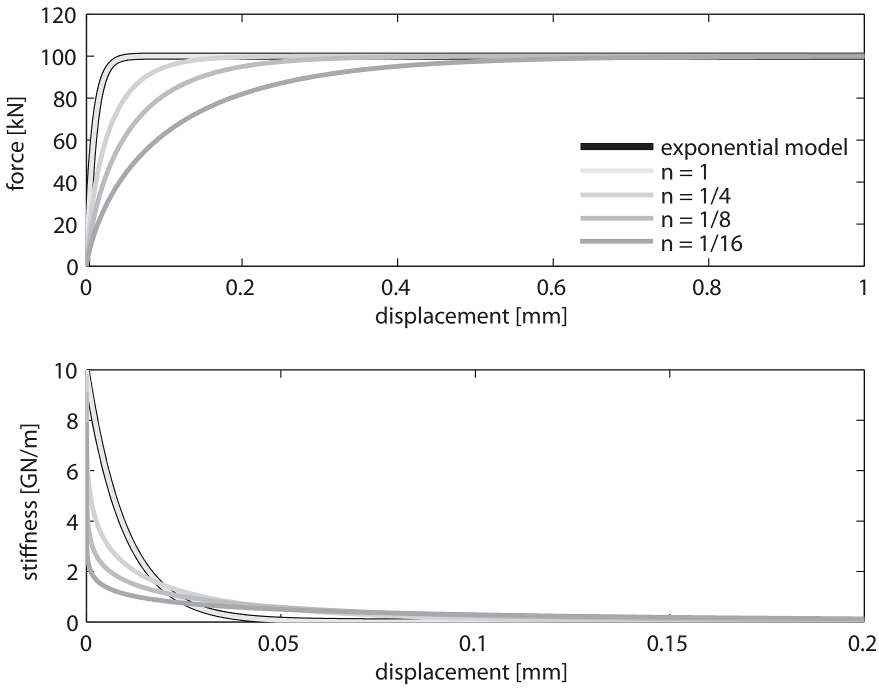

Figure 2.7: Some BW-model candidates for the roller bearing mechanism in the case 1 bridge. n is the model parameter described in section 2.1 (equation (2.3))

Table 2.1: Model parameters used in the benchmark test of the ABAQUS implementation of the univariate, classical Bouc-Wen model.

	k [GN/m]	m [kg]	c [kNs/m]	k_0 [GN/m]	a [-]	D [m]	n [-]	β [-]	γ [-]
x_1	0.180	306000	4.1	-	-	-	-	-	-
x_2	-	100000	4340	6.65	0.363	0.0005	1	0.1	0.9

that parameter. However, this mainly improved the robustness of the solutions, the time step required was still in the order of $10^{-5} - 10^{-4}$ s near the load reversal points of the hysteresis loops. This is probably also highly influenced by the rapid variation of the stiffness for very small relative displacements over the bearings, see figure 2.7.

Chapter 3

Modelling details

As described in the chapter 1, several factors influence the dynamic properties of railway bridges. Having shown that the modes of vibration of railway bridges can indeed have a non-linear amplitude dependency, the most likely candidates were identified and research was initiated to determine which of them are most relevant. Prior to the writing of paper III, the list of candidates was

1. Soil-structure interaction
2. Ballast/track superstructure

assuming that the material properties of the sub- and superstructure were linear. The work with paper III led to the conclusion that (1) the variation in the stiffness of the ballast during the warm period of the year is essentially negligible and (2) the bearing mechanisms are fixed for very small amplitudes of vibration. Thus, the list above was augmented with the bearing mechanisms

1. Ballast/track superstructure
2. Soil-structure interaction
3. Bearing mechanisms

These three modelling details were assumed to be the most relevant and will be shortly described in this chapter.

When introducing these modelling details, higher requirements are imposed on the geometrical modelling and on the modelling of damping. In beam models, the eccentricity between the support points, the track superstructure and the neutral axis of the beam elements must be carefully modelled. This can be achieved by standard techniques, using constraint equations. In a simply supported beam, this eccentricity becomes relevant only if we restrain the horizontal movement of the movable bearing. If the movable bearing is fully constrained, the beam is fixed at both ends. As will be shown in section 3.4, a detailed model of a movable bearing has a smooth transition from being fixed at very small displacements, to be moving at larger displacements. In ABAQUS, one can create these eccentricities by means of constraints or by using a form of mechanism-elements, referred to as connector-elements. Connectors can be used to define couplings between nodes with quite complicated constitutive relations, but here they have mainly been used to define linearised bearing mechanisms, linear SSI-elements and rigid links.

3.1 Modelling of damping

This section gives a short discussion of damping in railway bridges in general and the approach taken to the modelling of damping in the case studies described in section 5. Material and friction damping will be discussed in this section and specific sources of damping, other than material damping, which have been considered in the case studies will be treated in sections 3.2–3.4.

Damping in civil engineering structures is composed of contributions from several sources. These sources are:

1. Friction in e.g. bearings, joints, ballast, cracks in concrete.
2. Material damping, i.e. rearrangement of crystals, molecules or granules and heat transfer in solids (thermoelastic damping).
3. Radiation damping through foundations or abutments and embankments.

In addition to these sources, interaction effects such as train-bridge interaction and fluid-structure interaction may also dissipate energy from the vibrations of the structure. The total damping of a structure will be referred to as structural damping. Naturally, a complete review of this topic is beyond the scope of this thesis, but a short description of how damping from different sources have been defined in the case studies will be given in the following.

The complexity of the theoretical modelling of structural dynamics increases quite rapidly when one tries to separate the sources of damping, even if a linear structural response is expected. The reason for this is that each of the above mentioned sources of damping are areas of research of their own. Furthermore, the distinction between material and structural damping is not entirely clear in civil engineering structures.

Material damping

It is well known that the material damping only constitutes a very small part of the total structural damping. In general, it depends on the amplitude and frequency of vibration. Several linear rheological models have been proposed to describe material damping in various materials. Bert [8] provided a review of damping models commonly used until 1973 and the very same models are still in common use today as reflected by the contents of handbooks such as reference [27]. In civil engineering structural dynamics, the Kelvin-Voigt model (i.e. a spring and a dashpot in parallel) is the most commonly used linear, viscous damping model. Essentially, this model leads to the linear viscously damped oscillator, to which solutions are readily obtained by well-known techniques. However, most of the damping in a railway bridge appears to have its cause in radiation damping and frictional effects, although train-bridge interaction is also considered important. Radiation damping is described in section 3.2 and the frictional effects considered herein are described in sections 3.3 and 3.4.

The mechanisms which generate material damping varies considerably between different types of materials. In metals and other solid, crystalline materials, damping is generated by heat transfer and plastic work. Thermoelastic damping is a consequence of temperature gradients caused by material inhomogeneities and elastic deformations [43]. These temperature gradients give rise to a heat flux which in turn leads to dissipation of energy ultimately to the surroundings of the elastic body. However, it is clear that some form of very small plastic-like deformations (i.e. movements of dislocations) also occur at very small amplitudes of vibration, resulting in fatigue. The material damping in steel structures can therefore vary somewhat depending on manufacturing processes, the alloy and welding and other types of heat treatment.

In pure concrete, material damping of pure concrete depends on factors such as its age, the water-to-cement ratio, loading frequency and amplitude, aggregate proportioning and the presence voids [10]. In reinforced concrete, the material damping is dependent on the formation and propagation of cracks and thereby on the configuration of reinforcement, pre-stress and confining pressure but also the loading history and the history of the environmental variables. This, as well as other factors, complicates matters tremendously. In some sense, reinforced concrete is a composite structure and therefore, the distinction between material damping and structural damping is not clear and the need for simplifications based on experimental data is obvious.

In granular materials, the material damping is mainly caused by the rearrangement of the granules and the frictional inter-granular forces involved in that process. Therefore, the material damping ratio of granular materials is highly dependent on the confining pressure and the state of strain, see e.g. [26, 25] and [32]. Nevertheless, material damping within the granules is also present. A detailed theoretical description of the dissipation of energy in granular materials is also very difficult. Furthermore, it appears to be rather difficult to determine the correct initial state in natural soil deposits. However, in such cases, in-situ measurements can be used to obtain a realistic start point for theoretical analyses.

Nevertheless, reasonable values needed to be chosen for the material damping in the case studies performed within this project. Cremer et al. [18] have gathered experimental estimates of material damping ratios for many common materials from the literature. According to Cremer et al., the loss factor of steel is $\eta_{\text{steel}} = 2\cdot10^{-5} - 3\cdot10^{-4}$ and the loss factor of concrete is $\eta_{\text{concrete}} = 4\cdot10^{-3} - 8\cdot10^{-3}$. The corresponding damping ratios are $\xi_{\text{steel}} = 1 \cdot 10^{-5} - 1.5 \cdot 10^{-4}$ and $\xi_{\text{concrete}} = 2 \cdot 10^{-3} - 4 \cdot 10^{-3}$. In the analysis performed within this thesis, the material damping ratio of the steel-concrete composite beam in the case 1 bridge was fixed to $\xi_{\text{composite}} = 1.5 \cdot 10^{-3}$ and the material damping of concrete was fixed to $\xi_{\text{concrete}} = 4.5 \cdot 10^{-3}$.

Friction damping

The study of friction and wear in contact mechanics is referred to as tribology. This is a field of research in its own and has applications in essentially all forms of machines and structures. The friction force itself has its origin in the contact and deformation of small asperities on the surfaces in contact. Thus, on a microscopic level, the contacting surface pair consists of a number of small point-like contacts. Therefore, a distinction must be made between the apparent and the true contact area. The friction force is proportional to the normal stress on the contact surfaces (Amonton's first law of friction). Ultimately, it is given by a critical shear stress over the true contact area, which depends on the normal load and the deformation characteristics of the asperities. Thereby, the friction force is independent of the apparent area (Amonton's second law of friction).

In general, one must discern between dry and lubricated friction. In the present context we are mainly interested in dry friction, although some bridge bearings have lubricated PTFE-stainless steel contacts. Naturally, lubricated friction becomes more complicated than dry friction because we then also need to consider the flow of the lubricant between the contacting surfaces. In both dry and lubricated friction, one may also have to consider chemical processes on the contacting surfaces. In the case of dry friction, most materials react with the surrounding environment, creating a surface which has rather different properties than the bulk material. A simple example is of corrosion of steel, but water or even moisture in the air (which can adhere to the contact surfaces) can give rise to a certain degree of lubrication. A deeper discussion of this topic is outside the scope of this thesis. Nevertheless, it is clear that the multidisciplinary nature of the dynamic response of railway bridges also touches upon mechanical engineering.

However, a few common notions used in the tribological literature will be used and the following definitions have been adopted essentially from the textbook by Armstrong-Hélouvry [6]. We need to consider the distinction between static and kinematic friction. Static friction refers to the force needed to initiate motion, while kinematic friction refers to the force needed to maintain motion. However, the friction coefficient is in general highly dependent on the relative velocity between the contacting surfaces, especially in lubricated contacts. If the kinematic friction is independent of the relative velocity it is referred to as Coulomb friction. A linear dependence of the friction coefficient on the relative velocity is referred to as viscous friction. The transition from static equilibrium to dynamic equilibrium is referred to as break-away. Micro-slip or the Dahl effect refer to the deformation of the micro structure of the contacting surfaces which leads to increasing, partial slip, prior to motion. Finally, stick-slip is a phenomenon which occurs in cyclic motions, where

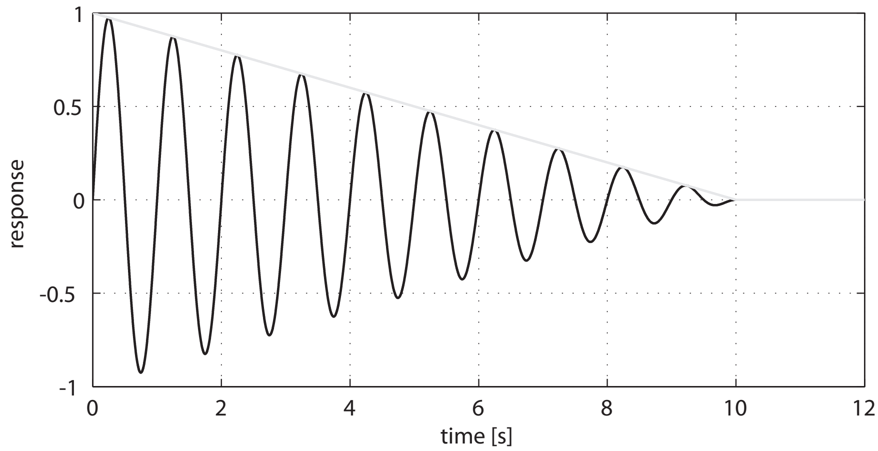

Figure 3.1: The free vibrations of a Coulomb damped ocsillator.

upon load reversal, the relative velocity becomes zero and the static friction has to be overcome in order to initiate the motion in the reverse direction, see also figure 3.2.

Oscillators with friction dampers have been studied by many authors, see for example long and Liu [34]. The most common friction model used in this context is the Coulomb model, in which the coefficient of friction is a constant. A uni-variate model with Coulomb damping has the form

$$m\ddot{x}(t) + kx + f_\mu(t) = f(t) \tag{3.1}$$

where x is the displacement, m is the mass, k is the stiffness, $f(t)$ is the external force and

$$f_\mu = -\mu N \operatorname{sgn} \dot{x} \tag{3.2}$$

is the friction force where μ is the coefficient of friction and N is the normal force on the friction device. It is quite straight forward to show that such an oscillator has a linear decay function (see figure 3.1) if subjected to free vibrations. The idealisation of the Coulomb friction is often too crude and more realistic models considering micro-slip and other effects such as velocity, pressure and temperature dependent friction, may become necessary. A model of micro-slip is inherently included in the Bouc-Wen model, which corresponds to the single degree of freedom system defined above when the parameter $n \to \infty$. Break-away friction for instance, cannot be described by the classical Bouc-Wen model, but with some slight modifications, the coefficient of friction could fairly easily be made dependent on the sliding velocity, as was done by Constantinou et al. [17]. These matters will be further described in section 3.4.

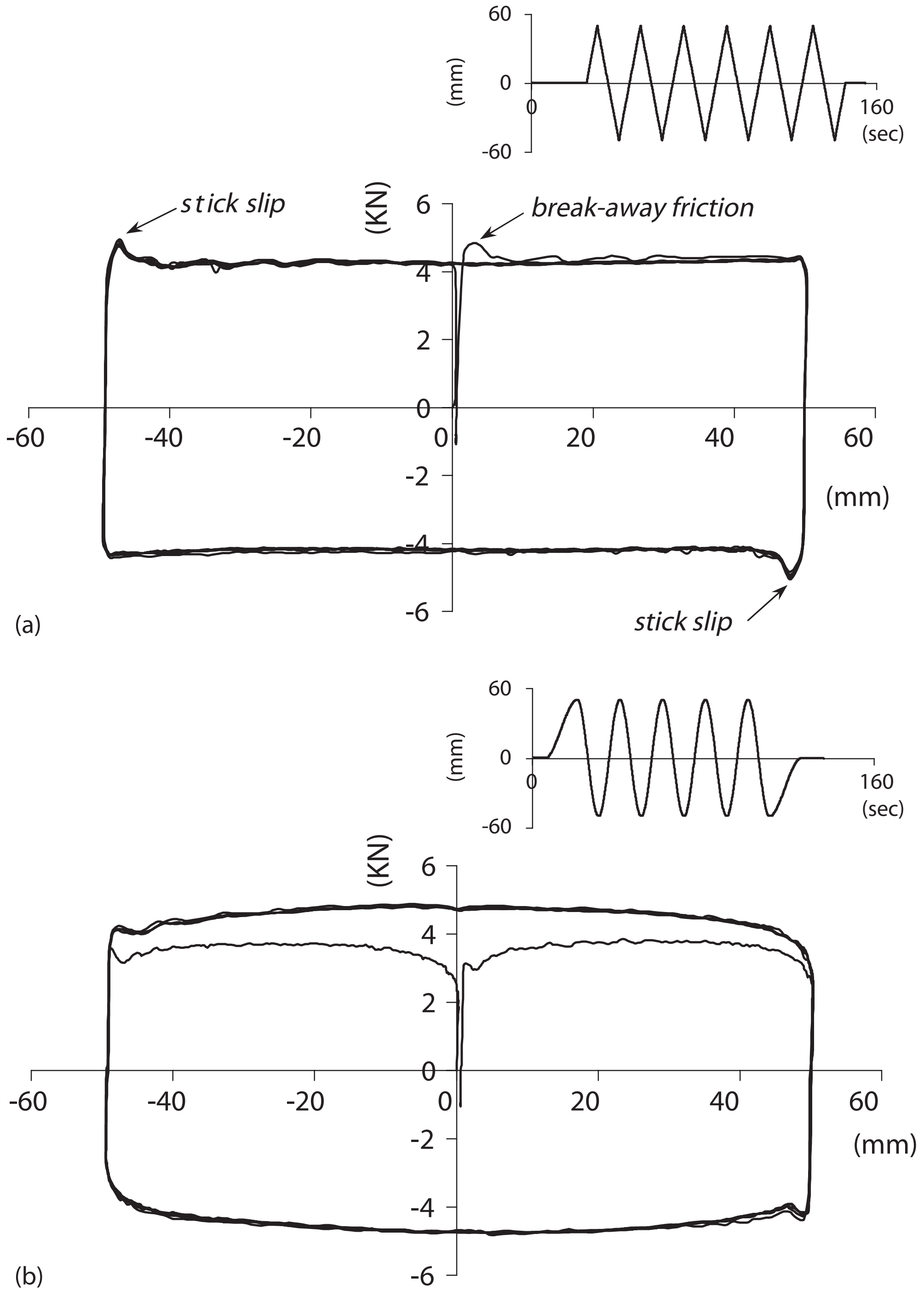

Figure 3.2: Typical frictional force-displacement loops recorded during (a) triangular and (b) sinusoidal tests at low peak velocities (about 10 mm/s). Both tests were conducted on non-lubricated interfaces, under the same air temperature ($-10\,^{\circ}$C), contact pressure (28.1 MPa) and displacement amplitude (50 mm) (from Dolce et al. [20]).

3.2 Soil-structure interaction

Soil-structure interaction is a vast topic and the purpose of this section is to highlight its most important aspects in the present context. A very useful resource is the chapter written by Gazetas in the handbook edited by Fang [22] and the licentiate thesis [47] produced by the author provides some literature studies and theoretical background relevant for applications in railway bridge dynamics.

The soil-structure interface is typically defined by the foundation structure, which can often be assumed to be a rigid body. In three dimensions, this rigid body has six degrees of freedom. Assuming that the soil is isotropic and linearly elastic and that the contact between the foundation structure and the surrounding soil is never lost, the dynamic stiffness functions of the foundation can be computed by standard techniques. As mentioned earlier, the dynamic stiffness functions can be used as a form of macro element.

It turns out that these dynamic stiffness functions are complex-valued functions of frequency, where the real part corresponds to a stiffness and the imaginary part corresponds to an equivalent viscous damping coefficient. An example of such dynamic stiffness functions is shown in figure 3.3 which has been taken form the paper by Padron et al. [40], who used the boundary element method (BEM) and a coupled BEM-FEM method to compute the dynamic stiffness functions for pile groups with inclined piles in a homogeneous, isotropic, linearly elastic soil. The frequency is described by the dimensionless quantity $a_0 = \omega d/c_s$, where d is the pile diameter and c_s is the shear wave speed of the soil material.

The damping coefficient has two components; radiation damping and soil material damping. When a foundation is excited by an external force, elastic waves are generated and travel away from the foundation. Therefore, the energy of the motion of the foundation is dissipated into the surrounding soil as elastic waves, radiating away from the foundation and can only return to the foundation if the elastic waves are reflected against some stiffer region of the subsoil. This can occur if bedrock is close to the soil surface, but also between layers of different soil stiffness and other structures embedded in the soil. If the variation in the soil stiffness is increasing continuously, such reflections can occur at layer boundaries of infinitesimal extent, causing a much less effective dissipation of energy. The soil material damping ratio ranges between 1–5 % but the total damping of typical foundations is dominated by the radiation damping.

Although the pile groups studied by Padron et al. are quite small, their results can give some indications on the order of magnitude of the stiffness and damping that can be expected from such foundations. The piles used in the piled foundations of the case 2 and 3 bridges (see chapter 5) are concrete piles with a square cross section with the side length $a = 270$ mm. A circle with the same area would have a diameter of $d = 304$ mm. The depth of the soil stratum studied by Padron et al. was $H = 15d = 4.5$ m, which coincides quite well with that of some of the pile groups in the case 2 and 3 bridges. If we consider the case with the ratio $E_p/E_s = 10^3$ where

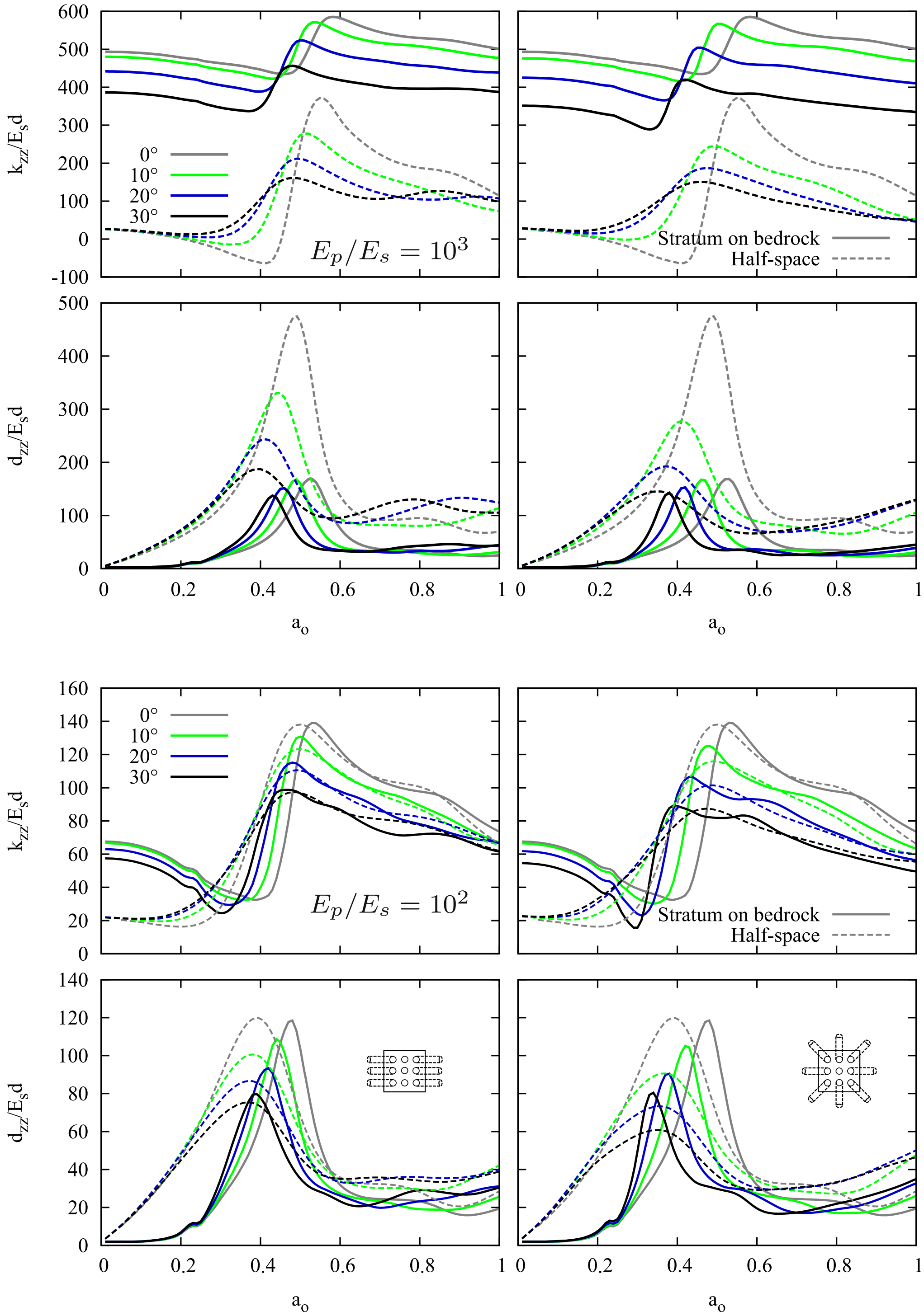

Figure 3.3: Theoretical vertical dynamic stiffness functions for 3×3 pile groups with inclined piles (from Padron et al. [40]). The ratio of the pile (head) spacing and the pile diameter is equal to 5 and E_p and E_s denote the modulus of elasticity of the piles and the soil, respectively.

E_p and E_s denote the modulus of elasticity of the piles and the soil, respectively and assume $E_p = 35\,\mathrm{GPa}$, we obtain $E_s = 35\,\mathrm{MPa}$, i.e. a soft soil. If it is furthermore assumed that the density of the soil is $\rho_s = 1600\,\mathrm{kg/m^3}$ and that its Poisson ratio is $\nu = 0.48$, we obtain the shear modulus $G_s = E_s/(2(1+\nu)) = 12\,\mathrm{MPa}$ and the shear speed $c_s = \sqrt{G_s/\rho_s} = 87\,\mathrm{m/s}$. Thus, the frequency range of figure 3.3 is approximately $\omega \in [0, 46]\,\mathrm{Hz}$. Furthermore, the scale factor $E_s d \approx 5\,\mathrm{MN/m}$. Thus, in the case studies presented herein, where the studied frequencies are all less than 6 Hz, the frequency dependency would not be very important, because in the range of $a_0 \in [0, 0.2]$, the variation of the stiffness and damping coefficients is not very large. The vertical stiffness would be in the order of $k_{zz} = 500 \cdot 5 = 2.5\,\mathrm{MN/m}$ and the damping coefficient would be much less. Actually, one cannot discern the damping ratio from zero for $a_0 \in [0, 0.2]$.

In all three studied cases within this thesis, a consideration of the flexibility and damping capacity of the foundations was needed in order to make the properties of the modes of vibration at very small amplitudes of vibration match the estimates from measurements of bridge deck accelerations during free vibrations. In paper III, a simple FE-model of the abutments were used to determine the stiffness coefficients of the support of the case 1 bridge and the damping was determined by means of the handbook formulas provided in [22]. The results provided by Padron et al. and discussed above show that the order of magnitude of the stiffness and damping coefficients used in cases 2 and 3 is reasonable.

3.3 Track-structure interaction

In Sweden, almost all tracks are ballasted and the three studied bridges all carry ballasted tracks. Therefore this discussion is limited to ballasted tracks and primarily to the longitudinal track resistance. A sketch of a track superstructure on a bridge and the BW-model of the longitudinal track resistance is shown in figure 3.4. Research regarding the track resistance has been geared mainly towards track stability in continuously welded tracks and longitudinal forces induced by changes in temperature or traction caused by trains accelerating or braking. The influence of the track superstructure on the dynamic response of railway bridges has not been given much attention at all. Ballast, although the particles are very large compared to typical soils, has been shown to abide to the same constitutive laws as sand [41]. A comprehensive description of the mechanical properties of ballast in general is given by Indraratna and Salim [31]. However, they, as well as other authors (see e.g. [44] and the references therein) seem to focus mainly on the long-term track quality issues. This is natural, since track maintenance is a major issue for most railway infrastructure managers. Here, the main emphasis is on short term effects during the free vibrations after a train passage. Of course, this simplifies matters considerably. Neglecting the degeneration of the track superstructure and the dependence of the modulus of elasticity of the ballast on the confining pressure, test results from the ERRI project D202 [1, 4, 2, 3] were used in paper IV to define a reasonably simple, phenomenological model of the longitudinal track resistance.

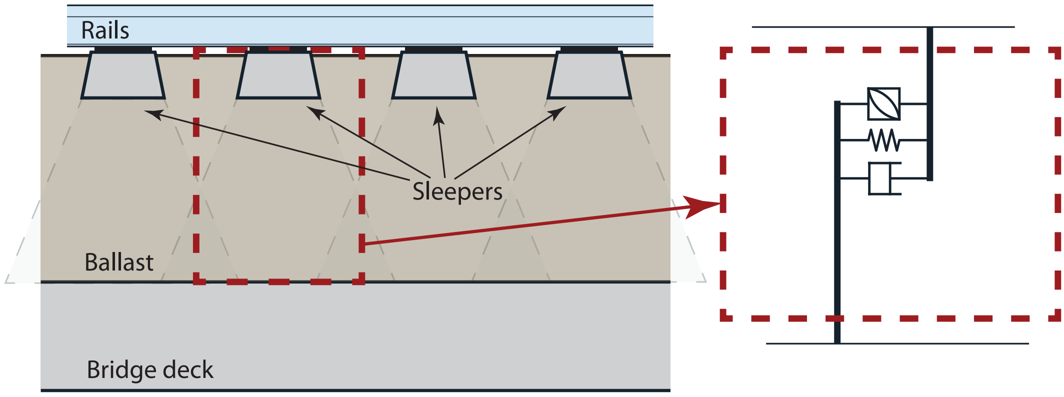

Figure 3.4: A sketch of the track superstructure and the definition of the longitudinal component of the Bouc-Wen track model.

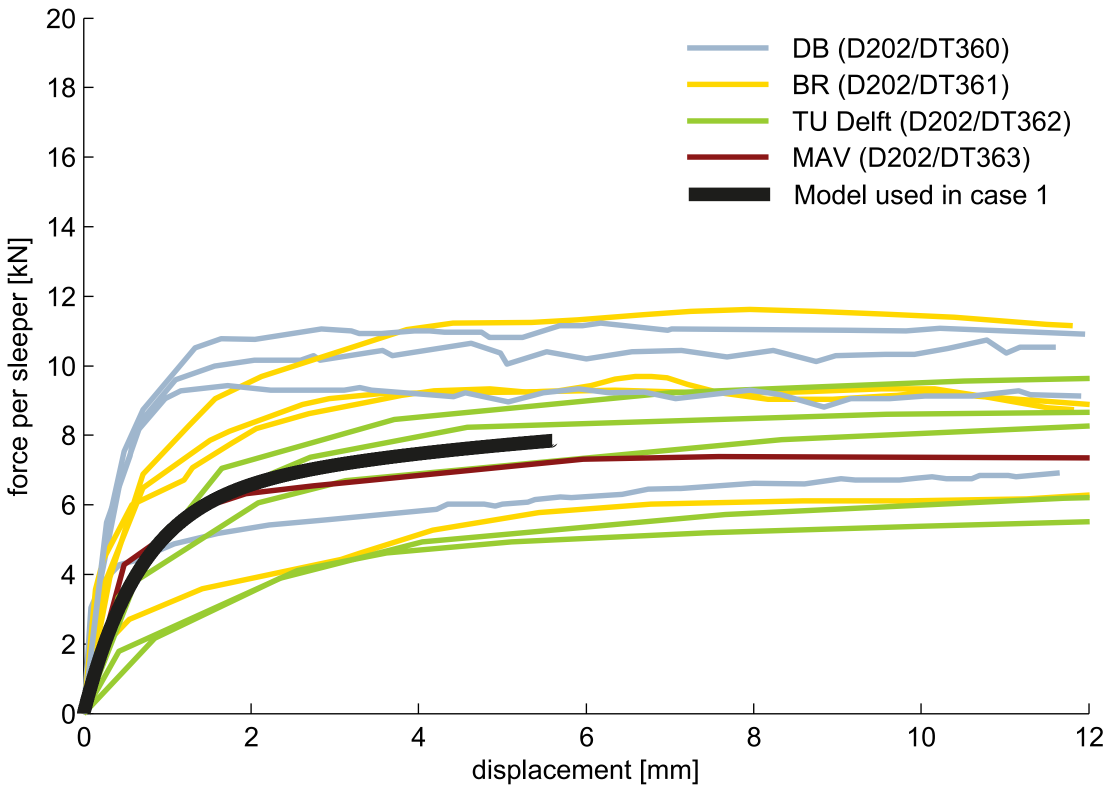

Figure 3.5: A summary of the test results for the longitudinal resistance of unloaded ballasted tracks (from the ERRI D202 project [1, 4, 2, 3]). The figure also shows the longitudinal track resistance used in the study of the case 1 bridge presented in paper IV.

For the longitudinal track resistance, the macro elements were defined to model one sleeper and a certain volume of the ballast assumed to be associated with it, see figure 3.4. The non-linear, hysteretic behaviour was modelled using the Bouc-Wen model (see section 2.1) and the form of the backbone curves used was determined using the experiments performed within the ERRI D202 project (see figure 3.5).

One important restriction on the theoretical studies presented herein is that only the warm period of the year was considered. In paper III it is clearly shown that very large differences in the stiffness of the case 1 bridge occur between the different seasons. It is also stated that large differences have been observed in the modal damping ratios between the different seasons, although those results have not yet been published. However, the ERRI tests referred to above were only performed in environmental conditions corresponding to summer or at least in temperatures above 0 °C. Thus, for cold regions such as Sweden, further research on the track resistance in environmental conditions corresponding to winter with snow, ice and long periods of temperatures $< 0\,^{\circ}\mathrm{C}$ is necessary.

3.4 Bridge bearings

Bridge bearings are used primarily to create sound constraints between different structural parts and to allow for deformations caused by variations in temperature and shrinkage and creep in concrete bridges. Two types of bearings are commonly used in Sweden; steel roller bearings and pot sliding bearings. Many other types of bearings exist, but they will not be considered here. The purpose of this section is mainly to describe how the pot bearings were modelled in case 2 and 3. The modelling of the roller bearings in case 1 is described in paper IV.

One important conclusion from paper III is that the roller bearings of the case 1 bridge can be either fixed or moving, depending on the amplitude of vibration. The basic features of the roller bearings of the case 1 bridge are described in paper IV and in figure 3.6, a sketch of a roller bearing is shown, together with the eccentricities which need to be considered. The eccentricity between the top bearing plate and the neutral axis of the superstructure can be modelled with rigid links when the Euler-Bernoulli hypothesis is assumed for the deformation of the superstructure.

The rotational function of a pot bearing is obtained by confining a circular rubber plate between a pot and a piston, see figure 3.7. Due to the incompressibility of rubber, a pressurised, confined rubber behaves like a fluid. Actually, the sealing ring (7) in figure 3.7 is absolutely necessary as without it, the rubber would flow out of its confinement when pressurised. In a pot bearing, the piston can rotate almost freely about the two horizontal axes. The sliding function of movable bearings is created by placing a sliding plate on top of the piston and the coefficient of friction is reduced by adding a sheet of polytetrafluoroethylene (PTFE) in between. The bearing is then free to translate in two directions. A uni-directional bearing is obtained by means of a groove and a notch.

In paper IV, a model of a roller bearing was defined on the basis of results from

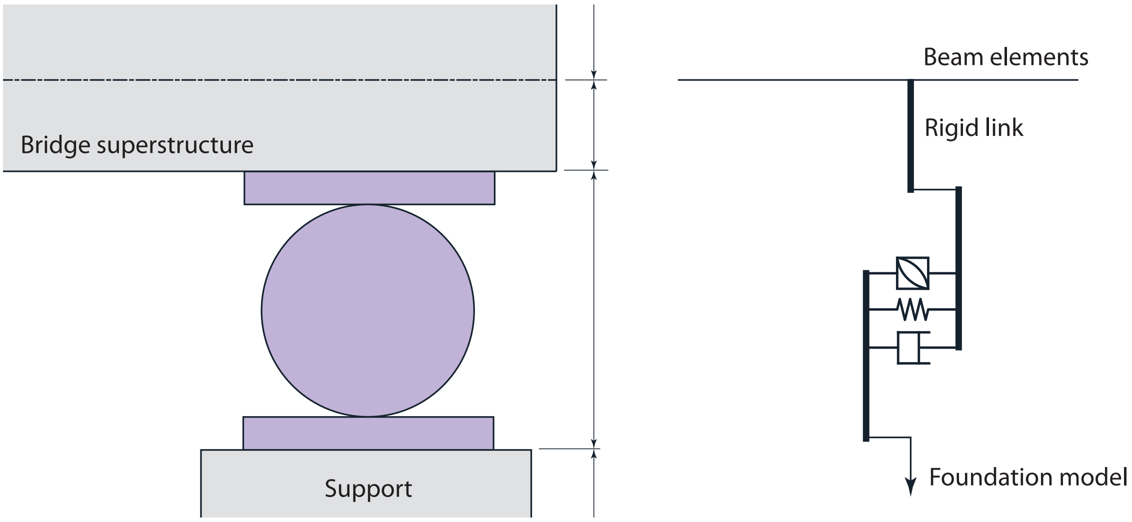

Figure 3.6: A sketch of the longitudinal component of the Bouc-Wen roller bearing element and the relevant eccentricities in the vertical direction.

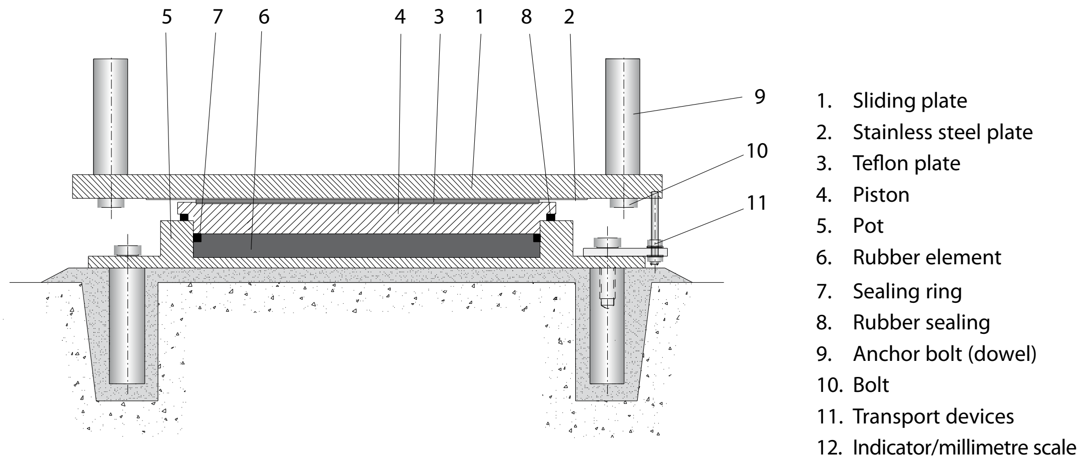

Figure 3.7: A section of a TOBE pot bearing (from http://www.spennteknikk.no).

the mechanical engineering literature. It was shown, by reference to the literature that such mechanisms can be modelled by means of Bouc-Wen models but the exact form of the Bouc-Wen model could not be determined. For that, some additional experimental efforts are needed. Instead, parametric studies on the Bouc-Wen model parameters were performed. A similar approach was used in the preliminary studies for the case 2 and 3 bridges presented in chapter 5. In the following, some additional information regarding the frictional properties of the PTFE-steel interface is given in order to clarify the simplifications made in chapter 5. Clearly, further experimental efforts are needed also in the case of pot bearings.

The PTFE-steel interface of a pot bearing has a more complicated behaviour than the rolling resistance of a roller bearing. This is mainly caused by the introduction

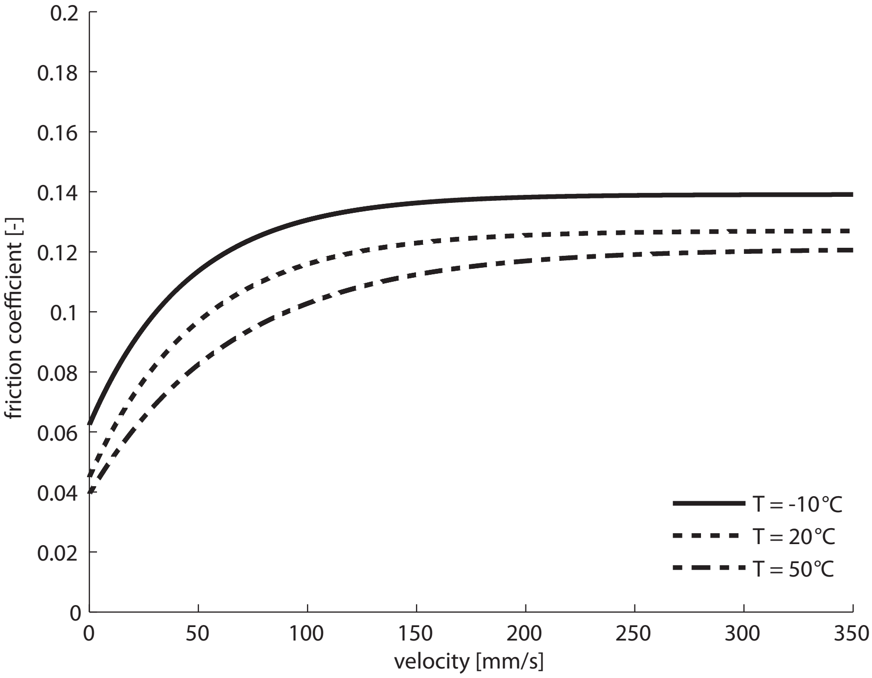

Figure 3.8: The coefficient of friction at a bearing pressure of 18.7 MPa as function of the sliding velocity, according to equation (3.3).

of the PTFE-sheet, the frictional properties of which are sensitive to factors such as temperature, sliding velocity and pressure. Lubrication also influences these properties, but typically, in the Swedish common practice, the PTFE-steel interface is unlubricated, so this factor will not be further discussed here. PTFE-steel contacts have been used in seismic isolation of buildings and structures, see e.g. [12, 17, 20, 29, 38] and the references therein. In such cases, the response is expected to be fast and at large amplitudes (corresponding to geometrical non-linearity) of vibration. However, it would appear as if the velocity dependency of the coefficient of friction cannot be ignored in serviceability limit state railway bridge dynamics.

Figure 3.8 shows the model function due to Constantinou et al. [17]

$$\mu(v) = \mu_{\max} - (\mu_{\max} - \mu_{\min}) \exp(-\alpha_\mu v) \tag{3.3}$$

where $\mu_{\max}$ and $\mu_{\min}$ are the maximum and minimum coefficients of friction, respectively, α_μ is a parameter depending on temperature, pressure and the condition of the PTFE-steel interface and v is the relative velocity between the sliding surfaces. Clearly, the dependency of the friction coefficient on the sliding velocity over the PTFE-steel interface varies the most at low sliding velocities and increases quite rapidly. For a simply supported bridge such as the case 1 bridge (the Skidträsk bridge, which was studied in papers I–IV), the sliding velocity can be estimated in the following way. Assuming a steady state and linearly elastic behaviour where the Euler-Bernoulli hypothesis holds in the fundamental model of vibration, the vertical displacement $v(x,t)$ may be written

$$v(x,t) = A\sin(2\pi f_{\mathrm{n}}t)\sin\left(\frac{2\pi x}{L}\right) \tag{3.4}$$

where A is the amplitude of vibration at mid-span, L is the length of the bridge and f_{n} is the frequency of the fundamental mode of vibration. If the height of the cross section over the supports is denoted by h, the maximum longitudinal displacement at the free support is given by

$$u_{\mathrm{l}} = \frac{2\pi Ah}{L} \tag{3.5}$$

and the maximum velocity is

$$\dot{u}_{\mathrm{l}} = \frac{4\pi^2 Ahf}{L} \tag{3.6}$$

Inserting the parameter values relevant for the Skidträsk (case 1) bridge, assuming $A = 10\,\mathrm{mm}$, we have $u_{\mathrm{l}} \approx 2\pi \cdot 0.01 \cdot 1/36 \approx 2\,\mathrm{mm}$ and $\dot{u}_{\mathrm{l}} \approx 4\pi^2 \cdot 0.01 \cdot 1 \cdot 3.9/36 \approx 40\,\mathrm{mm/s}$. Referring again to figure 3.8, it is clear that the coefficient of friction may increase with as much as a factor 2 due to the influence of the sliding velocity during a train passage or in a state of train-bridge resonance.

Furthermore, there is a more or less pronounced break-away effect in the first cycle. However, it is not expected to have any significant influence on whether sliding will occur or not, because otherwise, the bearings would behave as fixed bearings at all times. It is also possible that plastic deformations as well as corrosion and dirt in a roller bearing could give rise to a break-away like effect, which has not been considered within this thesis. Stick-slip however, does not appear to be very pronounced in sinusoidal cycles on PTFE-steel interfaces (see figure 3.2). In the preliminary studies presented in chapter 5 (case 2 and 3) the break-away friction and the influence of the sliding velocity was ignored. The pressure dependency was assumed to be negligible during free vibrations, although a slight variation in the bearing pressure is expected due to the vertical flexibility of the supports. Furthermore, the temperature was assumed to be constant. Under these assumptions, the classical Bouc-Wen model is applicable and the bearing model parameters were determined in an inverse sense by fixing all the other structural parameters to reasonable values (see chapter 5) and adjusting the bearing parameters so as to approximately match the experimentally determined instantaneous quantities. Thus, the theoretical results for the case 2 and 3 bridges presented in chapter 5 was not expected to fully resemble the real behaviour of those bridges and it is again stressed that the purpose was to obtain an indication of the influence of the bearing hysteresis on the global bridge response.

Chapter 4

Analysis of non-stationary signals

The result of paper IV and the other case studies presented in chapter 5 implies that the modes of vibration of typical railway bridges are non-linear. In structural dynamics, a mode of vibration is often associated with computational techniques based on the principle of superposition, which rests on the assumption that the studied structural system is linear. Therefore, the notion of a non-linear mode of vibration may be disturbing to some structural engineers. Therefore, the aim of this chapter is to define just that: a non-linear mode of vibration, and to discuss the restrictions needed in order to make such a definition meaningful. This chapter is based mainly on the textbooks by Mallat [36] and Flandrin [23] and the journal paper by Huang et al. [28].

4.1 Analytic signals and the Hilbert transform

The Fourier transform of the function $f(t)$

$$\hat{f}(\omega) = \int_{-\infty}^{\infty} f(t) \exp(-i\omega t) \mathrm{dt} \tag{4.1}$$

and its inverse

$$f(t) = \frac{1}{2\pi} \int_{-\infty}^{\infty} \hat{f}(\omega) \exp(i\omega t) \mathrm{d}\omega \tag{4.2}$$

is a well known mathematical tool which has been used in applications in most fields of engineering and science. Although this transformation and its inverse can be defined for any function $f(t)$ such that

$$\int_{-\infty}^{\infty} |f(t)| \mathrm{dt} < \infty \tag{4.3}$$

(see for example [50]), the physical interpretation of the result of the transformation is not straight forward. Here, the function $f(t)$ will be restricted to real-valued functions since we are considering signals from structural systems. In general, the Fourier transform $\hat{f}(\omega)$ is a complex function of the real variable ω and if $f(t)$ is an even function ($f(-t) = f(t)$), its Fourier transform will be a real-valued function while if $f(t)$ is odd ($f(-t) = -f(t)$), its Fourier transform will be a purely imaginary function. Furthermore, if $f(t)$ is real, it has the property $\hat{f}(-\omega) = \hat{f}^*(\omega)$ where * denotes the complex conjugate. If the independent variable t represents time however, the independent variable in the Fourier domain ω will represent a circular frequency and the notion of a negative frequency does not make sense, but there is a symmetry/antisymmetry over $\omega = 0$. Given the efficiency of using the Fourier transform in solving linear ordinary and partial differential equations, these somewhat strange features of the Fourier transform can be accepted. When it comes to functions $f(t)$ which are generated by non-stationary or non-linear systems however, some additional issues arise. Consider a rectangular wave with a certain time step Δt between changes in its sign. Its period is then $T_{\text{rect}} = 2\Delta t$ and with the definition of frequency in terms of the period of oscillation, $f = 1/T$, the frequency of this signal will be $f_{\text{rect}} = 1/(2\Delta t)$. However, the Fourier transform of this signal will have frequency components which extend towards $\pm\infty$. So, how should these higher frequencies be interpreted from a physical point of view? The cause of these higher frequencies lies in the fact that the Fourier transform gives a representation of our signal $f(t)$ composed of an infinite sum of sine and cosine functions, extending over the entire set of real numbers. It relies on the destructive and constructive interference between these trigonometric functions and in order to exactly represent the function $f(t)$ by its Fourier transform $\hat{f}(t)$ we need to include the entire range of ω. In this particular example, a finite number of Fourier components would give a good approximation. The real issues arise when transient phenomena are studied by means of the Fourier transform. Each Fourier component is completely non-local in time, so the information in the Fourier domain cannot tell us anything about what is going on at a given time instant, unless we integrate over the entire Fourier domain.

One way of dealing with these issues is the continuous wavelet transform, which is described in paper I. Although the wavelet transform does provide a great improvement in terms of time/frequency localisation, it is a very complex mathematical tool, where the basis on which the signal is projected is defined by a function, the mother wavelet, which can be chosen in many different ways. The mother wavelet typically has more than one parameter which may need to be adjusted and it is inherently two-dimensional, so the computational work involved is quite time-consuming. Having determined the wavelet transform, rather complicated operations are needed in order to extract the relevant information, i.e. the instantaneous amplitude and frequency. There is another, much more efficient way of dealing with the estimation of the instantaneous quantities, namely the Hilbert transform.

However, before we turn our attention towards the Hilbert transform, some further motivation for its use in the present context will be given. A signal $x(t)$ generated by a non-stationary or non-linear system can be represented by a frequency and amplitude modulated function on the form

$$x(t) = A(t)\cos(\phi(t)) \tag{4.4}$$

where $A(t)$ and $\phi(t)$ are the modulated (instantaneous) amplitude and frequency, respectively. However, this definition is not unique, a fact which can be easily shown.

Multiplying and dividing equation (4.4) with an arbitrary function $B(t)$ such that $0 < B(t) < 1$, we have

$$x(t) = \frac{A(t)}{B(t)} B(t) \cos(\phi(t)) = \bar{A}(t) \cos(\bar{\phi}(t)) \tag{4.5}$$

where $\bar{A}(t) = A(t)/B(t)$ and $\bar{\phi}(t) = \arccos(B(t)\cos(\phi(t)))$. Thus, there exists an infinite number of pairs $(A(t), \phi(t))$ which can represent the signal $x(t)$.

Given a real valued signal $x(t)$, the so called analytic signal $x_\mathrm{a}(t)$ corresponding to $x(t)$ is obtained by removing the negative frequencies from the Fourier transform of the signal. This does not remove any information from the signal, since $\hat{x}(-\omega) = \hat{x}^*(\omega)$. In the frequency domain, this can be achieved by the operation

$$\hat{x}_\mathrm{a}(\omega) = 2U(\omega)\hat{x}(\omega) \tag{4.6}$$

where $U(\omega)$ is the Heaviside function

$$U(\omega) = \begin{cases} 1, & \omega \geq 0 \\ 0, & \omega < 0 \end{cases} \tag{4.7}$$

The inverse Fourier transform of $\hat{x}_\mathrm{a}(\omega)$ can be written

$$x_\mathrm{a}(t) = x(t) + \frac{i}{\pi} \mathrm{P.V.} \int_{-\infty}^{\infty} \frac{x(\tau)}{t - \tau} \mathrm{d}\tau \tag{4.8}$$

where P.V. denotes the Cauchy principal value

$$\int_{-\infty}^{\infty} f(t)\mathrm{d}t = \lim_{R\to\infty} \int_{-R}^{R} f(t)\mathrm{d}t \tag{4.9}$$

Thus, the analytic signal is a complex function. The second term of equation (4.9)

$$H\{x(t)\} = \frac{i}{\pi} \mathrm{P.V.} \int_{-\infty}^{\infty} \frac{x(\tau)}{t - \tau} \mathrm{d}\tau \tag{4.10}$$

is known as the Hilbert transform, which is defined for arbitrary functions $f(t) \in L^p$, i.e. the functions for which

$$\int_{-\infty}^{\infty} |f(t)|^p \mathrm{d}t < \infty \tag{4.11}$$

with p a positive integer greater than zero. From this definition of an analytic signal, a modulus-phase pair can be defined in the following unambiguous way

$$a_x(t) = |x_\mathrm{a}(t)| \tag{4.12}$$

$$\omega_x(t) = \frac{\mathrm{d}}{\mathrm{d}t} \arg(x_\mathrm{a}) \tag{4.13}$$

where $a_x(t)$ and $\omega_x(t)$ are the instantaneous amplitude and frequency, respectively. Figure 4.1 shows an example of some mono-component signals and their analytic signal representations.

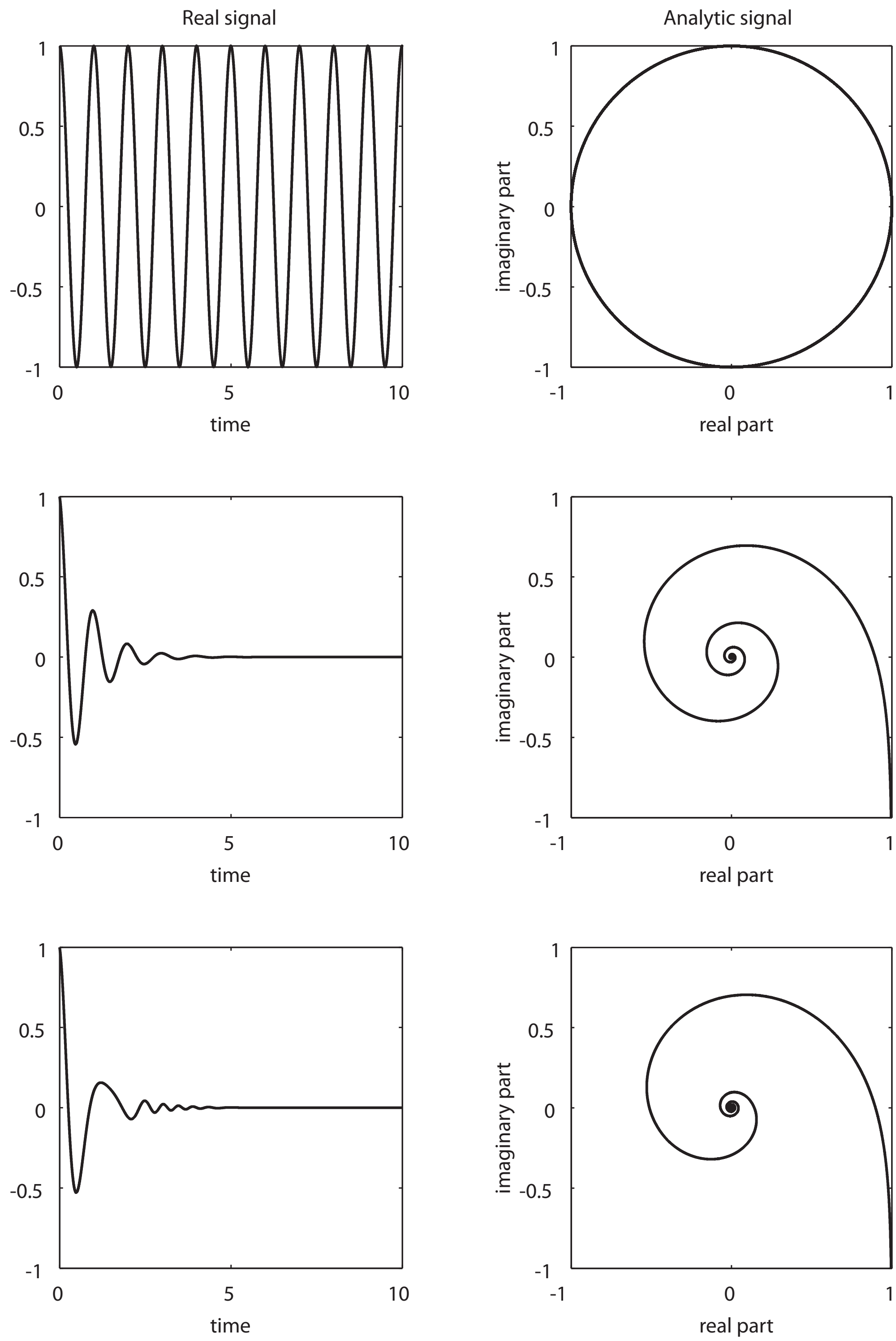

Figure 4.1: An illustration of the analytic signal corresponding to (top) a monochromatic signal, (middle) an amplitude modulated mono-component signal and (bottom) an amplitude and frequency modulated mono-component signal.

In this thesis, the studied signals are mono-component signals, i.e. only one mode of vibration is present. This was ensured by bandpass-filtering. In the analysis of the case 1 bridge however, the first vertical bending and the first torsional modes of vibration are closely spaced, and wether the first torsional mode is present in the free vibrations or not cannot be determined directly from the analytic signal. This becomes immediately obvious from the wavelet transform, due to the time/frequency representation obtained thereby. If several modes of vibration are present in the scalogram computed by the wavelet transform, they will appear as separate ridges (see paper I), unless they are extremely closely spaced and have essentially the same instantaneous variation. These ridges could cross each other if the frequency of some modes varies much faster with the amplitude of vibration than others. Such cases could be treated using the concept of the empirical mode decomposition which was defined by Huang et al. [28].

4.2 The instantaneous damping ratio

The variation in the amplitude is dependent on the type of damping in the structure generating the signal, a fact which raises the question: How should we define a measure of the damping in a free vibration signal from a non-linear structure? From the previous section, it is clear that the instantaneous frequency cannot be unambiguously defined unless certain restrictions are posed. That discussion led us to adopt the definition that the (non-linear) modes of vibration which we are interested in can be represented by a narrow band of frequencies. We also used our knowledge of the non-linear mechanisms involved and arrived at the conclusion that at very small amplitudes of vibration, a maximum frequency $f_{\max}$ exists, which is continuously reduced at larger amplitudes of vibration, due to the reduction in the structural stiffness imposed mainly by the non-linearities of the bearings. If we furthermore limit the large amplitudes of vibration to those which may occur in a serviceability limit state, a minimal frequency $f_{\min}$ which the mode in question can assume, can also be established. Thus, the modes of vibration which we are interested in are assumed to be well represented by a narrow-band process bounded, in frequency, essentially by $(f_{\min}, f_{\max})$. Then, there should also exist some natural restrictions on the variation of the damping ratio, but how should we compute it if only free vibration data is at hand?

Equation (2.7) could perhaps be used, with some approximation owing to the fact that we do not obtain full cycles form free vibrations. However in order to do so, we need to measure the reaction force corresponding to the generalised degree of freedom of the mode of vibration. As such data is typically not available, we need something that can be directly applied using only the information available in the instantaneous quantities of the free vibration signals. Ideally, we would use a displacement controlled excitation test to determine the damping ratio from full hysteresis loops, but as explained in the introductory chapter, such measurements were not available and would be much more expensive to obtain than free vibration data. Therefore, in paper I, we defined an equivalent instantaneous viscous damping ratio in order to have a measure of the damping properties that can be used when only free vibration output data is available. This measure of the instantaneous damping ratio was based on the linear, viscously damped oscillator and has the form

$$\xi_{\text{eq}} = -\frac{\dot{a}_x}{\omega_x a_x} \tag{4.14}$$

using the notation from the previous chapter. Please note that a slightly different notation was used in papers I–IV. It should be noted however, as shown in paper IV, that this measure of the damping ratio must be used with caution, as it may overestimate the damping ratio compared to the formal definition given by equation (2.7).

The identification of systems with frictional (Coulomb) damping has been studied by Tomlinson and Hibbert [46], Badrakhan [7] and Liang and Feeny [33], among others. Tomlinson and Hibbert [46] proposed a methodology, capable of determining the Coulomb model parameters from forced vibration tests on multi-degree of freedom systems, which could be used to estimate the properties of bearings and supports if their behaviour is close to that of Coulomb friction. Badrakhan as well as Liang and Feeny developed techniques for identification and separation of systems with combined friction (Coulomb) and viscous damping from measurements of free vibrations. Such techniques could be useful as first approximations of the non-linear component of the modes of vibration studied here.

However, the treatment of the friction-like mechanisms in a phenomenological manner, through the non-linear mode of vibration defined in this thesis, appears to be more relevant in the present context. First, forced vibration tests on existing railway bridges are very difficult to perform, although some tests of this kind seem necessary in order to gain support for the hypothesis proposed herein. Second, the frictional behaviour of these non-linear modes of vibration is not of the Coulomb type. Thus, methods for the identification of Bouc-Wen models or similar models of hysteresis seem to be more appropriate. Such methods exist in an abundance for the case of uni-variate BW-models, see e.g. references [13, 16, 45], which could be used as a start point for such developments.

4.3 Estimates of the instantaneous quantities

The techniques based on the continuous wavelet transform (CWT) and the Hilbert transform (HT) have in common that we need to compute derivatives of signals with noise. It is well known that such operations may lead to significant distortions. Here, the smoothing algorithms of Matlab were used to remove the most of this distortion, so having two different methods for the estimation gives an opportunity to validate the estimates. This deficiency does not exist with the method used by Rebelo et al. [42] and Lorieux [35]. In the method based on the CWT, the instantaneous frequency is given by the ridge of the CWT, so in that case we only need to differentiate the amplitude. However, in the method based on the HT, in order to compute our estimates as defined by equations (4.13) and (4.14), we need to differentiate both the phase and the amplitude in the HT. The implementation of the two methods are summarised below.

CWT

The CWT method consists of the following five steps:

1. Window, bandpass filter, and down-sample the signal
2. Compute the continuous wavelet transform
3. Determine the ridge and the instantaneous frequency
4. Determine the amplitude along the ridge
5. Compute the equivalent instantaneous damping ratio

The main computational effort lies in computing the CWT. Since it is a function of both frequency and scale/time, this can take some time if a fine resolution is needed. However, much of the computational effort lies in plotting the transform.

HT

The HT method consists of the following four steps:

1. Window, bandpass filter, and down-sample the signal
2. Compute the Hilbert transform
3. Compute the instantaneous frequency
4. Compute the equivalent instantaneous damping ratio

Here, the computational effort in each step is similar. The Hilbert transform is one-dimensional, and can be computed efficiently by means of the Fast Fourier transform, so the calculations are faster than the CWT method. Also, the end effects were found to be somewhat less pronounced in the HT method, compared to the CWT method.

Chapter 5

Case studies

In this section, some additional results to those published in papers I–IV will be presented. These consist in a validation of the CWT estimates of the natural frequency and damping ratio presented in paper I, where the HT has been used instead, and an extension of the analysis presented in paper IV on two other typical beam bridges. Section 5.1 gives a comparison between the estimates of the natural frequency and the damping ratio, as obtained from the CWT and the HT for the case 1 bridge. In sections 5.2 and 5.3 the two additional bridge cases will be shortly described, along with the CWT results obtained from measurements of free vibrations on the two bridges. In section 5.4, a preliminary analysis including BW-models of the bearings in the three bridges is presented. Finally, in section 5.5, some key parameters have been varied in the theoretical model of the case 3 bridge, with the purpose of studying the qualitative influence of different model parameters.

5.1 Wavelet versus Hilbert

A comparison between the frequency and damping functions estimated for the case 1 bridge using the CWT and the HT is shown in figure 5.1. The agreement between the two methods is quite good, but the HT has a much smaller end effect than the CWT. Furthermore, the CWT analysis took a few minutes to compute while the HT analysis took a few seconds. The data were taken from the cold period of the year, hence the larger variability (see paper III) than what was reported in paper I, were the data were taken from the warm period of the year.

5.2 Case 2 - Ullbrobäcken

The case 2 bridge is shown in figure 5.2 and the result of the CWT-based estimation scheme is shown in figure 5.3. The bridge is a two span concrete wide beam bridge with integrated abutments and it carries two ballasted tracks. The superstructure is prestressed and was assumed to be un-cracked, but the increased thickness over

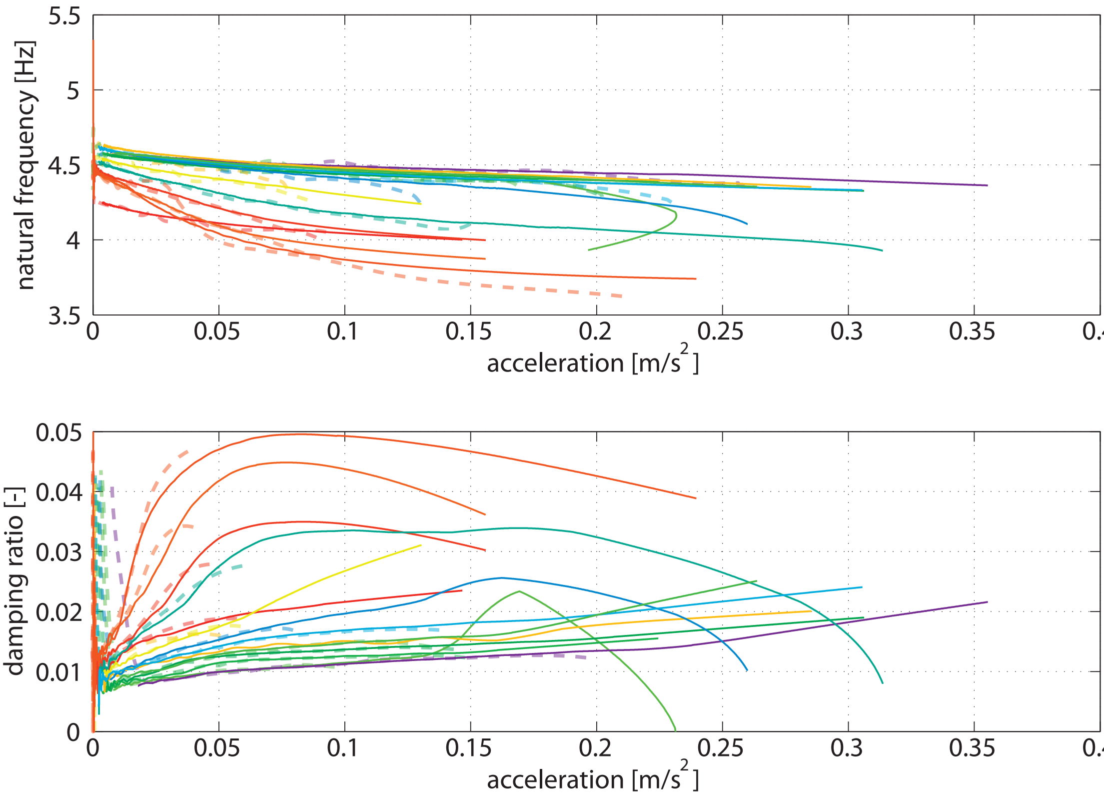

Figure 5.1: A comparison between the CWT (dashed) and the HT (solid) for the first vertical bending mode of the case 1 bridge.

the middle support was considered. The bridge is founded on pile groups which are quite similar for the end supports, consisting of 24 piles with a batter of 4:1, and a much larger pile group at the middle, consisting of 40 piles, again with a batter of 4:1. The stiffness of the foundations was approximated using the static stiffness of the piles alone, approximated as bars. The end supports are very low and the middle support consists of two concrete columns, resting on the pile cap of their foundation. However, in this very much simplified analysis, the substructures were ignored.

Material damping was assumed as discussed in section 3.1, i.e. Rayleigh damping was assigned with $\alpha = 0.11$ and $\beta = 1.1 \cdot 10^{-4}$. In order to obtain the modal damping ratio of 0.6 % at very small amplitudes of vibration (see figure 5.3), an additional radiation/soil material damping was applied as viscous dashpots with the damping coefficient $c = 7.5\,\mathrm{MNs/m}$ at the corresponding foundations. The density of the concrete was taken as $2500\,\mathrm{kg/m^3}$ and adding the mass of the ballast, the equivalent density was $3228\,\mathrm{kg/m^3}$ and $3053\,\mathrm{kg/m^3}$ for sections 1 and 2, respectively. With these parameter values, the modulus of elasticity of the concrete was set to 36.5 GPa, yielding the natural frequency of the first vertical bending mode $f^{\mathrm{case2}} \approx 5.0\,\mathrm{Hz}$. Apart from the mass of the ballast, the track superstructure was completely neglected.

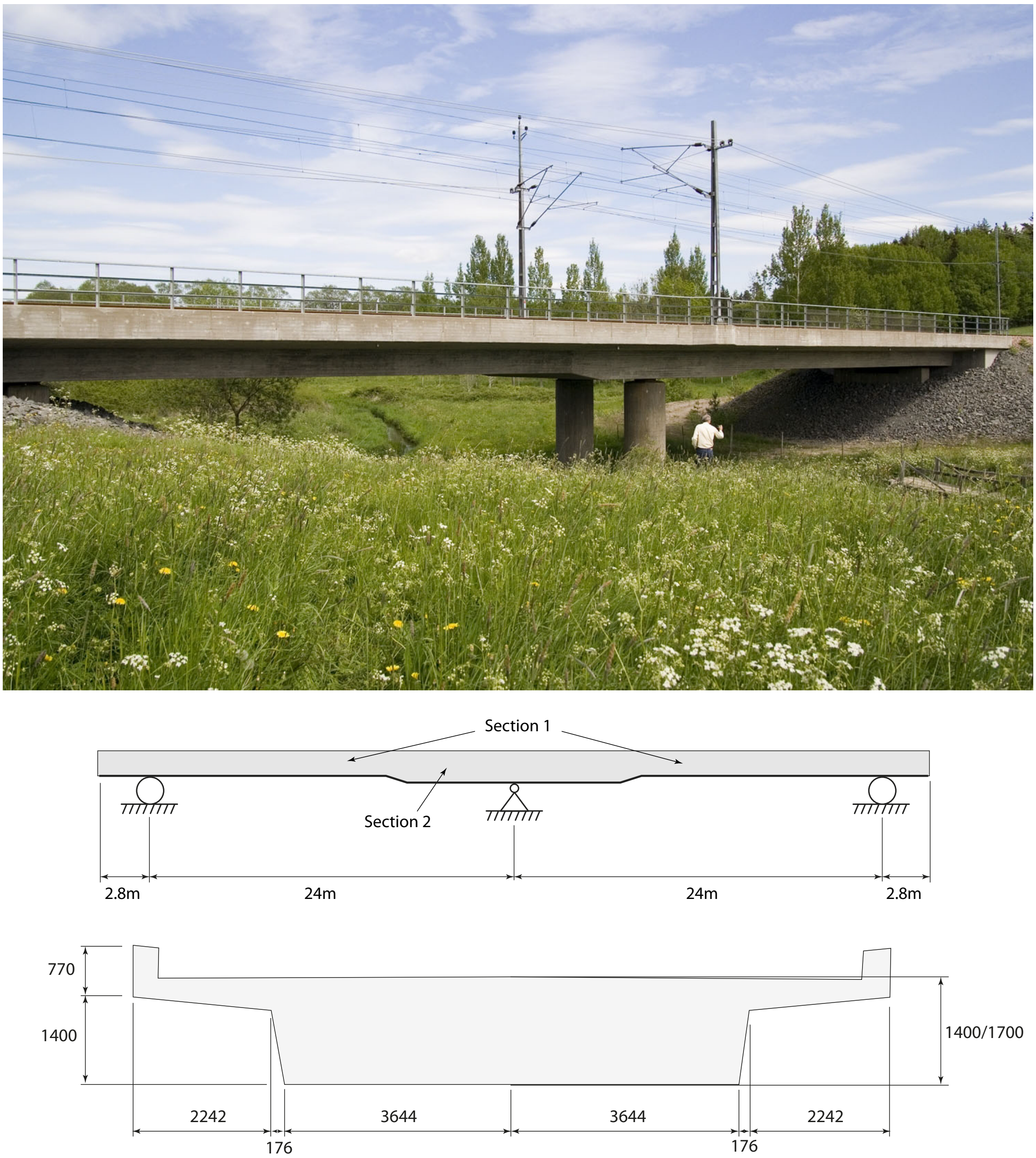

Figure 5.2: A photograph of the case 2 bridge (Ullbrobäcken) and a sketch of its 2D geometry and its cross section. Measures are in millimeters unless otherwise stated.

5.3 Case 3 - Sagån

The case 3 bridge is shown in figure 5.4 and the result of the CWT-based estimation scheme is shown in figure 5.5.

This bridge is a three span prestressed concrete girder bridge which carries one ballasted track. The cross section is solid as shown in figure 5.4. In the model,

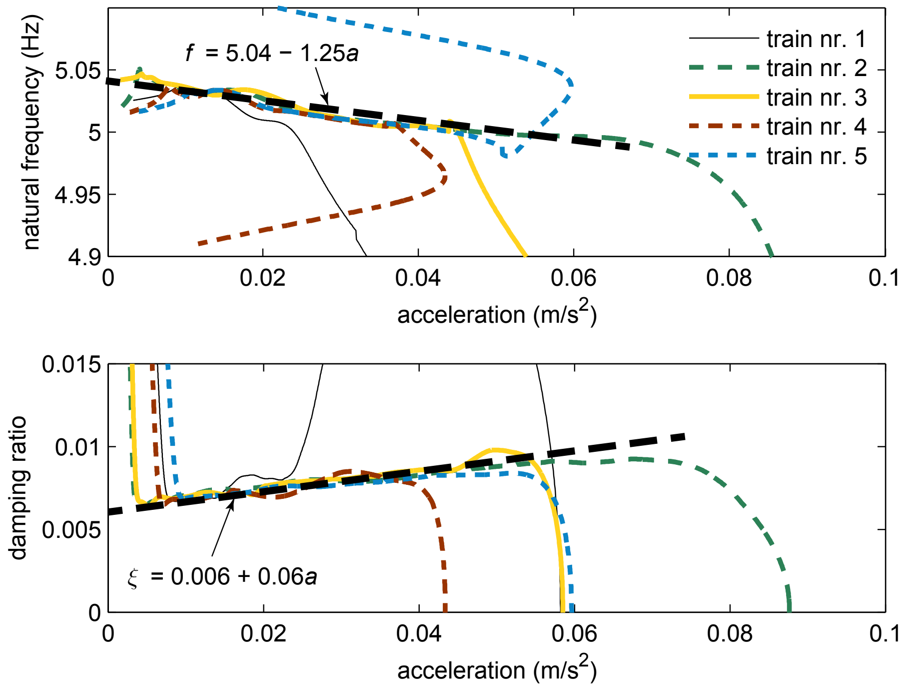

Figure 5.3: The frequency and damping ratio of the first vertical bending mode of the case 2 bridge, as given by the CWT

the cross section was approximated by a 3 m×1.7 m rectangle. The supports are numbered from left to right in figure 5.4. Supports 1, 3 and 4 are founded on pile groups while support 2 is founded on bedrock. Supports 1 and 4 are very similar pile groups consisting of 10 piles. The pile group of support 3 consists of 26 piles. As in case 2, the stiffness of the foundations was approximated using the static stiffness of the piles alone, approximated as bars. As in case 2, the material damping was modelled using Rayleigh damping with $\alpha = 0.11$ and $\beta = 1.1 \cdot 10^{-4}$. In order to obtain the modal damping ratio of 0.7 % at very small amplitudes of vibration (see figure 5.5), an additional radiation/soil material damping was applied as viscous dashpots with the damping coefficient $c = 3$ MNs/m at the corresponding foundations. The density of the concrete was taken as 2500 kg/m^3 and adding the mass of the ballast, the equivalent density was 3600 kg/m^3. With these parameter values, the modulus of elasticity of the concrete was set to 42 GPa, yielding the natural frequency of the first vertical bending mode $f^{\text{case3}} \approx 5.8$ Hz. Again, apart from the mass of the ballast, the track superstructure was completely neglected.

5.4 Influence of bearings - all cases

The result of the analysis for case 1 have been reported in paper IV. Here, the main results from a preliminary analysis of the influence of the bearing mechanisms on the case 2 and 3 bridges will be summarised and compared to those of the case 1

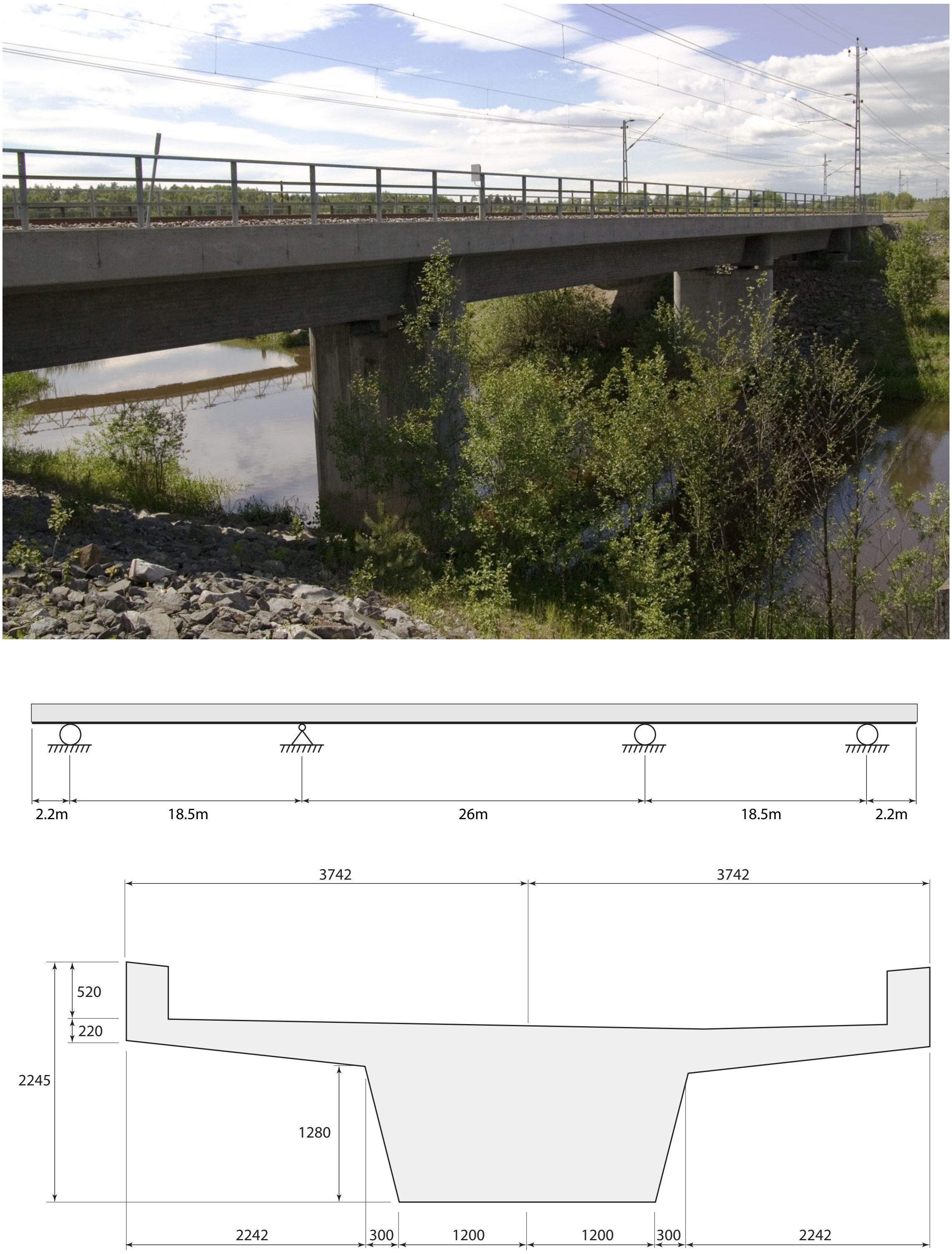

Figure 5.4: A photograph of the case 3 bridge (Sagån) and a sketch of its 2D geometry and cross-section. All measures are in millimeters unless otherwise stated.

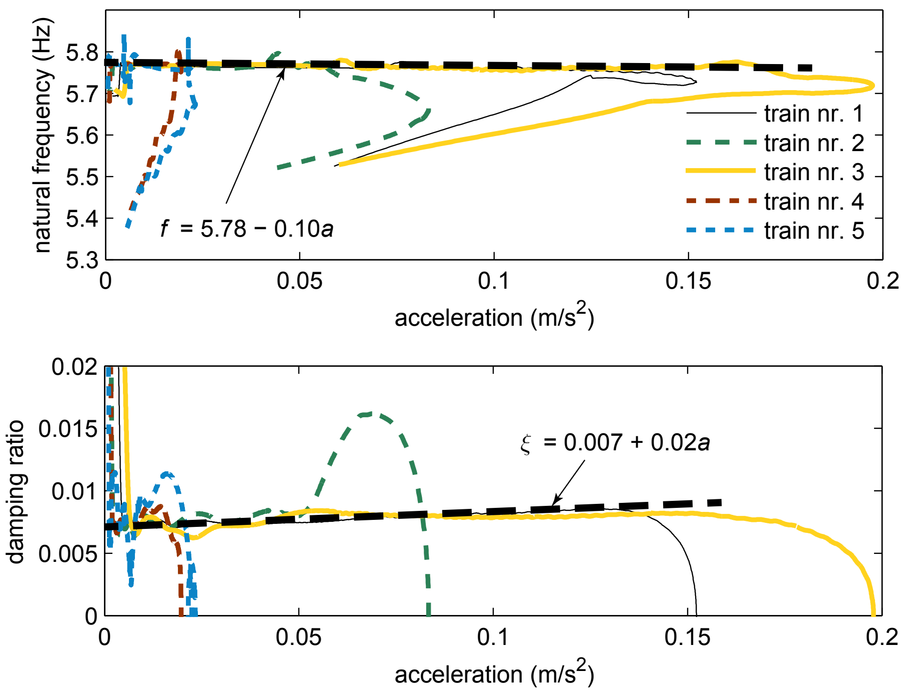

Figure 5.5: The frequency and damping ratio of the first vertical bending mode of the case 3 bridge, as given by the CWT.

bridge.

Due to the lack of experimental data for the backbone curves of the bearings, reasonable BW-model parameters were determined in the following way. The natural frequency of the fundamental mode of vibration was determined by fixing all stiffness parameters except the modulus of elasticity of the concrete. The modulus of elasticity of the concrete was then used to match the fundamental mode of vibration against the values determined from measurements at very small amplitudes of vibration. The material damping of the superstructures was fixed and the modal damping ratio at very small amplitudes of vibration was matched with the experimentally determined modal damping ratio by adjusting the dashpots at the foundations. These values seemed to be in agreement with the discussion provided in chapter 3. Then, BW-model parameters were determined so that the measured frequency and damping functions were reasonable well approximated in the range of accelerations $(0, 0.2)\,\mathrm{m/s^2}$. Obviously, this procedure is quite rough, but serves well as an illustration of what can be expected from the non-linear bearing mechanisms.

Figure 5.6 shows the frequency and damping functions of the "best" candidate models for each of the case studies, together with the measured frequency and damping functions for each of the bridges. Although these results are of a preliminary nature and the modelling of the bearings has not yet been verified, the results do provide some interesting indications. From the CWT analysis presented in the previous sections of this chapter, the observed non-linear effects were most pronounced in the case 1 bridge, slightly less pronounced in the case 2 bridge and only a weak

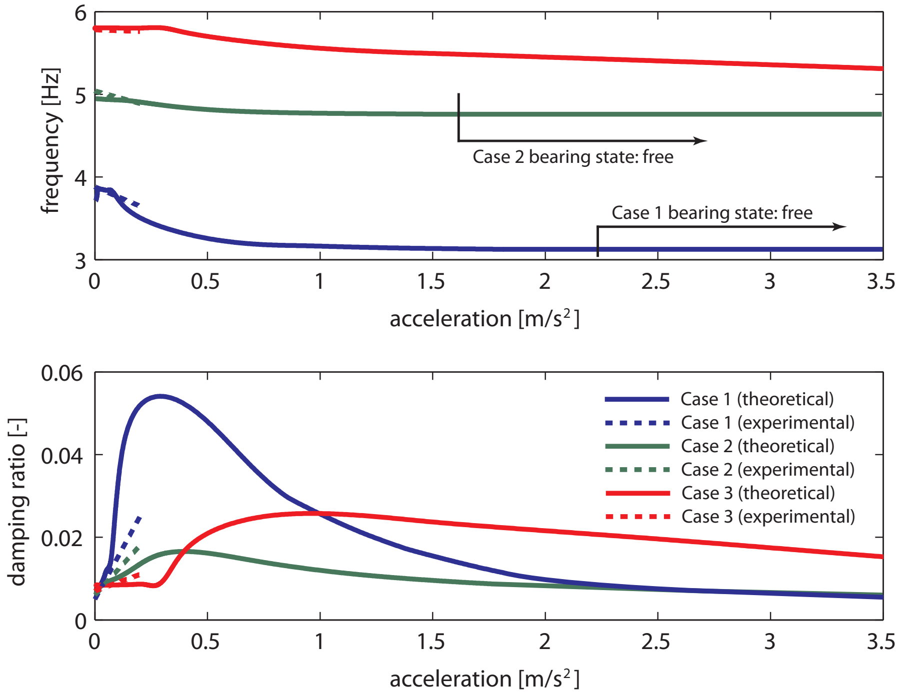

Figure 5.6: The "best" candidate models for each of the case studies.

indication in the case 3 bridge. The theoretical modelling allowed for some extrapolation to larger amplitudes of vibration and from these results, the following could be observed:

- For the case 1 bridge, the damping ratio increases very much but at $2\,\mathrm{m/s^2}$, it has already returned to the value at very small amplitudes of vibration.
- For the case 2 bridge, the damping ratio increases by a factor 2, but again at $2\,\mathrm{m/s^2}$, it has returned to the value at very small amplitudes of vibration.
- For the case 3 bridge however, the damping ratio does not increase at all until approximately $0.3\,\mathrm{m/s^2}$ but it maintains an elevated value all the way up to the Eurocode criteria for vertical bridge deck acceleration of $3.5\,\mathrm{m/s^2}$ for ballasted tracks.

5.5 Parameter variations - case 3

Given that the Euler-bernoulli hypothesis holds true for all three cases, the main differences between the three bridges, apart from the number of spans and the span lengths, lie in:

1. The height of the cross sections.

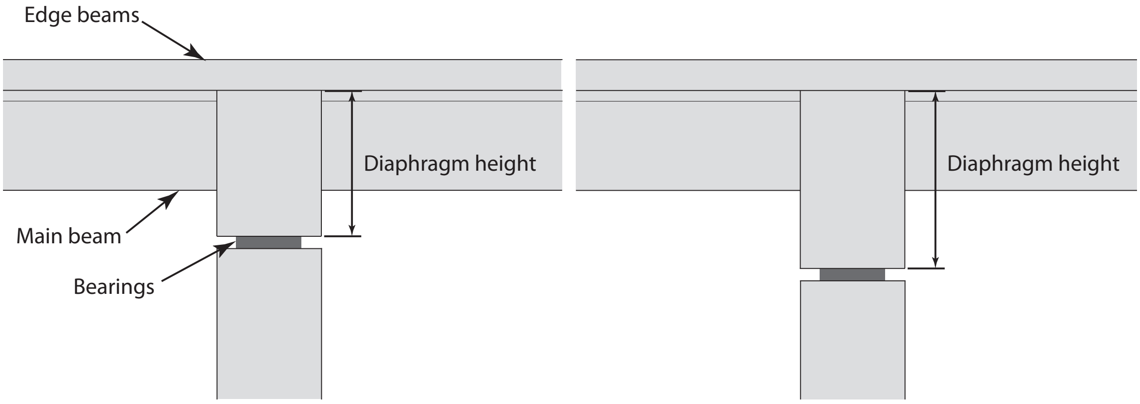

Figure 5.7: A sketch of the diaphragms at the supports of the case 3 bridge.

2. The longitudinal stiffness of the supports.
3. The boundary conditions at the ends of the superstructures.

These factors where varied in the case 3 model to evaluate their respective influence. The height of the cross section influences the longitudinal displacements over the bearings in a very simple way as long as it can be assumed that the cross sections remain undeformed. However, it is of course also coupled with the distribution of the bending stiffness along the superstructure and the division of the spans. Nevertheless, it is interesting to study how an increase in the cross section height over the supports influences the dissipation of energy in the bearings. In the case 3 bridge, a diaphragm wall is placed in the superstructure over each support (see figure 5.4). This could easily be changed as illustrated in figure 5.7, as long as the stiffness of the diaphragm is large enough to behave essentially as a rigid body.

The longitudinal stiffness of the supports carrying the roller/sliding bearings decreases from case 1 to case 3. The relation between the longitudinal stiffness of the supports and the pre-rolling/-sliding resistance of the bearings influence the dynamic properties by allowing for elastic deformations of the foundation instead of sliding or rolling. This occurs if the foundation stiffness is smaller than the initial stiffness of the bearings and has the effect that the transition zone between states 1 and 2 is spread over a larger range of amplitudes of vibration. This appears to partly explain the qualitative difference between the three cases.

The case 1 bridge is simply supported while the two other cases have integrated abutments. These restraints at the bridge ends are difficult to estimate, but they act so as to reduce the rotations over the end supports, which are typically equipped with movable bearings in multi-span bridges. They also provide translational constraints in the longitudinal direction. Thus, removing these constraints should lead to a larger response over the bearings and thereby, to more dissipation of energy in the bearings.

Based on the above listed reasons, a small study of the influence of these parameters on the free vibrations of the case 3 bridge was performed. The longitudinal stiffness

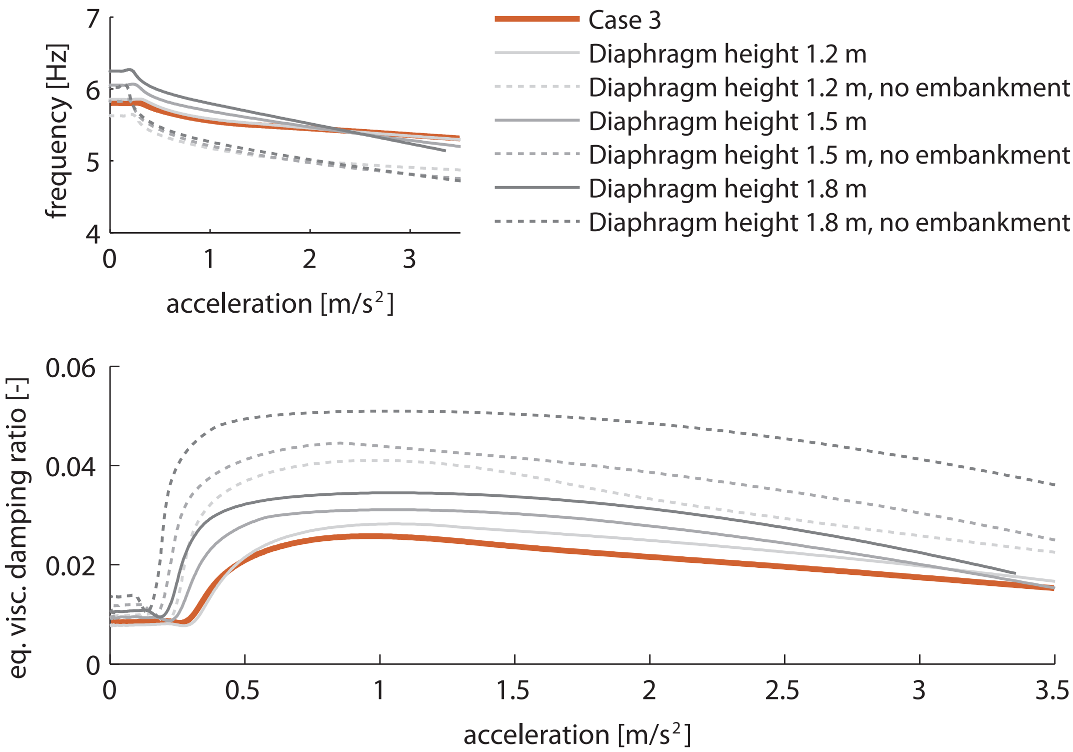

Figure 5.8: The result of the parametric study on the case 3 bridge.

of the pile groups at the end supports was increased by a factor 2 as compared with the case 3 best model candidate. This increased foundation stiffness was held constant in the study. The diaphragm height (from the neutral axis) was set at three different values: 1.2 m (the original design), 1.5 m and 1.8 m. For these three diaphragm heights, the calculations were performed with the assumed embankment stiffness and without the embankments, i.e. assuming that the bridge design could work also without integrated abutments. The results of this study are shown in figure 5.8.

Clearly, the increased foundation stiffness did not have any significant influence although it did increase the damping with approximately 10 % in the range of accelerations between 1 and 3 m/s^2. The increased diaphragm height led to a larger difference between the natural frequencies in the two states of the mode of vibration. Also, significant increases in the damping over essentially the whole range of amplitudes of vibration was obtained. Thus, the increased damping comes at the cost of a reduced critical train speed. The removal of the end restraints due to the integrated abutments increased the damping further and the natural frequency decreased faster with respect to the amplitude of vibration. Common for all the results of this study is that the elevated damping was kept over almost the entire range of amplitude of vibration.

Chapter 6

Discussion

The conclusions drawn from the research performed within this project are summarised in section 6.1. However, several extensions of the presented work are needed in order to draw more general conclusions. Apart from verifying the presented theoretical results using tests with controlled input forces, these extensions mainly consist in taking the influence of a passing train into consideration, but seasonal effects must also be further studied. Suggestions regarding the continued work within this field are briefly described in section 6.2.

However, a few words regarding the errors involved in the presented analyses need to be said. Three different techniques were used to determine the instantaneous natural frequency and damping ratio of the case 1 bridge and they all gave similar results. Thus, any error in this analysis would be systematic somehow. The sensors themselves could also introduce some errors, mainly due to noise, sensor misalignment and the calibration of the sensors. A formal error analysis of the numerical techniques used is beyond the scope of the thesis. Instead, the next best thing was done, i.e. to decrease the time step until convergence. Obviously, there are several possible sources of error in the modelling of the bearings and the longitudinal track resistance and these have been discussed in chapter 3. Nevertheless, it is the authors belief that those errors cannot be identified and remedied with the current state of knowledge. Also, the possible interaction between different mechanisms and the uncertainties associated with them, can only be handled in a robust manner by forced excitation tests at amplitudes of vibration which are relevant for a state of train-bridge resonance.

The model updating was performed "by hand" and much more could be done here, if proper OMA or EMA is performed. For example, the modulus of elasticity of the concrete differs quite much between the theoretical models of the case 2 (36.5 GPa) and case 3 (42.5 GPa) bridges, although both bridges were built using the same concrete quality (K40) with a characteristic modulus of elasticity of 32 GPa. This could be ascribed to variations in the density and the amount of ballast (due to ballast degradation and maintenance operations), but also to the rough estimates of the bending stiffness used in these preliminary calculations. Also, the stiffness of the pile groups and the embankments was modelled in a highly simplistic way.

However, given the state of knowledge regarding the properties of the bearings, further refinements of these models cannot be motivated at this stage. Nevertheless, the results do motivate further studies of the bearing mechanisms.

6.1 Conclusions

The analysis of measured free vibration data from three different beam bridges led to the following conclusions:

- The modes of vibration of the studied bridges are non-linear.
- The natural frequency appears to decrease with increasing amplitude of vibration. This could lead to a significant decrease in the critical train speed.
- Several techniques exist by which these non-linear modes can be estimated. Three different techniques have been implemented and used to determine the instantaneous quantities, i.e. the natural frequency and the damping ratio, associated with the fundamental mode of vibration and all three yield similar results within the available range of measured response.
- The wavelet based technique was much more efficient than the short-time Fourier technique. This efficiency was obtained at the cost of a reduced range of amplitudes due to the so called ”end effects” inherent in the wavelet transform.
- The most efficient technique was based on the Hilbert transform which is also distorted by end effects, although to a slightly smaller extent than the wavelet transform.
- The equivalent instantaneous viscous damping ratio defined in paper I was found to overestimate the damping ratio by as much as 20-25 %.

Modelling details were discussed mainly in papers III and IV and several conclusions were drawn from those studies:

- Soil-structure interaction is relevant and the variation of the state of stress and strain in the soil during a train passage appears to remain within the elastic regime. The flexibility of the foundations was needed to obtain correct natural frequencies for the first vertical bending and the first torsional modes of vibrations. The radiation and soil material damping constitute a considerable part of the structural damping at small amplitudes of vibration.
- Bridge bearings can have a significant influence on the dynamic properties of a non-linear mode of vibration. The initiation of rolling or sliding generates a non-linear mode of vibration which has two states; the fixed state at very small amplitudes of vibration and the free state at larger amplitudes of vibration. During the transition from the fixed state to the free state, the

natural frequency decreases monotonically towards an asymptotic value while the damping ratio behaves like a uni-modal function.

- The longitudinal track resistance was found to have a negligible influence on the structural stiffness and a significant although much smaller influence than the bearings on the damping ratio of the case 1 bridge during the warm period of the year.

- Seasonal effects have a significant effect on the dynamic properties of railway bridges in cold climates such as that in Sweden. Reluctance to taking seasonal effects in consideration may lead to erroneous decisions in assessments of existing bridges. The variation in frequency between different seasons depends on the type of mode and can be as large as 35 %.

The preliminary studies presented in chapter 5 indicate that it could be possible to design bridges with movable bearings so as to maximise the dissipation of energy at the movable bearings over a certain range of amplitudes of vibration. Naturally, the parameters which govern this behaviour are those which govern the movements over the bearings, i.e. the eccentricity between the neutral axis of the beam and the support points, the longitudinal stiffness of the supports and the beam end restraints provided by the track continuity and integrated abutments. Furthermore, the bridge (case 3) which showed the least non-linear tendency in the CWT analysis, provided the most beneficial non-linear behaviour, since its damping ratio was maintained at a high level all the way up to $3.5\,\mathrm{m/s^2}$ (the maximum allowed acceleration for ballasted bridges, according to the Eurocode). However, to verify these assertions, further studies are needed, as described in the following section.

6.2 Further research

In the authors opinion, the continued research within this field should focus on an extension of the presented analysis towards states of train-bridge resonance and a generalisation to a wider range of bridges. In order to take this leap, further research is needed along several different directions:

1. The proposed hypothesis regarding the influence of the bearings must be verified on existing bridges using forced excitation tests. However, the mechanism itself could probably be verified in scaled laboratory tests.

2. Laboratory tests on bearings should be used to determine appropriate Bouc-Wen models or extensions of such models for the hysteretic properties of rolling and sliding bearings.

3. An extension of the Bouc-Wen element to incorporate coupling of its degrees of freedom. This could be used to model the pressure dependence of the rolling resistance and the friction coefficient of the PTFE-steel interface, as well as the influence of the confining pressure of the ballast on the track longitudinal stiffness.

4. Improvements of the computational efficiency of the BW-element should be sought so that they can be incorporated in more detailed parametric studies and three dimensional models.

5. An increased wear is expected, especially in pot bearings, if bridges are designed to optimise the dissipation of energy in bearing movements. This must be carefully studied in order to estimate the costs involved with shorter maintenance intervals and to identify possible countermeasures.

Furthermore, a more detailed study of the formation of ice within the ballast and its evolution during the cold season needs to be further studied. Research within this project has shown that the damping ratio varies more during the cold season and it appears to be higher during the cold season than during the warm season.

An appropriate test methodology for railway bridges in general should be able to study arbitrary modes of vibration within a given range of frequencies and amplitudes of vibration. However, testing structures along operating railway lines is rather expensive, even when studying the modes of vibration at very small amplitudes of vibration. nevertheless, in order to verify the results presented within this project, at least a few bridges must be tested with known input forces at relevant amplitudes of vibration.

In practical cases where several bridges along a railway line need to be tested and operational modal analysis (OMA) can be applied successfully, a combination of OMA and free vibrations could be very efficient. OMA could then be used to determine the dynamic properties at very small amplitudes of vibration and guidance regarding the non-linear behaviour could be obtained from the Hilbert or continuous wavelet transforms of free vibration signals.

References

[1] *ERRI D 202/DT 360, Improved knowledge of forces in CWR track (including switches). Lateral resistance tests.* European Rail Research Institute, 1997.

[2] *ERRI D 202/DT 362, Improved knowledge of forces in CWR track (including switches). Ballast resistance under three-dimensional loading.* European Rail Research Institute, 1997.

[3] *ERRI D 202/DT 363, Improved knowledge of forces in CWR track (including switches). Measurements of of lateral resistance and change of neutral rail temperature (NRT) for ballasted track. Volume 2 – Determination of lateral and longitudinal ballast resistance of a railway track by experimental tests.* European Rail Research Institute, 1997.

[4] *ERRI D 202/DT 361, Improved knowledge of forces in CWR track (including switches). Measurement of lateral resistance characterisitcs for ballasted track.* European Rail Research Institute, 1998.

[5] *ERRI D 214 RP3, Rail Bridges for Speeds >200 km/h - Recomendations for calculating damping in rail bridge decks.* European Rail Research Institute, 2000.

[6] B. Armstrong-Hélouvry. *Control of machines with friction.* Kluwer Academic Publishers, 1991.

[7] F. Badrakhan. Separation and determination of combined dampings form free vibrations. *Journal of Sound and Vibration*, 100(2):243–255, 1984.

[8] C. W. Bert. Material damping: An introductory review of mathematical measures and experimental techniques. *Journal of Sound and Vibration*, 29(2):129–153, 1973.

[9] R. Bouc. Modèle mathématique d'hystérésis. *Acustica*, 24:16–25, 1971.

[10] A. G. Bowland. *Comparison and Analysis of the Strength, Stiffness, and Damping Characteristics of Concrete with Rubber, Latex, and Carbonate Additives.* Ph.D. Thesis, Virginia Polytechnic Institute and State University, 2011.

[11] CEN. *Eurocode 1: Actions on structures - Part 2: Traffic loads on bridges.* CEN, European Comittee for Standardization, 2008.

[12] K. C. Chang, J. S. Hwang, and G. C. Lee. Analytical model for sliding behavior of teflon–stainless steel interfaces. *Journal of Engineering Mechanics*, 116(12):2749–2763, 1990.

[13] A. E. Charalampakis and V. K. Koumousis. Identification of bouc-wen hysteretic systems by a hybrid evolutionary algorithm. *Journal of Sound and Vibration*, 314:571–585, 2008.

[14] A. E. Charalampakis and V. K. Koumousis. On the response and dissipated energy of bouc-wen hysteretic model. *Journal of Sound and Vibration*, 309:887–895, 2008.

[15] A. E. Charalampakis and V. K. Koumousis. A bouc-wen model compatible with plasticity postulates. *Journal of Sound and Vibration*, 322:954–968, 2009.

[16] A. E. Charalampakis and V. K. Koumousis. Identification of bouc-wen hysteretic systems using paritcle swarm optimization. *Computers and Structures*, 88:1197–1205, 2010.

[17] M. Constantinou, A. Mokha, and A. Reinhorn. Teflon beraings in base isolation. ii: Modeling. *Journal of Structural Engineering*, 116(2):455–474, 1990.

[18] L. Cremer, M. Heckl, and B.A.T. Petersson. *Structure-Borne Sound – Structural Vibrations and Sound Radiation at Audio Frequencies*. Springer, third edition, 2005.

[19] Dassault Systémes. *Abaqus Analysis 6.11 User's Manual*. 2011.

[20] M. Dolce, D. Cardone, and F. Croatto. Frictional behavior of steel-ptfe interfaces for seismic isolation. *Bulletin of Earthquake Engineering*, 3:75–99, 2005.

[21] S. Erlicher and N. Point. Thermodynamic admissibility of bouc-wen type hysteresis models. *Comptes Rendus Mecanique*, 322:51–57, 2004.

[22] H. Fang, editor. *Foundation Engineering Handbook*. Van Nostrand Reinhold, New York, second edition, 1991.

[23] P. Flandrin. *Time-Frequency/Time-Scale Analysis*. Academic Press, 1999.

[24] M. Friswell and J. E. Mottershead. *Finite Element Model Updating in Structural Dynamics*. Kluwer Academic Publishers, 1995.

[25] B. O. Hardin and V. P. Drnevich. Shear modulus and damping in soils: Design equations and curves. *Journal of the Soil Mechanics and Foundations Division, ASCE*, 98, SM7, 1972.

[26] B. O. Hardin and V. P. Drnevich. Shear modulus and damping in soils: Measurement and parameter effects. *Journal of the Soil Mechanics and Foundations Division, ASCE*, 98, SM6, 1972.

[27] C. M. Harris and A. G. Piersol, editors. *Harris' Shock and Vibration Handbook*. McGraw-Hill, fifth edition, 2002.

[28] N.E. Huang, Z. Shen, S.R. Long, M.C. Wu, H.H. Shih, Q. Zheng, C.C. Tung N-C. Yen, and H.H. Liu. The empirical mode decomposition and the hilbert spectrum for nonlinear and non-stationary time series analysis. *Proceedings of the Royal Society A*, 454:903–995, 1998.

[29] J. S. Hwang, K. C. Chang, and G. C. Lee. Quasi-static and dynamic sliding characteristics of teflon–stainless steel interfaces. *Journal of Structural Engineering*, 116(10):2747–2762, 1990.

[30] F. Ikhouane and J. Rodellar, editors. *Systems with Hysteresis - Analysis, Identification and Control using the Bouc-Wen Model.* Wiley, 2007.

[31] B. Indraratna and W. Salim. *Mechanics of Ballasted Rail Tracks.* Taylor & Francis, London, 2005.

[32] K. Ishihara. *Soil behaviour in earthquake geotechnics.* Oxford University Press, London, 1996.

[33] J. W. Liang and B. F. Feeny. Identifying coulomb and viscous friction from free vibration decrements. *Non-linear Dynamics*, 16:337–347, 1998.

[34] H.-K. Long and C.-S. Liu. Coulomb friction oscillator: Modelling and responses to harmonic loads and base excitations. *Journal of Sound and Vibration*, 229(5):1171–1192, 2000.

[35] L. Lorieux. *Analysis of train-induced vibrations on a single-span composite bridge.* Master thesis 263, Royal Institute of Technology, Stockholm, Sweden, (Available online: http://www.byv.kth.se/), 2008.

[36] S. Mallat. *A Wavelet Tour of Signal Processing - The Sparse Way.* Academic Press, 3:rd edition, 2008.

[37] H. K. Milne. The impulse response function of a single degree of freedom system with hysteretic damping. *Journal of Sound and Vibration*, 100(4), 1985.

[38] A. Mokha, M. Constantinou, and A. Reinhorn. Teflon bearings in base isolation. i: Testing. *Journal of Structural Engineering*, 116(2):438–454, 1990.

[39] M.Ülker-Kaustell, R. Karoumi, and C. Pacoste. Simplified analysis of the dynamic soil-structure interaction of a portal frame railway bridge. *Engineering Structures*, 32:3692–3698, 2010.

[40] L. A. Padrón, J. J. Aznárez, O. Maeso, and M. Saitoh. Impedance functions of end-bearing inclined piles. *Soil Dynamics and Earthquake Engineering*, 38:97–108, 2012.

[41] B. Prange. Resonant column testing of railway ballast. *Proceedings of the Tenth International Conference on Soil Mechanics and Foundation Engineering*, 3:273–278, 1981.

[42] C. Rebelo, L. Simões da Silva, and M. Pircher. Dynamic behaviour of twin single-span ballasted railway viaducts - field measurements and modal identification. *Engineering Structures*, 30(9):2460–2469, 2008.

[43] E. Serra and M. Bonaldi. A finte element formulation for thermoelastic damping analysis. *International Journal for Numerical Methods in Engineering*, 2008.

[44] A. S. J. Suiker. *The mechanical behavior of ballasted railway tracks*. Delft University Press, 2002.

[45] S. Talatahari, A. Kaveh, and N. Mohajer Rahbari. Parameter identification of bouc-wen model for mr fluid dampers using adaptive charged system optimization. *Journal of Mechanical Science and Technology*, 26(8):2523–2534, 2012.

[46] G. R. Tomlinson and J. H. Hibbert. Identification of the dynamic characteristics of a structure with coulomb friction. *Journal of Sound and Vibration*, 64(2):233–242, 1979.

[47] M. Ülker-Kaustell. Some aspects of the dynamic soil-structure interaction of a portal frame railway bridge. *TRITA-BKN. Licentiate thesis*, 102, 2009.

[48] K. C. Valanis. A theory of viscoplasticity without a yield surface. part i – general theory. *Archives of Mechanics*, 23:517–533, 1971.

[49] A. Visintin. *Differential models of hysteresis*. Springer, 1994.

[50] A. Vretblad. *Fourier analysis and its applications*. Springer, 2003.

Paper I

Application of the continuous wavelet transform on the free vibrations of a steel-concrete composite railway bridge

Engineering Structures, 33:911–919, 2011.

Engineering Structures 33 (2011) 911–919

Contents lists available at ScienceDirect

Engineering Structures

journal homepage: www.elsevier.com/locate/engstruct

Application of the continuous wavelet transform on the free vibrations of a steel–concrete composite railway bridge

Mahir Ülker-Kaustell *, Raid Karoumi

The Royal Institute of Technology, KTH, Brinellvägen 34, SE-100 44 Stockholm, Sweden

ARTICLE INFO

Article history:
Received 10 July 2010
Received in revised form
12 November 2010
Accepted 1 December 2010
Available online 15 January 2011

Keywords:
Railway bridges
Steel–concrete composite bridge
Train induced vibrations
Continuous wavelet transform
System identification

ABSTRACT

In this article, the Continuous Wavelet Transform (CWT) is used to study the amplitude dependency of the natural frequency and the equivalent viscous modal damping ratio of the first vertical bending mode of a ballasted, single span, concrete–steel composite railway bridge. It is shown that for the observed range of acceleration amplitudes, a linear relation exists between both the natural frequency and the equivalent viscous modal damping ratio and the amplitude of vibration. This result was obtained by an analysis based on the CWT of the free vibrations after the passage of a number of freight trains. The natural frequency was found to decrease with increasing amplitude of vibration and the corresponding damping ratio increased with increasing amplitude of vibration. This may, given that further research efforts have been made, have implications on the choice of damping ratios for theoretical studies aiming at upgrading existing bridges and in the design of new bridges for high speed trains. The analysis procedure is validated by means of an alternative analysis technique using the least squares method to fit a linear oscillator to consecutive, windowed parts of the studied signals. In this particular case, the two analysis procedures produce essentially the same result.

1. Background

The dynamic properties of railway bridges are known to depend on a rather large number of phenomena. These consist of soil–structure interaction, train–bridge interaction, interaction between the track and the bridge superstructure and the material properties of the structure. For certain bridge types, some of these phenomena give rise to more or less pronounced non-linearities, which may have noticeable effects on the dynamic properties of the structure [1].

Today, many railway owners wish to upgrade existing bridges to meet the increasing demand on train speed and axle loads. In this context, the damping ratio is highly important and can have a large influence on theoretical estimates of the dynamic response of the structure. Also, in the design of new railway bridges for high-speed railway lines according to the Eurocode [2], the vertical bridge deck acceleration is often decisive for the dynamic analysis. The vertical bridge deck acceleration must be limited in order to ensure that the wheel-rail contact is maintained and to eliminate the risk for ballast instability in the case of ballasted railway bridges. For these reasons, it would be desirable to learn more about the phenomena governing the dissipation of energy in railway bridges.

One approach to increasing our knowledge within this field would be to establish a reliable experimental methodology to determine how the damping ratio varies with the amplitude of vibration and then use that knowledge as a basis for theoretical studies of the phenomena which are believed to govern this behavior. For this purpose, alternative methods should be used to verify the outcome of the experimental procedures. This paper aims at describing the application of such an alternative, namely the *Continuous Wavelet Transform* (CWT). This mathematical tool has traditionally been applied in quantum mechanics and signal analysis [3,4], but during later years, several authors have presented applications in system identification and to some extent also damage detection (see [5] and the references therein), though most publications describe theoretical and/or laboratory studies. Staszewski [6] used the CWT to estimate the damping of simulated linear and non-linear multi degree of freedom systems with additive noise, based on the assumption that the system is viscously damped. Slavič et al. [7] succeeded in applying the CWT to experimental data produced in a laboratory, for a linearly elastic, viscously damped beam. Le and Argoul [8] described procedures to identify the eigenfrequencies, damping ratios and mode shapes of linear structural systems from free vibration data by means of the CWT. An extension towards applications of the CWT to identify non-linear systems was suggested by Staszewski [9] where the CWT was used to estimate the skeleton (the variation of the amplitude with time) of different signals. These concepts were further elaborated by Ta and Lardies [10], who applied their methodology to simulated numerical data and

* Corresponding author. Tel.: +46 8 7907949.
E-mail address: mahir.ulker@byv.kth.se (M. Ülker-Kaustell).

0141-0296/$ – see front matter © 2010 Elsevier Ltd. All rights reserved.
doi:10.1016/j.engstruct.2010.12.012

experimental data produced in their laboratory. Ta and Lardies also suggested a modification to the use of the Morlet wavelet in CWT's which optimizes the localization of the (Morlet) wavelet in the time/frequency domain for the signal at hand. Given a skeleton, a non-linear model was fitted to the measured response. Of course, in order to succeed in applying the methodology suggested by [10] to a given real-life mechanical system such as a railway bridge and draw any useful conclusions from those results, the nature of the underlying model must be known. In the present case, the underlying model is not known, but as indicated by the results presented in [10], the CWT may become a useful tool in determining such models for railway bridges. A recent publication by Chang and Shi [11] describes the application of wavelet transform techniques to identify the parameters and their time-dependencies in a Bouc–Wen model used to describe the hysteretic behavior of shear-buildings subjected to ground accelerations.

It should also be mentioned that several other methods which aim at identifying non-linear systems from measured data exist, see for example [12] where a method based on the Hilbert transform is applied to simulated non-linear single-degree-of freedom systems, and also [13] and the references therein.

This article presents some results of applications of the CWT to free vibration data measured from a ballasted, single-span steel–concrete composite bridge, with the main purpose of determining whether weak non-linearities are present or not. Suggestions based on the work by Staszewski [6] are given as to how an instantaneous equivalent viscous damping ratio can be estimated from the skeleton curve of the CWT, assuming that the signal can be modeled as a viscously damped linear oscillator at each time instant.

2. The continuous wavelet transform

The CWT is well described in textbooks such as [4] and the following is a short summary of the most important concepts needed in the proposed analysis of railway bridge dynamics based on the CWT. The CWT is an integral transform and is thus defined as the inner product

$$\langle u, K\rangle = \int_{-\infty}^{\infty} u(t)K(t, a, b)\mathrm{d}t \tag{1}$$

of the signal $u(t)$ with a kernel function $K(t, a, b)$ which is a scaled and shifted version of the complex conjugate of the wavelet $\psi(t)$. The wavelet can be chosen arbitrarily from the space of square integrable functions, given that it has a zero average

$$\int_{-\infty}^{\infty} \psi(t)\mathrm{d}t = 0 \tag{2}$$

and fulfills the following condition of admissibility

$$\int_{0}^{\infty} \frac{|\hat{\psi}(\omega)|^2}{\omega}\mathrm{d}\omega < \infty. \tag{3}$$

Throughout this text, $(\hat{\bullet})$ will be used to denote the Fourier transform. Furthermore, the wavelet is normalized $\|\psi\| = 1$ and centered around $t = 0$.

By scaling the wavelet by a and shifting it by b, a set of functions is obtained, which are compared to the signal by means of the inner product (1) giving a measure of the resemblance between the signal and the scaled and shifted wavelet. To preserve the normalization of the wavelet at each scale, the wavelet is divided by $\sqrt{a}$. The CWT is then defined by an integral of the form

$$T_\psi[u](a, b) = \frac{1}{\sqrt{a}}\int_{-\infty}^{\infty} u(t)\psi^*\left(\frac{b-t}{a}\right)\mathrm{d}t \tag{4}$$

where * denotes complex conjugation.

The duration Δt_u and bandwidth $\Delta\omega_u$ (or time and frequency support [3]) of any finite energy function u can be determined in terms of quantities which are equivalent to the standard deviation

$$\Delta t_u^2 = \frac{1}{E_u}\int_{-\infty}^{\infty} (t - t_u)^2 |u(t)|^2\mathrm{d}t \tag{5}$$

$$\Delta\omega_u^2 = \frac{1}{E_u}\int_{-\infty}^{\infty} (\omega - \omega_u)^2 |\hat{u}(\omega)|^2\mathrm{d}\omega \tag{6}$$

where the energy E_u of the signal is

$$E_u = \int_{-\infty}^{\infty} |u(t)|^2\mathrm{d}t < \infty \tag{7}$$

t_u and ω_u are the first moments of the squared absolute value of the function $u(t)$ and its Fourier transform $\hat{u}(\omega)$

$$t_u = \frac{1}{E_u}\int_{-\infty}^{\infty} t|u(t)|^2\mathrm{d}t \tag{8}$$

$$\omega_u = \frac{1}{E_u}\int_{-\infty}^{\infty} \omega|\hat{u}(\omega)|^2\mathrm{d}\omega. \tag{9}$$

It can be shown [3,4] that the duration and bandwidth of any finite energy function satisfies the inequality

$$\Delta t_u \Delta\omega_u \geq \frac{1}{2} \tag{10}$$

which is referred to as the Heisenberg–Gabor uncertainty principle. In the present context, this principle shows how an increase in the localization of a wavelet in time is connected to a decrease in the localization in frequency and vice versa.

The time (Δt) and frequency $(\Delta\omega)$ locality, or resolution, of the CWT depend on the scale and the duration Δt_ψ and bandwidth $\Delta\omega_\psi$ of the wavelet according to

$$\Delta t = a\Delta t_\psi \tag{11}$$

$$\Delta\omega = \frac{\Delta\omega_\psi}{a}. \tag{12}$$

Apparently, these quantities also obey the Heisenberg–Gabor uncertainty principle.

2.1. Scale and pseudo-frequency

The scale is inversely proportional to the frequency but it is not directly related to the frequency. A small scale contracts the wavelet so that it matches higher frequencies better and vice versa. One way to define a relation between frequency and scale is suggested in the Matlab Wavelet Toolbox manual [14] where a periodic signal of frequency f_c is associated to the wavelet. f_c is called the center frequency and it is given by the maximizer of $|\hat{\psi}|$. Then, a pseudo-frequency f corresponding to the scale a can be defined by

$$f = \frac{f_c}{a\Delta t} \tag{13}$$

where Δt is the sampling period of the analyzed signal.

2.2. Choice of wavelet

Le and Argoul [8] gave a thorough description of several common wavelet functions and discussed the choice between them for analyzing transient (free vibration) signals. The most common wavelet in the present context is the Morlet Wavelet, defined by

$$\psi(t) = \mathrm{e}^{-t^2/2}\mathrm{e}^{\mathrm{i}\omega_0 t} \tag{14}$$

and it has also been used in the present study, however with a slight adjustment. In [10] the notion of a modified Morlet wavelet was given with reference to the factor 2 in the denominator of the

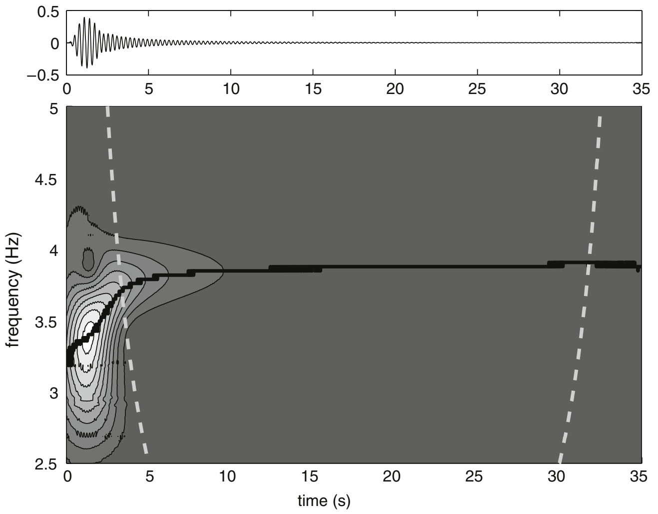

Fig. 1. The CWT of the first bending mode of the bridge at Skidträsk (see Section 3) together with its ridge (black solid line) and the boundaries (grey, dashed lines) within which the edge effect is negligible.

first factor of Eq. (14), whereas in the Matlab Wavelet Toolbox, the (complex) Morlet wavelet is directly defined with this parameter. This factor may be varied so that the variation of the amplitude of the Morlet wavelet is stretched or contracted. The center frequency ω_0 of the Morlet wavelet is approximately bounded from below by $\omega_0 \geq 5$ in order to fulfill the condition (3).

2.3. The edge effect

Due to the finite duration of the analyzed signal, there is a mismatch between the wavelet function and the signal at the beginning and end of the signal. This is referred to as the edge effect and there is no known procedure by which it can be removed. However, one can determine a domain D for a and b on which the edge effect is negligible [7,8]. In [8], the following bounds on the circular frequency were determined

$$\frac{2c_t Q\mu_\psi}{\omega_j} \leq b_j \leq L - \frac{2c_t Q\mu_\psi}{\omega_j} \tag{15}$$

$$0 < \omega_j \leq \frac{2\pi f_{\mathrm{Nyquist}}}{1 + \frac{c_f}{2Q}} \tag{16}$$

where $c_t \geq 1$ and $c_f \geq 1$ are parameters chosen so that when t and ω are outside the intervals

$$I_{c_t} = [t_\psi - c_t \Delta t_\psi, t_\psi + c_t \Delta t_\psi] \tag{17}$$

and

$$I_{c_f} = [\omega_\psi - c_f \Delta\omega_\psi, \omega_\psi + c_f \Delta\omega_\psi] \tag{18}$$

respectively, the wavelet and its Fourier transform have very small values. In [8] a good compromise was found in $c_t = c_f = 5$, which have also been used here. These bounds are shown in Fig. 1 using red dashed lines. Several methods to reduce the edge effect in short signals are described in [15], in the present context however, the above described bounds were found to be sufficient.

2.4. Asymptotic analysis

For a certain group of wavelets, referred to as analytic (or progressive) wavelets, the analysis can be much simplified if the signal is asymptotic. An analytic function f_a is characterized by having a Fourier transform which is zero for all negative frequencies

$$\hat{f}_a(\omega) = 0, \quad \forall\omega < 0. \tag{19}$$

A general monochromatic signal can be described in terms of an instantaneous amplitude $A(t)$ and phase $\phi(t)$ by functions of the form [16]

$$u(t) = A(t)\cos(\phi(t)). \tag{20}$$

Then, the instantaneous circular frequency can be defined as the time derivative of the phase

$$\omega(t) = \dot{\phi}(t). \tag{21}$$

If the amplitude $A(t)$ varies slowly compared to the phase $\phi(t)$, i.e. if the following conditions are met

$$\left|\dot{\phi}(t)\right| \gg \left|\frac{\dot{A}(t)}{A(t)}\right| \tag{22}$$

the signal is asymptotic. If the signal is asymptotic and the wavelet is analytic, the CWT can be approximated by [16]

$$\tilde{T}_\psi[u](a,b) \approx \frac{\sqrt{a}}{2} A(b) \mathrm{e}^{\mathrm{i}\phi(b)} \hat{\psi}^*(a\dot{\phi}(b)). \tag{23}$$

2.5. The ridge and skeleton of the CWT

Assuming that the signal consists of only one component, the maximum modulus of its CWT will be restricted to a curve in the

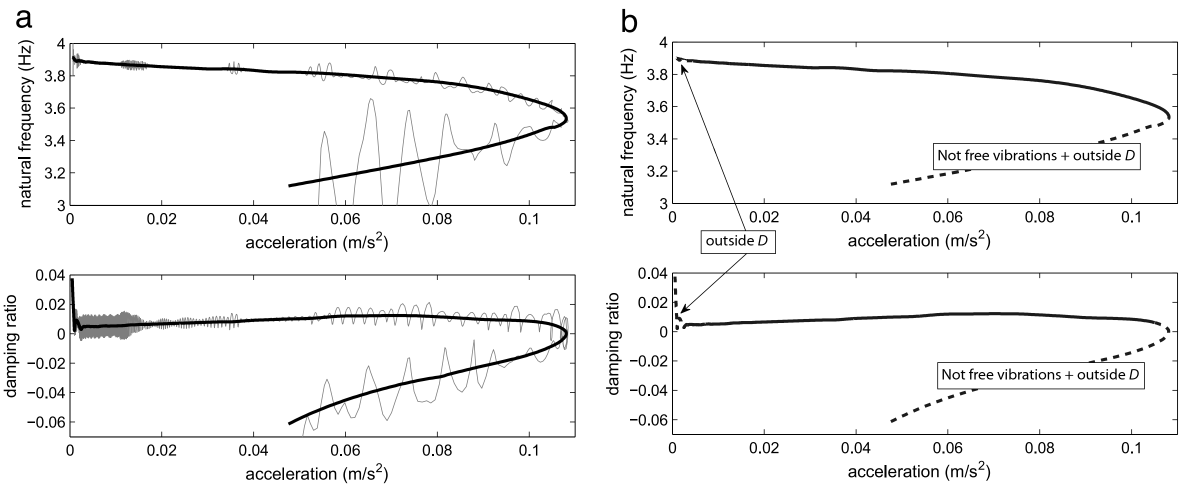

Fig. 2. The estimated natural frequency and the corresponding equivalent viscous damping ratio of the first bending mode of the bridge (see Section 3). (a) Without smoothing the amplitude and phase from the skeleton (grey), with smoothing (black). (b) The dashed parts of the lines illustrate the regions of the CWT-estimates which are affected by the edge effects and the part during which the train is still on the bridge.

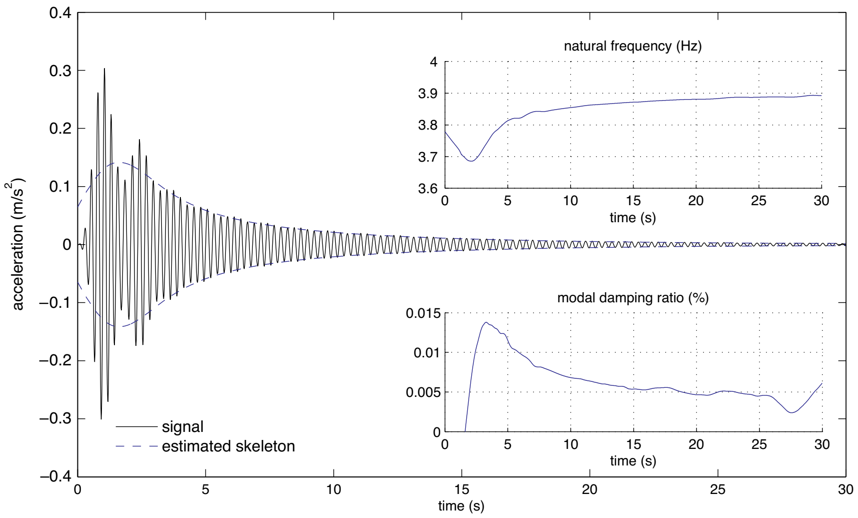

Fig. 3. The estimated natural frequency and equivalent modal damping ratio of the first bending mode of the bridge at Skidträsk (see Section 3).

time–frequency plane. This curve is referred to as the ridge $a_r(b)$ of the CWT and the modulus of the CWT, evaluated at these points $T_\psi[u](a_r(b), b)$ is referred to as the skeleton of the CWT (see Fig. 1). Given that an analytic wavelet is used, the amplitude $A(b)$ (i.e. the skeleton) of an asymptotic signal, can be determined from the modulus of the ridge of the CWT (Eq. (23))

$$A(b) = 2\frac{|T_\psi[u](a_r(b), b)|}{\sqrt{a}|\hat{\psi}^*(a\dot{\phi}(b))|} \tag{24}$$

and the phase $\phi(b)$ from its argument

$$\phi(b) = \arg(T_\psi[u](a_r(b), b)). \tag{25}$$

In the presence of considerable noise, the extraction of the ridge and skeleton of the CWT must be performed using rather complicated methods, see for example [17]. In the present context however, the Signal to Noise Ratio (SNR) is high and much simpler approaches may be used. The ridges were estimated simply by maximizing the modulus of the CWT along the frequency direction, at each discrete point in time. The skeletons obtained from these ridges were in many cases found to be very distorted and smoothing algorithms such as moving average filters and spline interpolation were used to decrease the distortion of the skeleton curves. Since the derivatives of the modulus and phase of the CWT along the ridge are needed, even very small fluctuations of these quantities may lead to very large distortions of their derivatives. Even though the fluctuations in the estimated functions ($A(b)$ and $\phi(b)$) are often not visible in the natural scale and the smoothed curves cannot easily be discerned from the un-smoothed curves, they lead to highly distorted derivatives as shown in Fig. 2(a) which shows a comparison between the estimated instantaneous dynamic properties of the bridge at Skidträsk (see Section 3) with and without smoothing. Fig. 2(b) illustrates the parts of the amplitude dependent relations of the natural frequency and the equivalent viscous damping ratio which are affected by the edge effects of the CWT and the presence of the train in the signal.

2.6. Estimating the instantaneous equivalent viscous damping ratio

The nature of damping is complicated and not fully understood. Therefore, the viscous damping model, which for many weakly damped systems is a rather good approximation, is most widely used. Due to the large model uncertainty inherent in using the viscous damping model and the great importance of the choice of the viscous damping ratio on the dynamic response in theoretical simulations, great care must be taken in estimating an equivalent viscous damping ratio from experimental data. Lower bounds are generally used and in the present context, an estimate at the lower amplitudes of vibration would be chosen to characterize the damping of the structure. In what follows, these rules will be set aside, though not forgotten, in order to enable an estimate of the variation in the damping ratio with the amplitude of vibration.

Assuming that the dissipation of energy at each time instant can be reasonably well modeled by viscous damping, an instantaneous equivalent viscous damping ratio can be determined from the skeleton of the CWT as follows. The free vibrations of the viscously damped linear oscillator are given by

$$u(t) = Ce^{-\xi\omega_n t}e^{i\omega_D t} = A_v(t)e^{i\omega_D t} \tag{26}$$

(where C is a constant, ξ is the damping ratio, ω_n is the undamped natural frequency and $\omega_D = \sqrt{1-\xi^2}\omega_n$ is the damped eigenfrequency) from which the amplitude of the viscously damped oscillator can be determined as

$$A_v(t) = Ce^{-\xi\omega_n t}. \tag{27}$$

Differentiating Eq. (27) we have

$$\dot{A}_v(t) = -\xi\omega_n Ce^{-\xi\omega_n t} = -\xi\omega_n A_v(t) \tag{28}$$

which gives an expression for the viscous damping ratio

$$\xi = -\frac{\dot{A}_v(t)}{\omega_n A_v(t)}. \tag{29}$$

This is a constant in the case of a linear system and independent on which kinematic variable (displacement, speed or acceleration) is used. However, if we replace $A_v(t)$ with the skeleton of the CWT A and ω_n with the instantaneous natural frequency $\dot{\phi}$ we have

$$\tilde{\xi} = -\frac{\dot{A}}{\dot{\phi}A} \tag{30}$$

as an estimate of the instantaneous equivalent viscous damping ratio. It should be mentioned that the same result was obtained by following the suggestions of Staszewski [6]. However, in [6] the damping of the studied theoretical systems was taken as a constant.

An example of the outcome of the above proposed estimate of the equivalent damping ratio is shown in Fig. 2(b).

2.7. Summary of methodology

Fig. 3 summarizes the proposed methodology in that it shows the original signal together with the estimated amplitude function

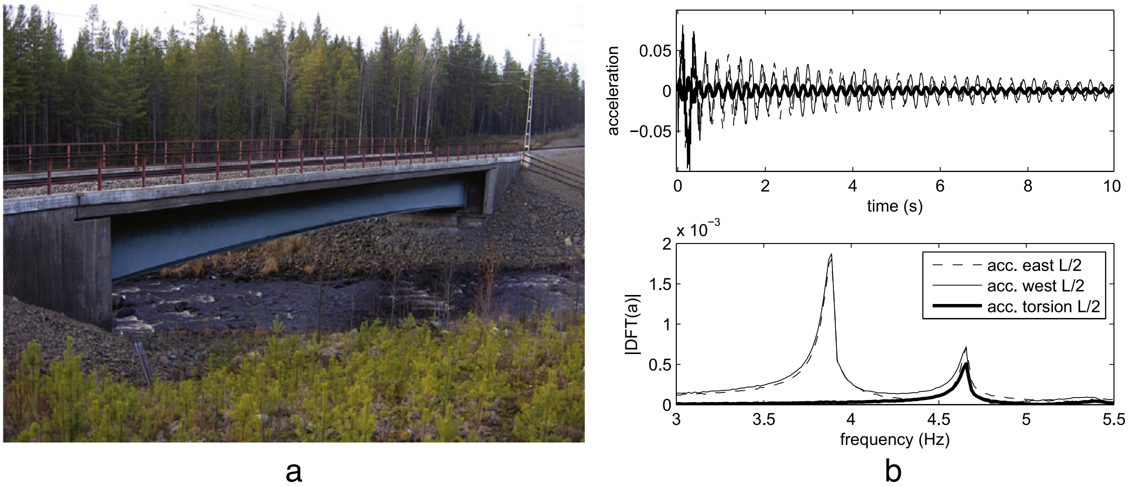

Fig. 4. (a) The bridge at Skidträsk. (b) The modulus of the Fourier transform of a typical outcome of free vibrations after the passage of a freight train (train 2, see Table 1) on the bridge at Skidträsk.

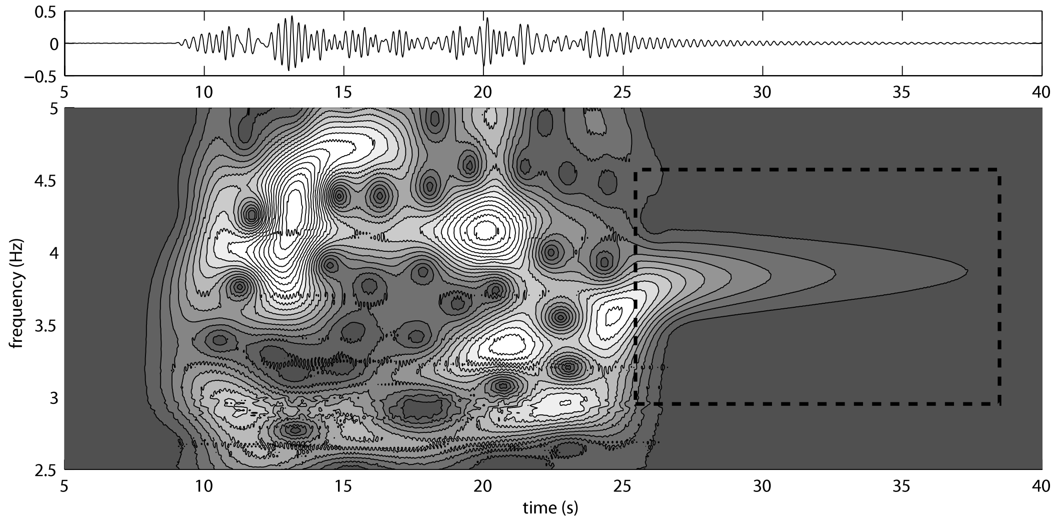

Fig. 5. The CWT for acceleration in the range of frequencies between 2.5 and 5 Hz of the entire passage of train nr. 5 (steel arrow). The dashed rectangle marks the region of interest in the present study.

Table 1
The train passages used in the present study and in [19]. The steel arrow is a freight train transporting iron ore between mines and steel mills in the northern parts of Sweden.

Train nr.	Lorieux [19]	Dominating mode	Train type	Speed (km/h)	Total length (m)
1	F-1	Vertical	Freight train	99	424
2	F-3	Vertical/torsion	Freight train	94	602
3	F-4	Torsion	Freight train	98	261
4	F-5	Vertical	Freight train	101	421
5	S-2	Vertical	Steel arrow	101	408

$A(t)$ and the estimated instantaneous dynamic properties, $f_n(t)$ and $\tilde{\xi}(t)$ of the non-linear single degree of freedom system which the original signal describes. The analysis procedures can be divided into the following steps:

1. Compute the CWT
2. Compute the ridge by maximizing the modulus of the CWT at each time instant
3. Extract the amplitude $A(t)$ and the phase $\phi(t)$ using Eqs. (24) and (25)
4. Apply an appropriate smoothing algorithm to the estimated amplitude and phase
5. Compute the instantaneous natural frequency and equivalent viscous modal damping ratio using Eqs. (21) and (30).

3. The bridge at Skidträsk

In order to test the capability of the CWT as applied to the dynamics of real railway bridges, a single span steel–concrete composite bridge was chosen as test subject. In the following, a short description of the bridge is given, together with a brief description of the experimental setup.

The bridge at Skidträsk (see Fig. 4(a)) is a single span, steel–concrete composite bridge carrying one ballasted track. Its span is 36 m. It was originally instrumented by the authors for the purpose of determining the maximum vertical bridge deck accelerations under normal operating conditions, bridge-weigh-in-motion [18] and to estimate the dynamic properties of the bridge. Here, only the part of the instrumentation which is related

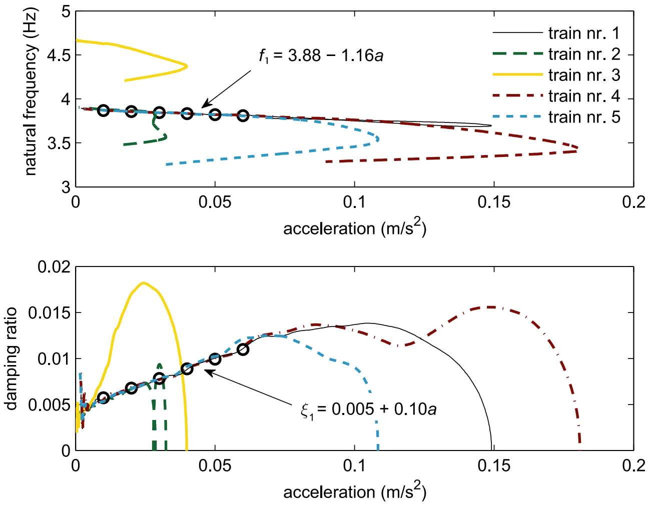

Fig. 6. This figure summarizes the results for the Skidträsk bridge in terms of natural frequency (top) for the first vertical bending mode (train nr. 3 mainly excited the first torsional mode) and the corresponding equivalent viscous damping ratio (bottom) estimates. The black circles show the fitted linear functions.

to the presented study will be described, see [19] for more details. Three accelerometers were placed on the edge beams of the bridge: two (one on each side) at mid-span and one at 1/4 of the span. Here, only data from one of the mid-span sensors have been used. However, the two sensors at mid-span can be used to detect torsional modes by studying the signal obtained from

$$a_t = \frac{a_1 - a_2}{B} \tag{31}$$

where a_t approximates the torsional acceleration at mid-span, a_1 and a_2 are the signals obtained from the two accelerometers at mid-span and B is the distance between the two accelerometers. The expression (31) is based on the assumption that the cross-section is rigid in its own place. Naturally, without a more detailed theoretical analysis of the mode shapes of the structure (or a more extensive instrumentation), it is impossible to discern such a "pure" torsional mode from modes which mainly involve an asymmetric deformation of the bridge deck. However, there appears to be some form of a torsional mode (∼4.6 Hz) quite close to the first vertical bending mode at around 3.9 Hz (Fig. 4(b)).

The accelerometers were of the MEMS-type (Colibrys,[1] Si-Flex SF1500S) and the data was gathered using an HBM[2] Spider8 data logger. The measurement system was controlled from a PC.

4. The influence of the train mass

Before presenting the results of the proposed analysis procedures, the most obvious cause for variations in the natural frequencies of a railway bridge excited by a passing train, namely the mass of the train, must be discussed.

The influence of the additional mass of the train on the natural frequency of the first vertical bending mode can be approximated using the Euler–Bernoulli beam theory, assuming that the mass of the train may be distributed over the length of the beam. On this particular railway, the maximum allowable axle load is 22.5 tons. The steel arrow iron ore trains have a well known mass as they utilize the maximum allowable axle load optimally. Furthermore, they have a special permit to use axle loads of 25 tons. The length of the steel arrow wagons is approximately 10 m. Thus, a fully loaded steel arrow adds around 400 tons to the mass of the bridge. This causes a reduction in the first bending mode frequency of approximately 20% considering a distributed mass of the bridge alone of 16–17 tons/m. This is clearly illustrated by Fig. 5 in which the CWT of the entire passage of train 5 is shown. The signal was band-pass filtered (using a fourth order Butterworth filter) over the range of frequencies 2.5–5 Hz so that the shown signal corresponds to the energy content of the CWT. The figure shows that when the train is on the bridge, the first bending mode frequency takes values around 3 Hz which conforms well with the estimate suggested above as the small amplitude frequency was found to be 3.9 Hz (see Eqs. (32) and (33)) giving $0.8 \cdot 3.9 = 3.1$ Hz. Such large variations have not been observed in the analyzed signals.

The dashed rectangle in Fig. 5 marks the region which has been analyzed in the present study. The observed variation in the natural frequency is rather slow and takes around 10 s. The speed of the train is around 100 km/h (see Table 1) so the time it takes for the last four wagons to leave the bridge is approximately

1 http://www.colibrys.com.
2 Hottinger Baldwin Messtechnik, http://www.hbm.com.

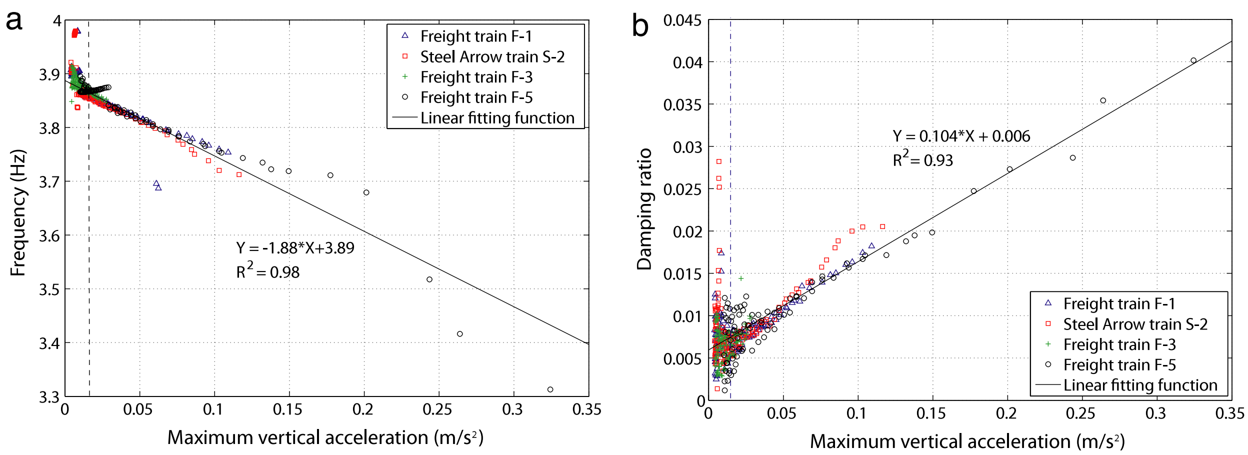

Fig. 7. The variation of (a) the natural frequency and (b) the damping ratio corresponding to the first vertical bending mode of vibration of the bridge at Skidträskån as a function of the maximum vertical acceleration (during the windowed part of the signal).
Source: Figures from [19].

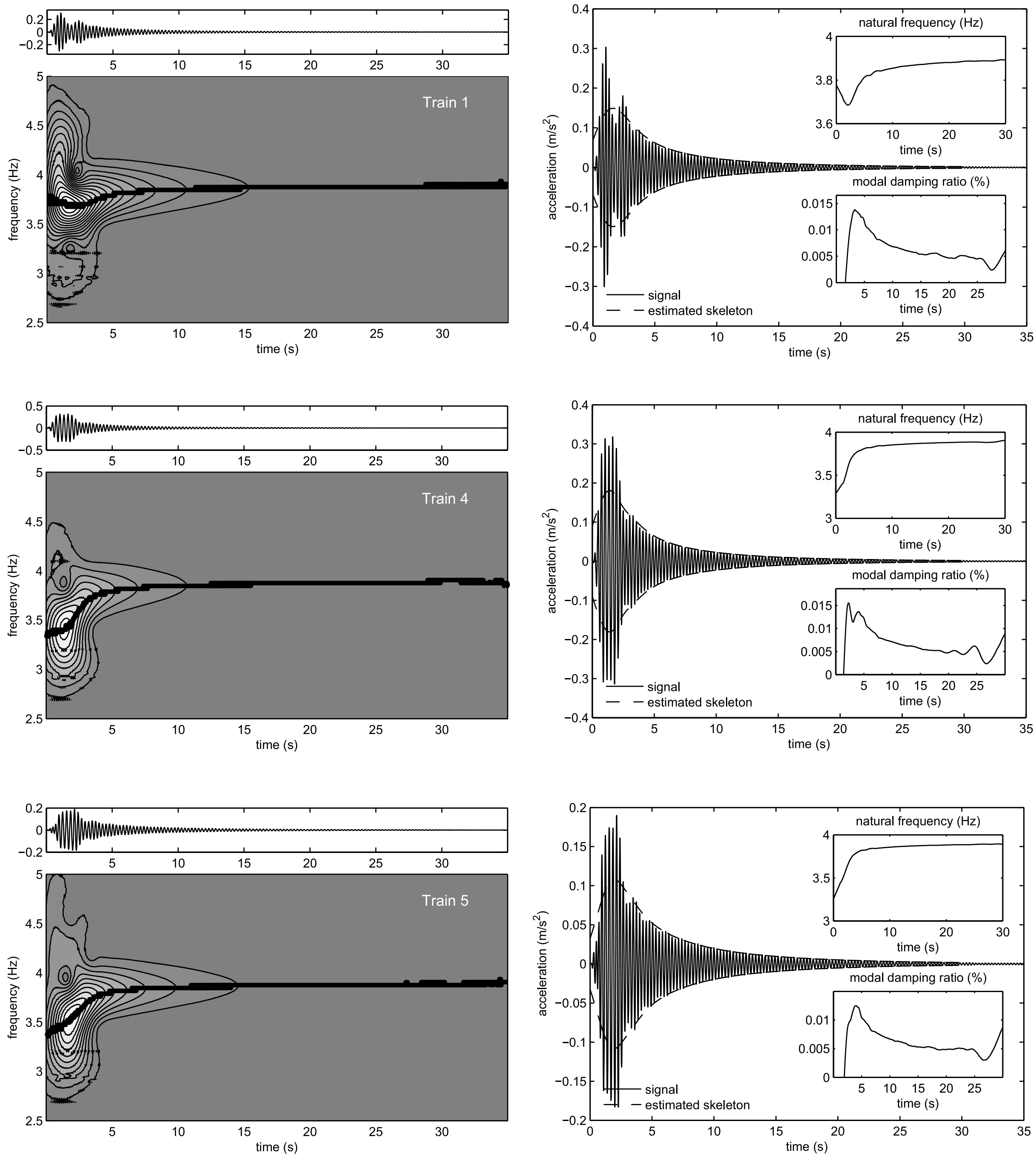

Fig. 8. The CWT (left) and the estimated skeleton curves (right) computed on basis of the free vibrations of the train passages which mainly excited the first vertical bending mode of the Skidträsk bridge.

$L_{\text{bridge}}/v_{\text{train}} = 36 \cdot 3.6/100 = 1.3$ s. Clearly, the slow variations in the eigenfrequencies cannot be explained by the variation in bridge mass caused by the passing train.

5. Result

Five train passages with comparatively large acceleration amplitudes in their free vibrations were chosen for this study. These train passages are summarized in Table 1, together with the notation used for these trains in [19].

The results obtained using the CWT in the proposed manner show that for the bridge at Skidträsk, variations in the natural frequency and the corresponding equivalent viscous damping ratio occur during the free vibrations of the structure. The estimated equivalent viscous damping ratios as well as the natural frequency of the first vertical bending mode appear to agree well between the different train passages. The free vibrations of train 3 were dominated by what is believed to be the first torsional mode of vibration (see Eq. (31) and Fig. 4(b)).

Rebelo et al. [20] used a windowed Fourier transform technique to estimate the instantaneous natural frequency of a number of single span reinforced concrete plate bridges. By applying a window function with a length of a few periods of the free vibrations, the instantaneous natural frequency and damping ratio was computed by a least square fit of the damped linear oscillator (26) to the windowed signals. It was then found that the natural frequency of the first bending mode of the analyzed bridges decreased as the amplitude of vibration increased. The authors

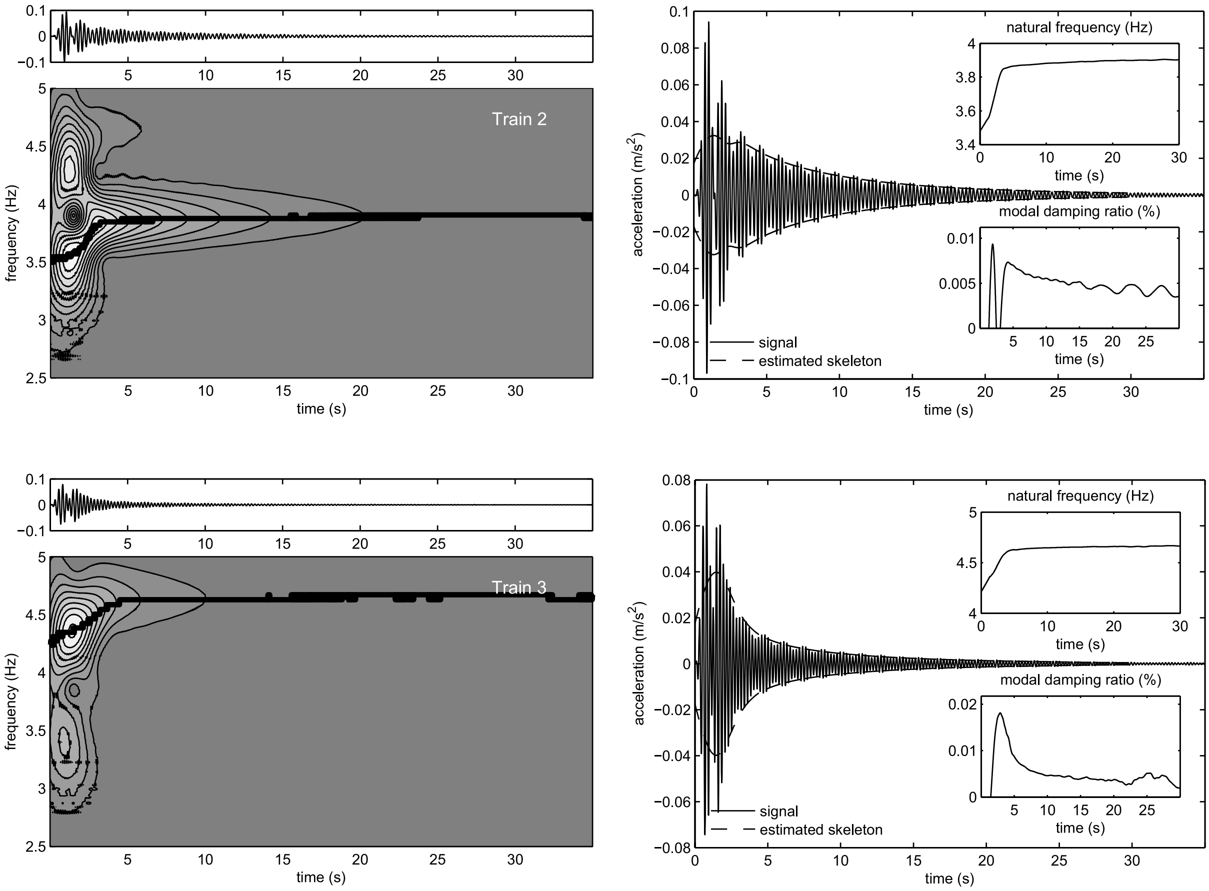

Fig. 9. The CWT (left) and the estimated skeleton curves (right) computed on basis of the free vibrations of the train passages which generated substantial vibrations in the first torsional mode of the Skidträsk bridge.

supervised a master thesis [19] in which this approach was applied to the data used in the current study. As will be shown in Section 5, this behavior is confirmed by the analysis based on the CWT.

Fig. 6 shows a rather encouraging summary of the estimated natural frequencies and equivalent viscous damping ratios for the bridge. Both the natural frequency and the damping ratio of the first vertical bending mode converge towards the same values at low amplitudes of vibration and as far as the different train passages can be compared, they follow the same curve. This curve is approximately linear over the available range of acceleration. By fitting a linear function to the estimated data the following relations were obtained:

$$f_1(a) = 3.88 - 1.16a \quad (32)$$
$$\xi_1(a) = 0.005 + 0.100a.$$

The corresponding linear functions determined by Lorieux [19] using the method based on windowed Fourier transforms (see Fig. 7), were

$$f_1(a) = 3.89 - 1.88a \quad (33)$$
$$\xi_1(a) = 0.006 + 0.104a.$$

The linear functions are plotted in Fig. 6 using black circles. The domain of these functions was chosen so that mainly the free vibration part of the relations was included. The estimates of the natural frequencies are valid everywhere in the domain D (Section 2.3). However, the estimated equivalent viscous damping ratios are only meaningful in a region where both the edge effect and the fact that free vibrations was assumed in establishing Eq. (30) are respected (see Figs. 1 and 2).

The free vibrations after train nr. 3 are dominated by a mode at ∼4.6 Hz which is believed to have a torsional character as discussed in Section 3. Unfortunately, only one train excited this mode well enough to get a clear estimate of its properties. However, it appears that the damping ratio of this mode is much more sensitive to the amplitude of vibration than the first vertical mode of vibration.

The estimated damping ratios are in excellent agreement between the two methods and the natural frequency have the same constant term. The linear term of the natural frequency does not agree well but for the available amplitude range, the discrepancy is not severe. Fig. 8 shows the CWT's and the estimated skeleton curves for the train passages in which the free vibrations were dominated by the first vertical bending mode. In Fig. 9, the corresponding results are shown for train passages in which the free vibrations are more or less influenced by the presumed first torsional mode. In time, the frequency changes quite rapidly in the beginning (of the domain D in which the edge effect is negligible as described in Section 2.3) and then slowly converges towards the low-amplitude value of the natural frequency. Before the ridge enters D it is much affected by the presence of the train which shows a large decrease in the natural frequency, most likely caused by the additional mass of the train.

It should also be noted that the damping ratio at small amplitudes of vibration, as estimated by the two methods, are in perfect agreement with the recommendations of the Eurocode ($\xi = 0.005$) for this bridge type. The recommendations of the Eurocode are based on extensive experimental work on a large number of bridges (see ERRI, European Rail Research Institute D 214, [21] and Frybá [1]).

Both methods were implemented using the functions provided in Matlab. In terms of computational time, the CWT took in the order of minutes to produce the presented results whereas the windowed Fourier transform took in the order of hours. The main reason for this is the relatively large number of least-squares problems which have to be solved in the implementation of the windowed Fourier transform. However, a specialized implementation of the two methods, aiming at optimizing the computational time may very well give a different result in terms of computational time.

6. Conclusions

The presence of weak non-linear effects in a steel–concrete composite bridge was detected and quantified using the continuous wavelet transform on the free vibrations after the passage of a train.

The following conclusions can be drawn from the present study:

– The identified natural frequencies were found to decrease whereas the corresponding equivalent modal damping ratios were found to increase with increasing acceleration.
– The obtained results were validated against the results of a method based on the windowed Fourier transform. The agreement between the two methods was satisfactory and it may thus be concluded that the observed non-linear behavior does exist in this type of structures.
– The presented results took a few minutes of computational time to produce using the CWT whilst the windowed Fourier transform method produced similar results taking a computational time in the order of several hours.
– A qualitative difference between the dynamic properties of the first vertical bending mode and the first torsional mode was found in that the damping ratio of the first torsional mode appears to increase much faster than that for the first vertical bending mode.
– Simple arguments regarding the influence of the mass of the train have clearly shown that this factor alone cannot explain the observed variations in the estimated natural frequencies.

The nature of the observed non-linearity is not well understood today. In the author's opinion, the phenomena most likely to cause effects such as those observed are interaction between the structure and the ballasted track, soil–structure interaction, and the non-linear material properties of cracked concrete. The authors intend to perform further studies within this field in order to study the influence of the above mentioned phenomena and to classify those bridge types in which the observed behavior can be expected. Extensions of the used method, geared towards identifying parameters in non-linear single and multi-degree-of-freedom models may become useful in future work within this field.

References

[1] Frybá L. Dynamics of railway bridges. London: Telford; 1996.
[2] CEN. Eurocode 1: actions on structures—part 2: traffic loads on bridges. CEN. European Committee for Standardization; 2008.
[3] Flandrin P. Time-frequency/time-scale analysis. Academic Press; 1999.
[4] Mallat S, Wavelet A. Tour of signal processing—the sparse way. 3rd ed. Academic Press; 2008.
[5] Liu K, Roeck GD. Damage detection of shear connectors in composite bridges. Struct Health Monit 2009;8(5):345–56.
[6] Staszewski WJ. Identification of damping in mdof systems using time-scale decomposition. J Sound Vib 1997;203(2):283–305.
[7] Slavič J, Simonovski I, Boltežar M. Damping identification using a continuous wavelet transform. J Sound Vib 2003;262:291–307.
[8] Le T-P, Argoul P. Continuous wavelet transform for modal identification using free decay response. J Sound Vib 2004;277:73–100.
[9] Staszewski WJ. Identification of non-linear systems using multi-scale ridges and skeletons of the wavelet transform. J Sound Vib 1998;214(4):639–58.
[10] Ta M, Lardiès J. Identification of weak nonlinearities on damping and stiffness by the continuous wavelet transform. J Sound Vib 2006;293:16–37.
[11] Chang C, Shi Y. Identification of time-varying hysteretic structures using wavelet multiresolution analysis. Internat J Non-Linear Mech 2010;45:21–34.
[12] Feldman M. Non-linear free vibration identification via the Hilbert transfrom. J Sound Vib 1997;208(3):475–89.
[13] Feldman M. Identification of weakly non-linearities in multiple coupled oscillators. J Sound Vib 2007;303:357–70.
[14] Matlab Wavelet Toolbox. The MathWorks. 2010.
[15] Boltežar M, Slavič J. Enhancements to the continuous wavelet transform for damping identification on short signals. Mech Syst Signal Process 2004;18:1065–76.
[16] Delprat N, Escudié B, Guillemain P, Kronland-Martinet R, Tchamitchian P, Torrésani B. Asymptotic wavelet and Gabor analysis: extraction of instantaneous frequencies. IEEE Trans Inf Theory 1992;38(2):644–64.
[17] Carmona RA, Hwang WL, Torresani B. Characterization of signals by the ridges of their wavelet transforms. IEEE Trans Signal Process 1997;45(10):2586–90.
[18] Liljencrantz A, Karoumi R. Twim—a matlab toolbox for real-time evaluation and monitoring of traffic loads on railway bridges. Struct Infrastruct Eng 2009;5(5):407–17.
[19] Lorieux L. Analysis of train-induced vibrations on a single-span composite bridge. Master thesis 263. Stockholm (Sweden): Royal Institute of Technology; 2008. Available online: http://www.byv.kth.se/.
[20] Rebelo C, da Silva LS, Pircher M. Dynamic behaviour of twin single-span ballasted railway viaducts—field measurements and modal identification. Eng Struct 2008;30(9):2460–9.
[21] ERRI. ERRI D 214 RP3. Rail bridges for speeds >200 km/h—recommendations for calculating damping in rail bridge decks. European Rail Research Institute; 2000.

Paper II

Influence of non-linear stiffness and damping on the train-bridge resonance of a simply supported railway bridge

Engineering Structures, 41:350–355, 2012.

Engineering Structures 41 (2012) 350–355

Contents lists available at SciVerse ScienceDirect

Engineering Structures

journal homepage: www.elsevier.com/locate/engstruct

Influence of non-linear stiffness and damping on the train-bridge resonance of a simply supported railway bridge

Mahir Ülker-Kaustell *, Raid Karoumi

KTH Royal Institute of Technology, Brinellvägen 34, SE-100 44 Stockholm, Sweden

ARTICLE INFO

Article history:
Received 7 November 2011
Revised 26 March 2012
Accepted 30 March 2012

Keywords:
Railway bridges
Dynamics
Non-linear stiffness and damping
Train-bridge resonance

ABSTRACT

Previous experimental work has identified variations in the natural frequency and the modal damping ratio of the first vertical bending mode of vibration of a simply supported, single span steel–concrete composite bridge. It was found that the natural frequency decreased and the modal damping ratio increased with increasing amplitudes of vibration. This paper illustrates the influence of these variations on the train-bridge resonance of this particular bridge by means of a non-linear single degree of freedom system, based on the previously mentioned experimental results. As one might expect, the results indicate that the influence of the increasing damping ratio leads to a considerable decrease in the resonant amplitude whilst the decreasing natural frequency decreases the critical train speed at which resonance occurs. Further studies along this line of research may help us reduce the uncertainties in dynamic assessments of existing bridges based on dynamic measurements and improve our understanding of the dynamic properties of railway bridges in general.

1. Introduction

The dynamic response of railway bridges subjected to high-speed trains is mainly governed by different states of resonance between the bridge and the train. The load induced by the train will, at certain train speeds, have components with frequencies that match eigenfrequencies of the structure. Thus, many possible combinations of train configurations and train speeds can exist which cause states of train-bridge resonance. This is one of the main issues in design of new bridges for high-speed railway lines and in dynamic assessments of existing bridges, which is becoming increasingly interesting for railway owners who wish to increase the maximum allowed train speed and axle loads.

From an analysis of single degree of freedom systems, one knows that in a state of resonance, the amplitude of vibration is mainly governed by the damping of the system. This also holds true for multi degree of freedom systems as well as for continuous systems, although in such cases, different combinations of modes may be relevant. However, variations in the eigenfrequency are also likely to influence the state of resonance, mainly by altering the critical train speed.

Previous studies [2,4] have given indications that for certain bridges, the damping ratio and the natural frequency have a dependency on the amplitude of vibration. The nature of these non-linearities are not well known but candidates have been suggested in the non-linear material properties of soil materials and concrete, which both have the same tendency: the damping increases and the stiffness decreases with the deformation of the materials. Fink and Mähr [3] reported experimental findings from a scaled laboratory model of a ballasted railway bridge which support the hypothesis that the ballast is one of the main sources to this behavior.

This paper aims at illustrating the influence of the non-linear dynamic properties of a simply supported, ballasted composite bridge on its response at resonance. A simple single degree of freedom system representing the first vertical bending mode of the bridge is used to simulate the response caused by a typical freight train and for a theoretical study of the train bridge resonance based on the Eurocode HSLM (*High Speed Load Model*) trains [5].

As the state of resonance is often dominated by a single mode of vibration, a qualitative analysis of this type of models may provide some insight into the real behavior at resonance. A formalized knowledge of the railway bridge response at resonance may lead to substantial savings for society, if it turns out that at resonance, the increased damping leads to a much smaller response than that predicted by linear theories.

2. Theory

2.1. A non-linear single degree of freedom system

Without explicitly knowing the sources to the non-linear behavior, models can only be devised in a "black-box" sense.

* Corresponding author.
E-mail address: mahir.ulker@byv.kth.se (M. Ülker-Kaustell).

0141-0296/$ - see front matter © 2012 Elsevier Ltd. All rights reserved.
http://dx.doi.org/10.1016/j.engstruct.2012.03.060

Measurements can give estimates of the relations between the dynamic properties (natural frequency and damping ratio) of different modes of vibration and the amplitude of vibration in those modes, see [4] and the references therein. Given such relations, a non-linear single degree of freedom system can be established

$$m\ddot{x} + c(x)\dot{x} + k(x)x = f \quad (1)$$

where x is the generalized coordinate of the fundamental mode of vibration, m is the generalized mass, $c(x)$ is an amplitude dependent viscous dashpot coefficient, $k(x)$ is a non-linear spring constant and $f = f(t)$ is the generalized forcing function.

The non-linearities are assumed to be small in the sense that the frequency does not vary much around the limit value at $\ddot{x} = 0$ and the mode shape is assumed to be constant, independent on the amplitude of vibration. Furthermore, the "black-box" nature of the proposed model presumes that variations in support stiffness and damping and the interaction between the structure and the embankments and with the track superstructure are all grouped together in the eigenfrequency and the damping ratio.

The load model used to define the generalized force function $f(t)$ is also subjected to some simplifying assumptions, namely that the train-bridge interaction may be neglected, thus leaving out the variation in mass damping and perhaps to some extent in stiffness, caused by the passing train.

Frybá [1] derived a solution for the response of a simply supported beam subjected to a pulse train moving along the beam. In the present analysis, we wish to solve for the temporal coordinate using a numerical technique in order to include the non-linear system parameters, but the generalized force for the first mode of vibration is approximated in the same way as in [1]:

$$f(t) = \sum_{i=1}^{N} F_i \epsilon_i(t)\phi(ct - d_i) \quad (2)$$

where F_i is the axle load of axle number i, N is the number of axles, $\epsilon(t)$ is a function defined by

$$\epsilon_i(t) = H(t - d_i/c) - H(t - (d_i + L)/c) \quad (3)$$

where $H(t)$ is Heaviside's function. Furthermore, d_i is the distance from the ith axle to the first point on the beam, L is the length of the beam and $\phi(x)$ is the first (vertical bending) mode of vibration

$$\phi(x) = \sin\left(\frac{\pi x}{L}\right) \quad (4)$$

This representation of the load function is a consequence of expanding the spatial coordinate in a Fourier series. This series will repeat itself indefinitely along the spatial coordinate, but we are only interested in $x \in (0, L)$. The function $\epsilon_i(t)$ simply ensures that the load is not applied to the repeated occurrences of the physical structure. Otherwise, the analysis would comprise a structure equivalent to an infinite continuous beam on simple supports.

The parameters of Eq. (1) can be rearranged so that the following equation is obtained

$$\ddot{x} + 2\xi(x)\omega_n(x)\dot{x} + \omega_n^2(x)x = \frac{f}{m} \quad (5)$$

where $\xi(x)$ and $\omega_n(x)$ are the amplitude dependent damping ratio and natural circular frequency of the fundamental mode of vibration.

A methodology to determine the amplitude dependency of the natural frequency and damping ratio from measured free vibrations after the passage of a train using the continuous wavelet transform (CWT) have been presented in [4]. More general applications of the CWT have been presented in several papers, see for example [6]. In this paper, bilinear relations based on the analysis presented in [4], were used to model the amplitude-dependency of the dynamic properties of the first mode of vibration. These relations, which may be represented by the generic relation

$$g(\ddot{x}) = \begin{cases} g_0 + k|\ddot{x}|, & |\ddot{x}| \leqslant \ddot{x}_c \\ g_c, & |\ddot{x}| > \ddot{x}_c \end{cases} \quad (6)$$

are shown in Fig. 1 with the parameters given in Table 1. The linear part of these functions were determined by means of the CWT, based on five train passages at slightly different speeds. For further details, the reader is referred to [4]. The constant parts of these functions have been assumed and reflect the lack of knowledge about these relations at accelerations greater than 0.3 m/s^2.

The relations given by Eq. (6) were derived using measurements of acceleration. However, in solving non-linear differential equations it is much more convenient to have the non-linearity on the displacement and/or the velocity as then, well-known numerical methods may be directly applied. In the present context, this does not pose any serious difficulties, because the non-linear relations given by Eq. (6) are defined using the free vibrations of a single mode of vibration. Therefore, the displacement during the free vibrations can be determined from measurements of acceleration simply by applying a high-pass filter to the signal and integrate it numerically. By doing so, and normalizing the results it is easy to verify that the displacement during free vibrations is proportional to the accelerations according to

$$u(t) \sim \frac{\ddot{u}(t)}{\omega^2} \quad (7)$$

with a phase-shift π. This is shown in Fig. 2, where ω was taken as $2\pi 3.9$ rad/s which clearly shows that the variation in frequency is slow enough to make this approximation feasible, i.e. the acceleration of the free vibrations may be obtained from the displacement function by applying a scaling and a translation. Formally, this means that the frequency and amplitude modulated signal which is considered here

$$u(t) = A(t)\cos(\omega(t)t) \quad (8)$$

has the property that $\dot{\omega}(t) \ll 1$, i.e. slow variations in $\omega(t)$. Thereby, the generic relation (6) can be restated as a function of displacement, simply by making the change of variables $\ddot{x} = -\omega_0^2 x$, with ω_0 being the natural frequency at small amplitudes of vibration.

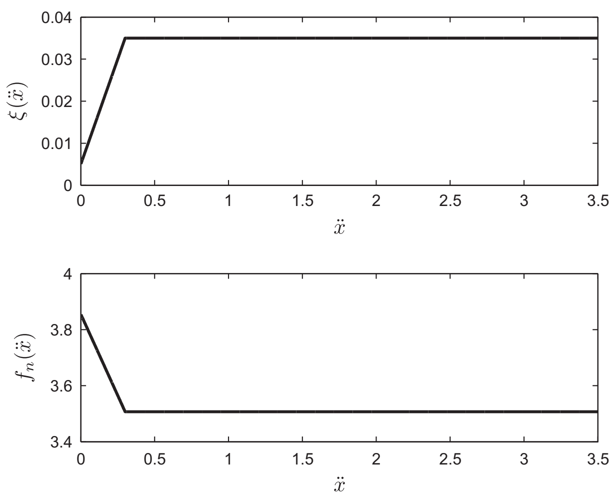

Fig. 1. Top: The damping ratio function (in %) for the SDOF-model. Bottom: The frequency function (in Hz) for the SDOF-model.

Table 1
Parameters in the bilinear relation given by Eq. (6).

	g_0	g_c	k (s/m)	$\ddot{x}_c$ (m/s^2)
ξ	0.005	0.035	0.1	0.3
f_n	3.9 Hz	3.5 Hz	−1.2	0.3

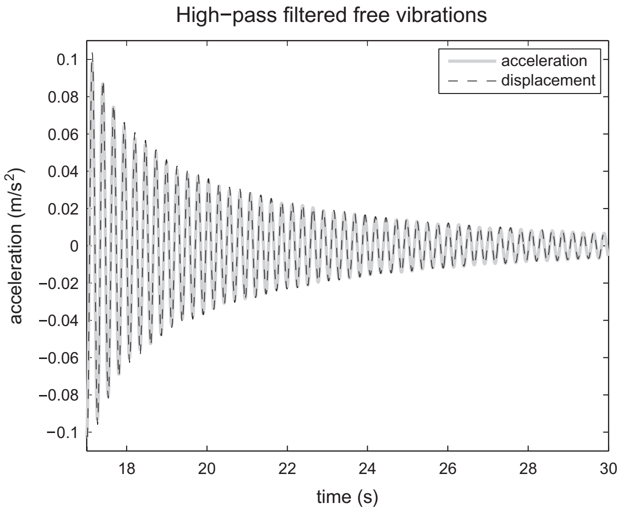

Fig. 2. Comparison between the measured acceleration and the acceleration computed from high-pass filtered and integrated acceleration assuming slow frequency variations.

2.2. Numerical procedures

Solutions to Eq. (5) are most conveniently determined by means of numerical methods. In this particular case, an explicit method based on central differences was found to give quick and robust solutions. Hence, the first and second derivatives were approximated by

$$\dot{x}_i \approx \frac{x_{i+1} - x_{i-1}}{2\Delta t} \tag{9}$$

$$\ddot{x}_i \approx \frac{x_{i+1} - 2x_i + x_{i-1}}{\Delta t^2} \tag{10}$$

If the initial values are zero, we can set $x_{i-1} = 0$ and step forward in time using the force term

$$\hat{f} = f_i - ax_{i-1} - bx_i \tag{11}$$

where the coefficients a and b are given by

$$a = m\left[\frac{1}{\Delta t^2} - \frac{\xi(x_i)\omega_n(x_i)}{\Delta t}\right] \tag{12}$$

$$b = m\left[\omega_n^2(x_i) - \frac{2}{\Delta t^2}\right] \tag{13}$$

and a stiffness $\hat{k}$

$$\hat{k} = m\left[\frac{1}{\Delta t^2} + \frac{\xi(x_i)\omega_n(x_i)}{\Delta t}\right] \tag{14}$$

so that

$$x_{i+1} = \hat{f}(x_{i+1})/\hat{k}(x_{i+1}) \tag{15}$$

Having performed these operations for time step $i+1$, $\dot{x}_i$ and $\ddot{x}_i$ can be computed using Eqs. (9) and (10), respectively.

As the method is explicit, one has to ensure that the time step Δt is sufficiently small, so as to avoid numerical instabilities.

3. The Skidträsk bridge and the Steel Arrow train

The question at hand is whether the amplitude dependency of the dynamic properties of the bridge has any influence on its dynamic response due to passing trains. Thus, a comparison will be made between the proposed model and the corresponding linear single degree of freedom system which would have been devised without this information. Primarily, the Steel Arrow train will be used in this comparison, as measurements of passages with this train are available.

In this section, a short description of the Skidträsk bridge and the part of the instrumentation of the bridge which was used in this paper will be given. Also, the Steel Arrow train will be defined in terms of the parameters needed to model it using Eq. (2).

3.1. The Skidträsk bridge

The skidträsk bridge is a simply supported composite bridge with a span of 36 m carrying one ballasted track, see Fig. 3. It was instrumented with a number of sensors, of which two vertical accelerometers at mid span, one on each upper flange of the steel beams, which were used in this paper. A more detailed description of the bridge and its instrumentation may be found in [7,8]. The parameters used to model the bridge with a linear single degree of freedom system were E = 210 GPa, I = 0.82 m^4 and m = 17,000 kg/m, where E is the elastic modulus of an equivalent steel section, I is the area moment of inertia of this equivalent cross section and m is bridge mass in which the mass of the ballast has been considered. In accordance to the Eurocode [5], the damping ratio for such a bridge should be chosen as 0.5%.

3.2. The Steel Arrow train

The Steel Arrow train is used for steel ore transports in the northern parts of Sweden. Each wagon has a length of 13.9 m, a bogie distance of 8.6 m and the axle distance within a bogie is 1.8 m. For the locomotives, the corresponding distances are 13.9 m, 7.7 m and 2.7 m, respectively. The axle loads are comparatively well known for this train type, as the wagons are typically filled with an equal amount of ore pellets. The axle loads of the locomotives and wagons are 19.5 and 22.5 metric tons, respectively. The train set studied in this paper consists of 24 wagons, pulled by two locomotives.

Fig. 3. The bridge at Skidträsk.

4. Result

4.1. Comparison with measurements

The model based on information about the first mode of vibration can of course only be compared to the measured reality in a frequency range which resembles the contributions related to this mode. Thus, a band-pass filter is necessary in order to make a just comparison in the time domain. However, in the real structure, a torsional mode exists with a frequency quite close to that of the first vertical bending mode. This is likely to cause some disturbances in a comparison, but the most severe errors are most likely caused by reducing the number of degrees of freedom to one and the simplicity of the load model.

Fig. 4 shows a comparison between the model and the measured response due to a Steel Arrow train moving at approximately 102 km/h. The free vibrations after the train passage are shown in Fig. 5.

4.2. Theoretical impulse responses

The impulse response of the model was computed for input forces $F = 5$, 10 and 50 kN. The result is shown in Fig. 6.

4.3. Theoretical response at train-bridge resonance

The train-bridge resonance was studied by simulating train passages at different train speeds $v \in (50, 300)$ (km/h) with a step of $\Delta v = 1$ km/h. This was done using the Steel Arrow configuration described in Section 4.1 and with the HSLM trains of the Eurocode. In this analysis, the linear model based on parameter values according to the Eurocode is compared to the proposed non-linear model. The results obtained for the Steel Arrow are shown in Figs. 7 and 8. However, it is also interesting to see what influence a variable frequency may have on the critical train speed. Therefore, a model in which the damping ratio was taken constant, whilst the natural frequency was allowed to vary with amplitude in accordance with Eq. (6) was also studied. This result is shown in Fig. 9.

5. Discussion

5.1. Comparison with the Steel Arrow train measurements

Given the highly simplified model used, the agreement between the measured signal and the simulation is quite good. However,

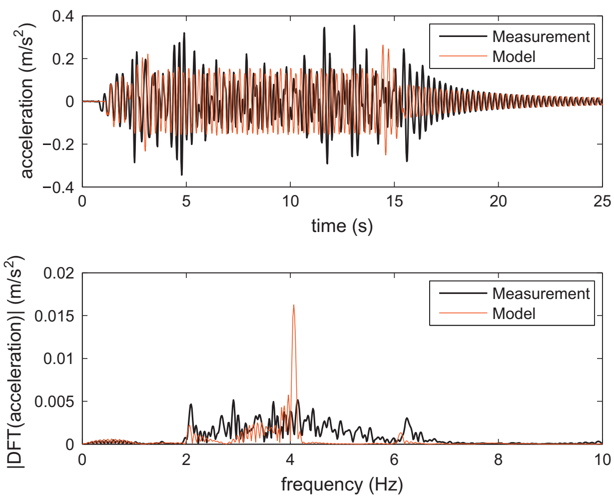

Fig. 4. Comparison between measured and simulated response during the passage of a Steel Arrow freight train at 102 km/h.

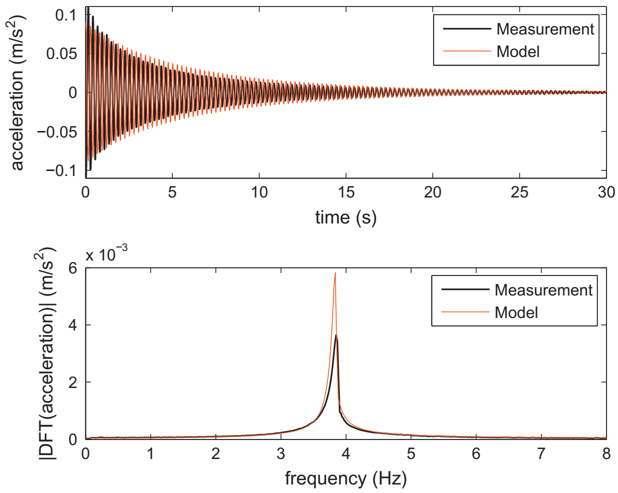

Fig. 5. Comparison between measured and simulated free vibrations after the passage of a Steel Arrow freight train at 102 km/h.

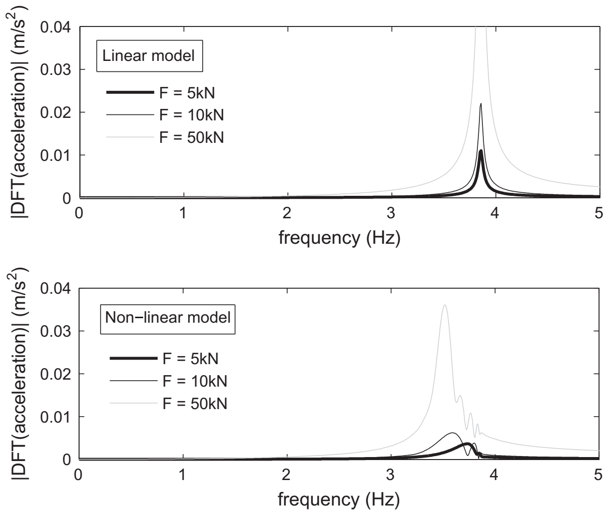

Fig. 6. Comparison of impulse responses for the linear (top) and non-linear models (bottom).

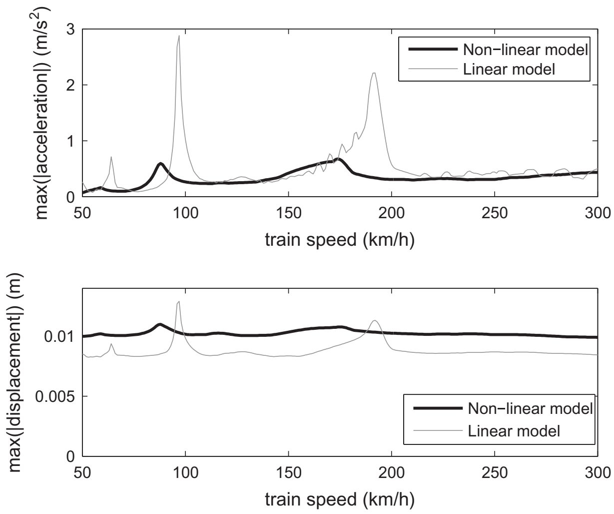

Fig. 7. Maximum absolute values of the vertical acceleration (top) and vertical displacement (bottom) as function of train speed for the Steel Arrow freight train.

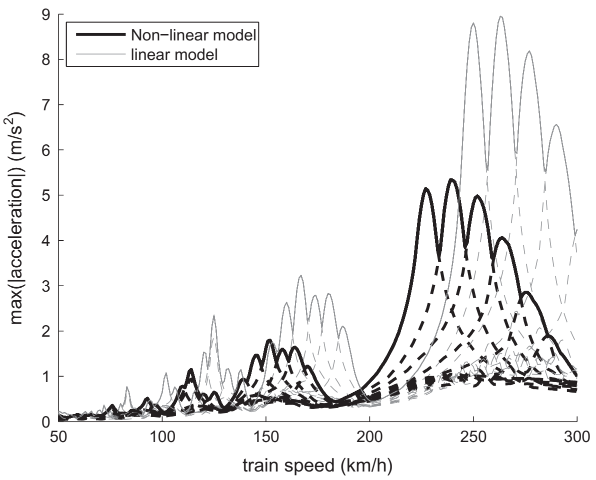

Fig. 8. Maximum absolute values of the vertical acceleration as function of train speed for the ten HSLM-A trains of the Eurocode.

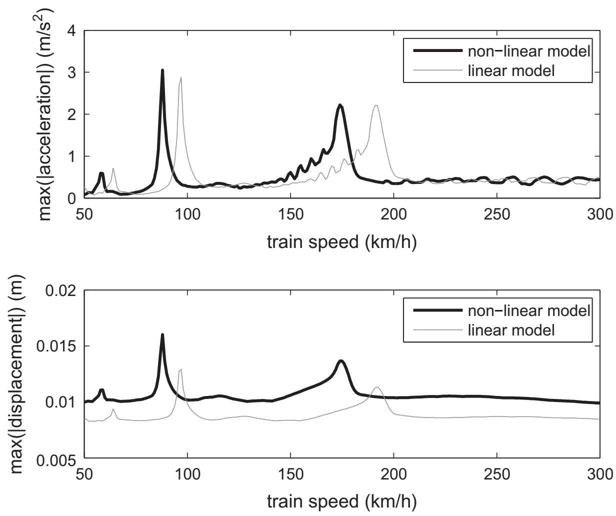

Fig. 9. Maximum absolute values of the vertical acceleration (top) and vertical displacement (bottom) as function of train speed for the Steel Arrow freight train assuming constant damping.

some aspects of reality will not be correctly represented with such a simple model as that proposed here. The most likely source to the discrepancies which can be observed in Fig. 4 is the highly simplified load model and the assumption that the mode shape is constant.

It goes without saying that the used load model is questionable in a comparison against the measured reality. The chosen load model does not include the variation in mass, stiffness and damping caused by the presence of the train. Nor can it describe defects in the train set and the rail-wheel contact which is known to give rise to impulses which may be "felt" by the bridge even though they often include much higher frequencies than what is customary in the bridge community.

The issues regarding the choice of mode shape and possible variations in the mode shape with the amplitude of vibration can, presumably, be ascribed to soil-structure interaction at the foundations/abutments and to the interaction between the bridge and the track superstructure. Such effects are not represented in the proposed model. In order to overcome these difficulties, further research regarding the nature of the observed non-linearities must be performed.

The comparison between the model and the measurements of the free vibrations which is shown in Fig. 5 show a much higher resemblance, which is encouraging, but not completely unexpected as the parameters of the model are based on such measurements.

To summarize this comparison, the agreement between the proposed model and the measured reality gives some confidence in the proposed model and it is therefore appropriate to use it in a theoretical study of the critical train speed for this particular bridge. Due to its simplicity, both in terms of instrumentation needs and analysis, it may also be used in a first check on existing railway bridges along lines for which an increase in maximum allowed train speed is planned.

5.2. Impulse responses

Fig. 6 shows the impulse response functions for the proposed model and the corresponding linear model. It is clear that the variation in the dynamic properties of the system leads to a decreased resonance amplitude and a spreading of the frequency content over the range of frequencies in which the natural frequency varies. This observation may be useful when analyzing measurements from railway bridges as estimates of mode shapes using "output-only" methods such as the Frequency Domain Decomposition [9] sometimes lead to several very similar modes with closely spaced frequencies.

5.3. Critical train speeds

A comparison of Figs. 7 and 9 clearly shows that it is the increased damping which gives rise to the decreased resonance amplitude of the non-linear model. The variation (decrease) in the natural frequency leads to a decreased critical speed, apparently a scaling of the train speed, and an increase in the displacement, due to the weakening of the system at higher amplitudes of vibration.

5.4. Possible sources of the observed non-linearity and future work

The presented analysis is the outcome of work with two issues related to high-speed railway bridges; the choice of design parameters and the analysis of existing bridges in capacity assessments. These are closely interrelated as we need to understand the underlying physics in order to gain confidence in the implications of the presented results, but also in order to device appropriate testing procedures for existing bridges.

As mentioned earlier, the most probable sources of the observed non-linear behavior is the soil material properties of either the foundations or the ballasted track superstructure. However, other conceivable sources such as bearing friction and cracks in the concrete deck cannot, at the state of understanding at which we are now, be completely ruled out. Of course, any combination of these sources may also be possible. The reason for taking the soil material properties as the most likely candidate is motivated by the relation between soil strain and elastic moduli and material damping ratio. Figs. 10 and 11 show generic curves based on the so-called hyperbolic model (see for example [10,11]) describing the variation of the soil shear modulus (normalized against the shear modulus for small strain) and damping ratio with strain. However, these quantities are also dependent on the state of stress (or rather, the mean effective stress, as indicated in the figures). In the thesis by Neild [12], a similar behavior, i.e. increasing damping and decreasing stiffness with amplitude of vibration, is reported based on experiments on cracked reinforced concrete beam.

From a theoretical point of view, the development of elasto-plastic and hypoplastic material models and macro-element

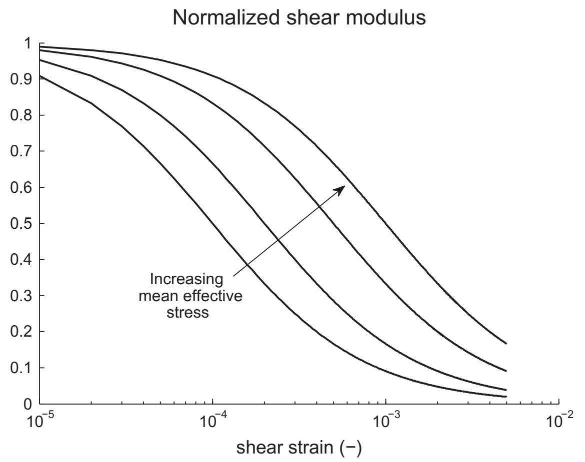

Fig. 10. Typical relations between soil shear modulus and shear strain.

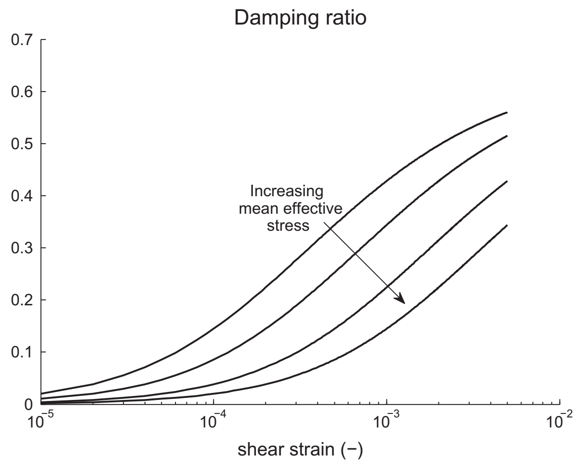

Fig. 11. Typical relations between soil damping ratio and shear strain.

models for shallow foundations should be sufficient to model this behavior. However, from a practical point of view, such efforts cannot be justified unless some more conclusive experimental findings can support the developments this far. Furthermore, procedures for determining model constants for relevant ranges of vibration amplitudes from non-destructive tests must be devised. This can be achieved in more than one way, but in the authors opinion, two types of tests should be devised for this purpose:

i. Measurements during the construction stages.
ii. Measurements on existing bridges.

Both types of experiments should be based on excitation with known forces, i.e. using a hydraulic exciter, so that both force and displacement control can be used. The first type of tests would enable a qualitative and to some extent quantitative study of the influence of the foundations and the track superstructure on the dynamic properties of a tested bridge. Naturally, such tests would have to be performed on a number of bridges of different type and span lengths, preferably also on different soil configurations. The main purpose of these tests would be to validate theoretical models and the inclusion of the results of geotechnical surveys in such models. In doing so, issues related to the choice of model parameters in constitutive relations and macro-element formulations would have to be handled. Given that the type one tests really gives conclusive results regarding the influence of the foundation and track superstructure on the dynamic properties of a set of typical bridges, type two tests could be performed on arbitrary existing bridges, thus making a much more systematic study possible. Such studies could take phenomena such as seasonal variations and the influence of track realignment in consideration.

5.5. Concluding remarks

In order to draw general conclusions regarding the observed behavior, a more thorough investigation of the presented results must be made. The sources of the observed non-linearities must be understood in order to implement an approach such as that used here in dynamic assessments of existing bridges with sufficient confidence. If for example, the track superstructure is the main source to these effects, winter conditions may alter the functions which describe the variation in natural frequency and damping ratio due to freezing of the ballast, especially if the railway line in question is not heavily trafficked. Also, the bilinear relations used here cannot be directly applied with full confidence in a state of resonance, where the acceleration are much higher than 0.3 m/s^2.

Acknowledgements

This work was made possible by the Railway Group at KTH Royal Institute of Technology, Stockholm, Sweden and Tyréns AB. The experimental work was performed by Claes Kullberg and Stefan Trillkott at KTH, Civil and Architectural Engineering.

References

[1] Frybá L. A rough assessment of railway bridges for high speed trains. Eng Struct 2001;23:548–56.
[2] Rebelo C, da Silva LS, Pircher M. Dynamic behaviour of twin single-span ballasted railway viaducts-field measurements and modal identification. Eng Struct 2008;30(9):2460–9.
[3] Fink J, Mähr T. Influence of ballast superstructure on the dynamics of slender railway bridge, NSCC; 2009.
[4] Ülker-Kaustell M, Karoumi R. Application of the continuous wavelet transform on the free vibrations of a steel–concrete composite railway bridge. Eng Struct 2011;33:911–9.
[5] CEN. Eurocode 1: Actions on structures – Part 2: Traffic Loads on Bridges, CEN, European Committee for Standardization; 2008.
[6] Ta M, Lardiès J. Identification of weak nonlinearities on damping and stiffness by the continuous wavelet transform. J Sound Vib 2006;293:16–37.
[7] Liljencrantz A, Karoumi R. Twim-a matlab toolbox for real-time evaluation and monitoring of traffic loads on railway bridges. Struct Infrastruct Eng 2009;5(5):407–17.
[8] Lorieux L. Analysis of train-induced vibrations on a single-span composite bridge. Master thesis 263, Royal Institute of Technology, Stockholm, Sweden; 2008. <http://www.byv.kth.se/>.
[9] Brincker R, Zhang L, Andersen P. Modal identification of output-only systems using frequency domain decomposition. Smart Mater Struct 2001;10:441–5.
[10] Ishihara K. Soil behaviour in earthquake geotechnics. London: Oxford University Press; 1996.
[11] Kondner RL, Zelasko JS. A hyperbolic stress–strain formulation of sands. In: Proceedings of the second Pan-American conference on soil mechanics and foundation engineering, vol. 1; 1963.
[12] Neild SA. Using non-linear vibration techniques to detect damage in concrete bridges. PhD thesis, Department of Engineering Science, University of Oxford; 2001.

Paper III

Seasonal effects on the stiffness properties of a ballasted railway bridge

To appear in Engineering Structures.

Seasonal effects on the stiffness properties of a ballasted railway bridge

Ignacio Gonzales[a], Mahir Ülker-Kaustell[a,*], Raid Karoumi[a]

[a]*KTH Royal Institute of Technology, Brinellvägen 23, SE-100 44 Stockholm, Sweden*

Abstract

In this article it is shown empirically that ballasted bridges in cold climates can exhibit a step-like variation of their eigenfrequencies as the yearly season changes. The bridge under study was observed to have significantly higher natural frequencies (as much as 35 %) during the winter months compared to the summer. This variation was rather discrete in nature and not proportional to temperature. Furthermore the increase in natural frequencies took place only after the temperatures had dropped below 0 °C for a number of days. It was thus hypothesized that this change in natural frequencies was due to changes in the stiffness parameters of some materials with the onset of frost. In low temperature conditions not only the mean value of the measured frequencies increased, but also their variance increased considerably. Given the large spread of the measured natural frequencies, the stiffness parameters were assumed to be stochastic variables with an unknown multivariate distribution, rather than fixed values. A Bayesian updating scheme was implemented to determine this distribution from measurements. Data gathered during one annum of monitoring was used in conjunction with a finite element model and a meta model, resulting in an estimation of the relevant stiffness parameters for both the cold and the warm condition.

Keywords: Railway bridges, Dynamics, Ballasted track, Seasonal effects, Bayesian updating, Markov-Chain Monte-Carlo Sampling

1. Introduction

The influence of long periods of low temperature on the dynamic properties of ballasted railway bridges has not been given much attention. This paper presents a study of the influence of seasonal effects on the natural frequencies of a ballasted single span steel-concrete railway bridge. It is shown that the natural frequencies of the first vertical bending and torsional modes of vibration increase markedly during the cold period of the year. An analysis of measured free vibration signals during one annum is used as a basis for a Bayesian updating procedure, which is applied on a three dimensional finite element model of the structure.

In dynamic assessments of existing railway bridges with the purpose of increasing the allowable train speed and/or axle loads, the analyst primarily needs information regarding the natural frequencies and the corresponding modal damping ratios of the first few modes of vibration. This information can be obtained by fairly simple instrumentations using the free vibrations from passing trains. However, as will be shown, the natural frequencies estimated during the cold season can be misleading. The natural frequencies are needed to estimate the critical train speeds at which train-bridge resonance may occur [1, 2, 3] and can be used in various model updating schemes, see for example [4, 5], preferably together with their corresponding mode shapes. The damping ratios are needed to estimate the response amplitudes for different train speeds and will not be treated here. Naturally, estimates of the properties of higher order modes would also be desirable, but are more difficult to obtain.

In applications of structural health monitoring (SHM), an awareness of temporal variations in the dynamic properties of the structure being monitored is also very important. Such systems need to update the "healthy" state according to the seasonal variations so as to avoid false positives as suggested by Peeters et al. [6].

*Corresponding author
Email address: `mahir.ulker@byv.kth.se` (Mahir Ülker-Kaustell)

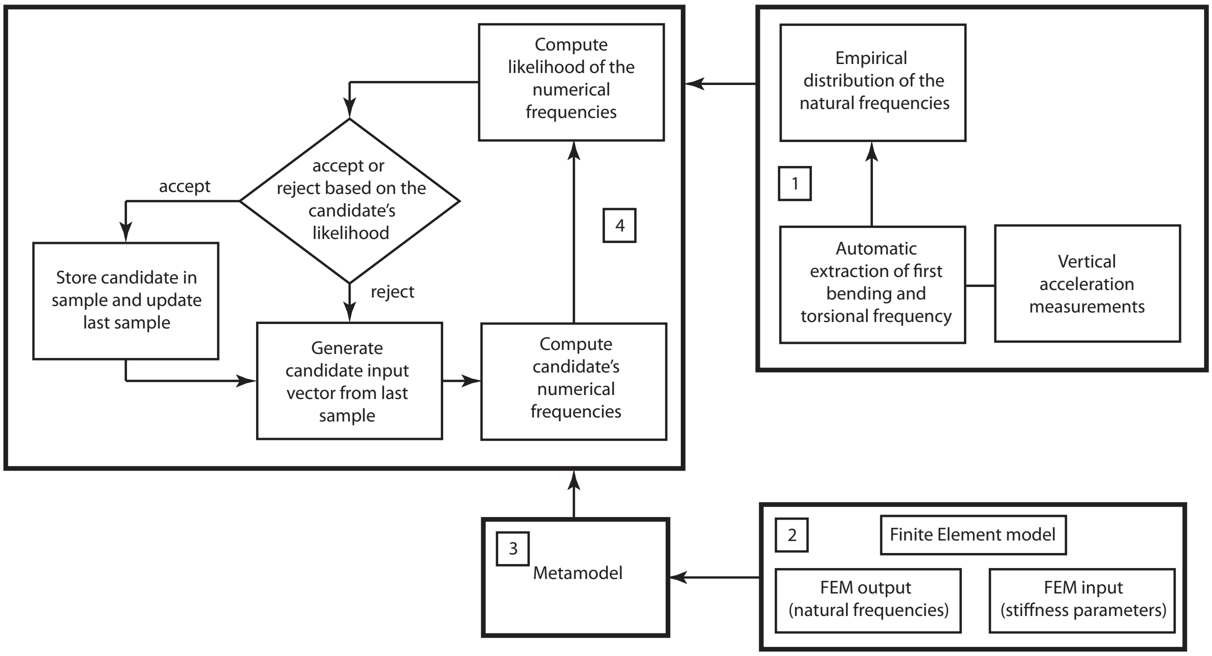

Figure 1: Schematic diagram of the updating method used in this study. It includes the acquisition and analysis of data (upper-right section), the development of the model and meta model (lower-right corner) and the updating procedure (left section) that builds on the results of the two previous steps.

Resonance between the train and the bridge can occur whenever the train passing frequency (i.e. the ratio between the train speed v and some characteristic length L such as the boggie distance or the carriage length) coincides with a natural frequency f_n of the bridge. Clearly, the modes of vibration with the lowest frequencies will be more sensitive to this phenomenon because they will be excited by lower train speeds, but also because they are not as efficiently attenuated as higher order modes. Therefore, accurate estimates of the natural frequencies are very important and overestimated frequencies may lead to unsafe decisions as the critical train speeds are then also overestimated. It is a well known fact that for linearly elastic, lightly damped structures, the natural frequencies and their corresponding mode shapes essentially depend on the spatial distribution of stiffness and inertia. The inertial properties of the structure can typically be fairly well estimated using the design drawings, although some variability in the amount of ballast and in the density of the ballast is expected due to track maintenance operations.

The goal of this study is to infer some stiffness properties of the ballast and subsoil from measurements carried out on the bridge, taking seasonal effects in consideration. However, as will be shown, other mechanisms may be relevant in describing the theoretical modes of vibration of the structure in a sufficiently accurate way. Bayesian updating of a 3D finite element (FE) model with Markov-Chain Monte Carlo (MCMC) sampling is applied to determine posterior distributions of the uncertain parameters in the warm and cold states of the bridge. The process used to obtain the distributions of the chosen uncertain parameters/mechanisms can be divided in the following steps:

1. Data collected for over one year of monitoring was analyzed. The eigenfrequencies for the first vertical bending mode and the first torsional mode were extracted from the data and studied.
2. A FE model of the structure was devised. The model was parameterized so that the parameters representing the uncertain parameters/mechanisms could be treated as unknown variables. The FE model thus represents a function that takes the uncertain stiffness pa-

rameters as arguments and returns the eigenfrequencies corresponding to the studied modes of vibration.

3. A large number of inputs (uncertain parameter sets) were evaluated in the model and the sought eigenfrequencies obtained by solving the corresponding eigenvalue problem. The parameter ranges were chosen to cover all the values that can be expected within reasonable limits. From this result a meta model was constructed by fitting a Gaussian Process. The purpose of the meta model was to bypass the computationally expensive model in the following step.
4. A Bayesian updating scheme was used to update the distribution of the chosen stiffness properties, using the meta model to calculate the likelihood of any given input.

The result of this process (graphically depicted in figure 1) is an estimation of the distributions of the uncertain parameters, which result in a frequency distribution in the theoretical model that matches the observed one. In section 3, we describe the structure, its instrumentation and an analysis of the estimated natural frequencies. The Bayesian updating scheme is described in detail in section 4 and the finite element model used to define our theoretical model is described in section 5. The results of the model updating are presented in section 6 and its implications are discussed in section 7, which also presents a summary of the conclusions drawn from the study and suggestions for future research.

2. Background

Studies of this kind are not very common in the literature. However, some references do treat the issue and related questions.

Xia et al. [10] presented a review of temperature effects in the context of vibrations of civil structures, but the temperature span mainly covered temperatures above the freezing point.

Yang et al. [11] reported variations in the natural frequencies of the first transversal modes of vibration of a road bridge of several spans due to seasonal variations. The frost in the ground was found to be a likely cause. Similarly, [12] observed large variations in the first three modes of vibration in a steel-concrete composite road bridge during a 9 month period and suggested that the freezing of the supports could give a reasonable explanation to these observations.

Simonsen et al. [8] presented results of laboratory tests on the resilient modulus of soil materials ranging from marine clay to gravelly coarse sand. The resilient modulus was found to increase by 1-2 orders as the temperature was decreased from 0°C to -10°C and the most considerable increase appeared in the temperature interval $(-5, 0)$°C. The resilient modulus in the unfrozen state, after one freeze-thaw cycle, was found to decrease by approximately 20 % for the gravelly sand and as much as 60 % for some of the other tested soils. One must therefore conclude that these relations are more complicated in an in-situ soil, being subjected to repeated freeze-thaw cycles. Nevertheless, the results presented by Simonsen et al. serves well to illustrate the variability in the elastic properties of soil materials due to seasonal variations.

Li et al. [9] performed cyclic triaxial tests on different sand specimens and found that the dynamic modulus of elasticity increased with decreasing temperature, much in the same way as in [8], and that the material damping ratio decreased by a factor 2 or more as the temperature decreased form 0 to -10°C.

Ice is a highly complicated material, the mechanical properties of which depends on the way it was formed, temperature and variations in temperature, air humidity and several other factors [13]. Due to the complexity of this material, there are not many tabulated values of its properties, but there are many publications which discuss the topic. Here, we simply state that many sources imply that the elastic modulus of ice is in the order of 1–10 GPa, which indicates that the observations made in the above cited references regarding the elastic properties of soil materials in a frozen state are reasonable.

3. The bridge

In this section, the bridge, its instrumentation and an analysis of the measured data are presented. The studied bridge is situated in the northern parts of Sweden and has its longitudinal axis in the north-south direction. A photo of the bridge is shown in figure 2. It has a horizontal skew of 30°, a span length of 36 m and carries one ballasted track. The thickness of the reinforced concrete deck varies between 320–350 mm and its total width is 6.7 m. The cross section of the two main steel beams varies

Figure 2: The bridge at Skidträsk.

along the bridge and have an average height of approximately 1.7 m. The main beams are connected with transverse braces at 4 sections along the beam as well as at the beam ends. One of the supports is fixed, but free to rotate over the transversal axis and the other end is supported on roller bearings to relieve constraints essentially caused by annual temperature variations. The bridge is founded on shallow foundations on an approximately 5 m thick layer of silty moraine. The geotechnical survey estimated the modulus of elasticity of the subsoil to be approximately 30 MPa and its density was determined as 1700 and 2000 kg/m^3 for the drained and undrained state, respectively. This estimate of the elastic modulus of the subsoils is intended for calculations of long-term settlements and is therefore a lower bound, characteristic value. The foundation plates have the width $W = 9.2\,\text{m}$ and the length $B = 5.8\,\text{m}$ and are placed with a skew of 30° with respect to the bridge center line.

3.1. Instrumentation

The instrumentation used in the current study consisted of three accelerometers and a temperature gauge. The data acquisition system consisted of a Spider8 data logger from HBM[1] and a laptop PC. The accelerometers are of the MEMS-type, manufactured by Colibrys[2] and encased by the laboratory personnel at KTH, Department of Structural Design and Bridges. These were placed under the top flanges inside the bridge, one on each main beam at mid span and one on one of the main beams at the quarter point. The temperature gauge was placed so as to measure the outdoor air temperature.

The accelerometers could thereby be used to identify the first vertical bending mode by taking the mean value of the response at mid span and the first torsional mode by taking the difference between the responses at mid span. However, there should be a transversal mode within the range of frequencies where the first vertical bending and the first torsional mode reside. The instrumentation did not include any device measuring in the transversal direction and therefore, it could not be identified from the measurements. The accelerometer at the quarter point could be used to identify the second vertical bending and torsional modes, but they were generally not well excited in the free vibrations.

3.2. Estimation of natural frequencies

The frequencies were determined by peak picking in Fourier transforms of the windowed free vibrations signals. All train passages that could be clearly identified by an automated procedure from the approximately 7000 logged train passages were used. However, the instrumentation was not initially designed for the current purpose. Therefore, some of the train passages were truncated very early in the free vibrations, so that the average time of free vibrations was sometimes only 10 seconds or even less. Complete train passages show that the free vibrations last for approximately 30 seconds, so even if the trigger system would have been able to correctly capture the free vibrations, the frequency resolution would still only be $\Delta f = 1/30 = 0.033\,\text{Hz}$. The studied natural frequencies lie in the range 3.5–8 Hz so an absolute error of $1/10 = 0.1\,\text{Hz}$ is not acceptable. To overcome this problem, we used zero padding so that each signal was 500 seconds long.

Another issue lies in the fact that the natural frequencies are dependent on the amplitude of vibration during free vibrations [7]. Therefore, the signals used in the updating procedure were truncated so that the maximum amplitude of vibration was $0.02 m/s^2$. The analysis presented in [7] was based on signals from the same bridge during autumn and showed that the natural frequency f_1 (given in Hz) of the first vertical bending mode is well described

[1] http://www.hbm.com
[2] http://www.colibrys.ch

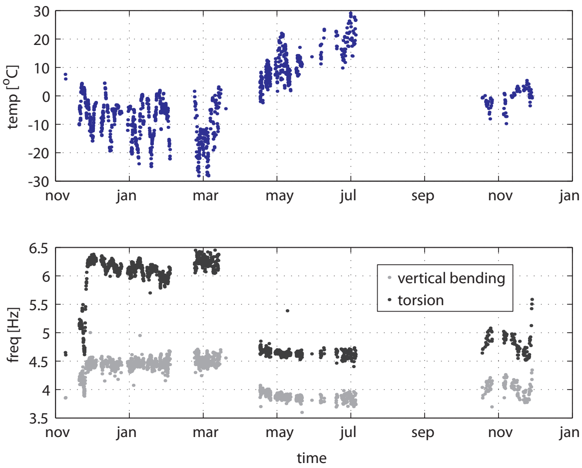

Figure 3: The variation in the estimated frequencies and the temperature during the periods of measurement.

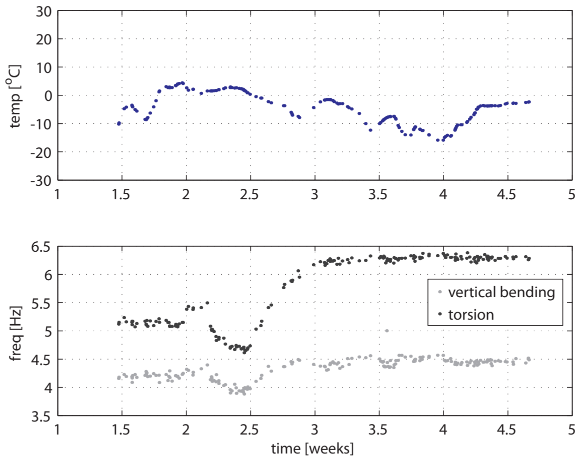

Figure 4: The variation in the estimated frequencies and the temperature during the first 4 weeks of measurement.

by the linear function

$$f_1(a_{\mathrm{m}}) = 3.88 - 1.16a_{\mathrm{m}} \qquad (1)$$

where $a_{\mathrm{m}} \in (0, 0.2)\mathrm{m/s}^2$ is the vertical acceleration.

3.3. Estimated natural frequencies

We wish to use the term *cold period* for the time of the year when the frost in the ground is permanent, i.e. approximately between December and April at this particular location and the term *warm period* for the part of the year when there is no frost in the ground. The transition periods between the cold and the warm period are simply referred to as *transition periods.*

Figure 3 shows the variation in the natural frequencies and the temperature over the whole period of measurements. Unfortunately, technical problems with the data acquisition system caused a few gaps in the time series, but they still give a good picture of the annual variation in the natural frequencies. In figure 5, the frequencies of the studied modes are plotted as functions of temperature. The frequency estimates have been color coded so that the transition zones into the warm state (corresponding to the months of March and April) gradually change from black to grey. This clearly shows how the frequency of the first vertical bending mode tends towards their warm state values (3.8 Hz), but it takes weeks of temperatures above 0 °C to reach it. The frequency of the first torsional mode can be seen to reach it warm state level much quicker.

A reasonable explanation for this behavior could be the development of the frost in the ground and the formation of ice within the track superstructure. However, since the superstructure is more exposed to the climate than the soil, the frost in the ground can be expected to vary slower than in the ballast. It typically takes in the order of days of temperature above or below the freezing point to cause relevant variations in the frost front. As can be seen in figures 3 and 4, the natural frequencies appear to vary somewhat in a daily basis, but major changes caused by a few days of temperatures above 0 °C can only be seen in the torsional frequency. This was consistent with the finding that in the theoretical model (described in section 5), the torsional frequency depended mostly on the ballast stiffness, while the bending frequency was more affected by the soil stiffness.

Another possible mechanism which may be involved is the fouling of the ballast, i.e. the emergence of finer materials within the ballast which appear as a consequence of the deterioration of the track caused by the traffic loads, but also by maintenance operations such as tampering and realignment of the track [14]. Eventually, these finer particles will fill the voids between the ballast particles and provide the ballast bed with a hydraulic conductivity, see [15] and the references therein. Hence, if the ballast is fouled to a certain degree,

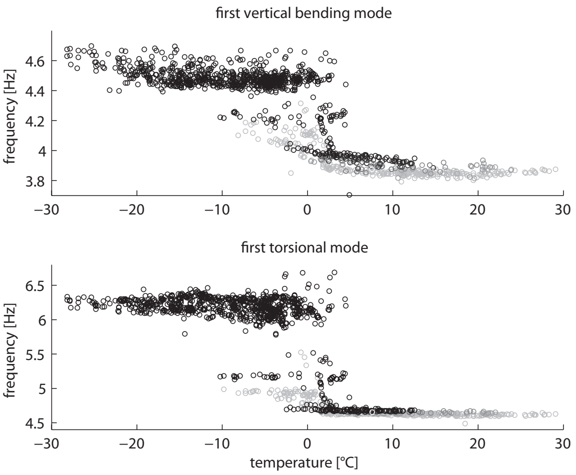

Figure 5: The variation in the frequency of the first vertical bending mode (top) and the first torsional mode (bottom) as function of temperature.

it appears likely that it holds a certain amount of water which could freeze. When spring begins, the temperature increases continuously, and the frost in the subsoil and in the track superstructure gradually disappears, which manifests itself in a more well-behaved variation in the natural frequencies of the structure. It should be noted that within this reasoning, the natural frequencies cannot be regarded as functions of temperature, but rather as functions of the freezing index, a quantity used in the geotechnical community to estimate the depth of the frost front [16, 17]. Simply put, the freezing index is the time integral of the temperature (at the ground surface) below the freezing point from the beginning of the cold period. Other factors such as snow cover and the location of the phreatic surface may also influence the frost depth.

To the authors knowledge, there are no studies available regarding frozen ballast in railway applications and thus, the above reasoning is mainly based on qualified guesses. Nevertheless, these findings imply that the cold state is more favourable than the warm state in terms of train-bridge resonance, since the natural frequencies increase and thereby, the critical train speeds. Furthermore, these implications should hold true for railway bridges in general and particularly for ballasted railway bridges. However, in a state of resonance, the structural damping is the governing parameter and further research is therefore needed.

4. MCMC Bayesian updating

Bayesian updating is a technique to take into consideration new knowledge (also called evidence) about stochastic variables. If a certain variable, due to epistemic or statistic uncertainty, is given an initial probability distribution, subsequent measurements of that variable can improve the available knowledge about it and thus lead to a modified and more accurate probability distribution. This process can be performed in a rigorous and systematic way using Bayes theorem [18]. The initial assigned probability distribution is called the prior distribution, while the updated distribution that takes the new evidence into consideration is called the posterior distribution. Bayes theorem states that the (posterior) probability P_{post} of a certain event x given a set of observed evidence Y_{obs} equals the normalized product of the likelihood of the evidence given the event, and the probability of the event disregarding the evidence

$$P_{\text{post}}(x|Y_{\text{obs}}) = \frac{P_{\text{prior}}(x)L(Y_{\text{obs}}|x)}{\int_x^\infty P_{\text{prior}}(x)L(Y_{\text{obs}}|x)\mathrm{d}x} \quad (2)$$

This normalizing constant given in the denominator of equation (2), called Bayes integral, is the likelihood of the evidence disregarding the event (i.e. the integral over all possible events). Bayes integral is expensive to evaluate, because it generally involves multidimensional numeric integration, but there are methods to obtain the posterior distribution without having to evaluate this integral [19]. In this study, Markov-chain Monte Carlo (MCMC) sampling was used [20].

A drawback of using MCMC is that the direction of each computational step is determined by the Markov-chain and hence, are not known beforehand. Therefore, the algorithm cannot be parallelized and the computationally expensive evaluations of the 3D finite element structural model must be performed sequentially. However, this can be improved by means of a meta model (see section 5.4), which can be evaluated very quickly.

In our study we attempt to find the probability distribution of the stochastic properties of our model given our evidence (i.e. the measured eigenfrequencies). The variables considered stochastic in our model were the modulus of elasticity of the ballast, the subsoil and the concrete, the longitudinal track stiffness and the mechanism controlling the longitudinal motion of the roller bearings. All the variables were updated together, resulting in a multivariate distribution that considers the interdependence of the variables.

In other words, we want to determine the multivariate distribution of the properties of the bridge, that we chose to update, that will result in a theoretical frequency distribution that approximates the observed one. The observed frequency distribution is bivariate, since two eigenfrequencies are considered. Naturally, when the first eigenfrequency is high it is expected to be due to high stiffness parameters, which should lead to a high value of the second eigenfrequency also, so the distribution for the two first eigenfrequencies is obtained considering their interconnection.

4.1. Markov-chain Monte Carlo sampling

As mentioned above there are methods for updating a distribution according to Bayes theorem without having to compute Bayes integral. One well-established family of such methods is the Markov-chain Monte Carlo sampling methods. As the name indicates, in these algorithms a Markov Chain is generated which, asymptotically, can be shown to behave as the sought distribution. MCMC methods are designed to sample from distributions with a known algorithmic expression, but that are difficult to sample from analytically.

The modified version of the Metropolis-Hasting sampling algorithm [21, 22] used in this study was first suggested by Tarantola [23]. The algorithm starts from an initial point X_i in the space to explore. This X_i can be set manually or chosen at random from the prior distribution and it constitutes the first sample of the collections of samples to generate. X_{last} denotes the last X generated. Initially X_{last} is X_i. The theoretical (meta) model M is evaluated with input X_{last} and the eigenfrequencies F_{last} are obtained. Two likelihoods are then obtained L^1_{last} which is the likelihood of the input X_{last} with respect to the prior distributions

$$L^1_{\text{last}} = P(X_{\text{last}}) \tag{3}$$

and L^2_{last} which is the likelihood of the output $M(X_{\text{last}})$ and is computed from the known distribution of eigenfrequencies

$$L^2_{\text{last}} = P(F_{\text{last}}) = P(M(X_{\text{last}})) \tag{4}$$

A candidate X_{can} is picked from a distribution that depends only in the previous sample X_{last}. Typically a normal distribution centered in X_{last} is used to generate the candidate X_{can}.

$$X_{\text{can}} = X_{\text{last}} + N(0, \sigma) \tag{5}$$

where σ is some predefined variance. Then, the likelihoods L^1_{can} and L^2_{can} of X_{can} are computed as above, the first with respect to the prior distributions and the second as

$$L^2_{\text{can}} = P(F_{\text{can}}) = P(M(X_{\text{can}})) \tag{6}$$

and their ratios a and b are computed

$$a = L^1_{\text{can}}/L^1_{\text{last}} \tag{7}$$

$$b = L^2_{\text{can}}/L^2_{\text{last}} \tag{8}$$

The candidate X_{can} is accepted with certainty if $a > 1$ and $b > 1$ (i.e. if the likelihood of the candidate is larger than that of the latest accepted sample) and, if $a \leq 1$ and/or $b \leq 1$ X_{can} is accepted with respect to the prior distribution with probability a and with respect to the known distribution of eigenfrequencies with probability b. For this, a random number between 0 and 1 is generated from a uniform distribution. If this random number is less than a (or b) then X_{can} is accepted with respect to the prior distribution (or with respect to the known distribution of eigenfrequencies). If not, X_{can} is rejected. It is necessary that X_{can} passes both tests in order to be accepted. If X_{can} is accepted it is added to the list of samples and X_{last} is updated as

$$X_{\text{last}} = X_{\text{can}} \tag{9}$$

and the process is repeated. If the candidate is rejected a new candidate is generated and the process is repeated. The two acceptance/rejection tests are done in sequential order. The test with respect to the known distribution of eigenfrequencies is computationally more expensive since it requires an evaluation of the meta model and is therefore performed only if the test with respect to the prior distribution has been successfully passed.

Each new sample X requires at least one call to the model (more if some candidates are rejected). Any sample X will be directly dependent on the previous sample. Thus, the process cannot be parallelized. This justifies the use of a meta model to avoid evaluating the computationally expensive FE model. The MCMC algorithm requires a larger number of evaluations of the theoretical model than the determination of a reliable meta model. More importantly, when computing the meta model each evaluation of the theoretical model is independent and can thereby be parallelized, rendering the computation much faster. Both the theoretical finite element model and the meta model are described in section 5.

There is a certain transient period before the samples converge to the desired distribution, so the first N samples obtained in this way are discarded. The discarded samples are called the burning period. The number of iterations required for the algorithm to converge, the burning period and the distribution from which the candidates are sampled are open parameters that the user must set, but there exist convergence monitoring algorithms [24].

4.2. Prior distributions

The prior distributions where chosen to be uniform for the elastic modulus of the ballast and the soil, reflecting our lack of knowledge regarding their variation over the seasons. For the concrete stiffness the prior was chosen to be normal with mean 38 GPa and standard deviation 2.5 GPa. The characteristic elastic modulus of the concrete quality used in the bridge deck was 32 GPa and the coefficient of variation for this parameter is approximately 0.1. The mean value was chosen assuming that the concrete is un-cracked and that the dynamic nature of the loads motivates an increase in the modulus of elasticity with a factor 1.2 (corresponding to a dynamic modulus of elasticity). The mechanisms of the roller bearings were set to be fixed, following the conclusion from the 2^n factorial design used to determine which parameters to study and their ranges (see section 5.1). Finally, the longitudinal track stiffness was found to have very little influence and therefore it was ignored in the updating scheme.

5. Finite element modelling

The commercial finite element code ABAQUS[3] was used to model the structure and the abutments. Combinations of beam, shell and solid elements were used where appropriate. Different element types and geometrical entities were coupled together using constraint equations and a type of elements referred to as connector elements. The connector elements are used to couple two nodes in

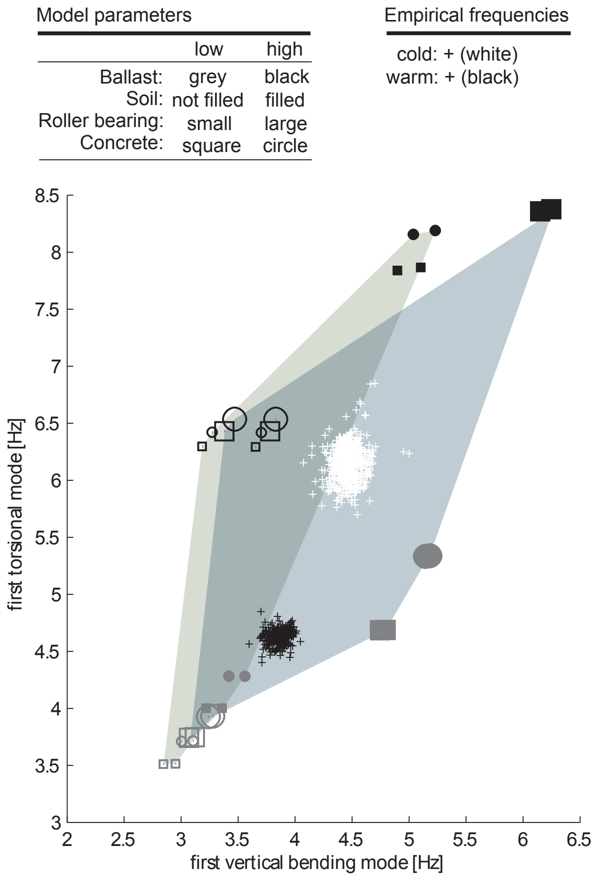

Figure 6: The result of the final 2^n factorial design, together with a the natural frequencies (+) of the bridge for the cold (white) and warm (black) states, as estimated from the measured free vibrations (the transition zone frequencies have been left out for clarity).

quite arbitrary ways; they can be used to define constraints, but the constitutive relation between the two nodes can include stiffness, viscous damping, friction, stop and lock elements in various combinations. Thus, connector elements are highly useful for modelling mechanisms such as roller bearings.

5.1. Relevant parameters and mechanisms

It goes without saying that in order to obtain a well-posed inverse problem, the theoretical model must describe the underlying physics in an appropriate manner. The so called 2^n factorial design (see for example [25] for details) provided an efficient method to determine which parameters to study in detail. In the present context, where a numerical model is studied with a factorial design,

[3]http://www.3ds.com

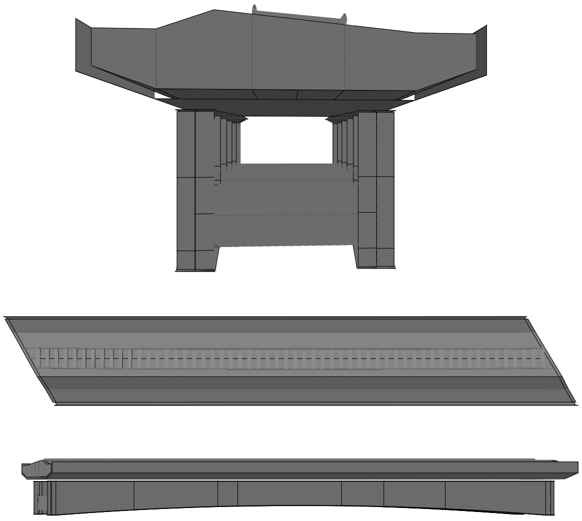

Figure 7: Views of the 3D finite element model

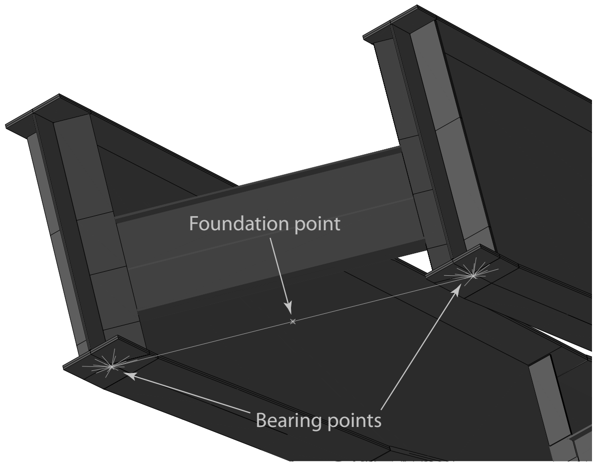

Figure 8: Description of constraint definitions at the supports.

the errors (model error and numerical errors) are deterministic. Thus, the method simply consists in choosing a number n of parameters to vary and then to compute the model response, assigning these values a high or a low value. Hence, one performs 2^n tests and then use some convenient method to visualize the results. An example is given in figure 6, which shows the final factorial design used to define the meta model on which the Bayesian updating procedure was based, together with the natural frequencies estimated from the measurements during the warm and the cold states, i.e. the transition periods have been left out for clarity.

A few different versions of the model was studied in order to determine a final set of parameters and mechanisms to include, namely

i. The modulus of elasticity of the subsoil and embankments E_{s}
ii. The modulus of elasticity of the ballast E_{b}
iii. The modulus of elasticity of the concrete E_{c}
iv. The fixation of the roller bearings
v. The longitudinal track stiffness

As can be seen in figure 6, this set of model parameters spans the domain of frequencies defined by the frequencies estimated from the measurements. Thus, it was assumed that this model is representative for the bridge during all seasons, under small amplitudes of vibration. The longitudinal track stiffness did not have any significant influence on the theoretical frequencies, but was kept as it did not increase the computational work. It can be seen from the figure that it is the large markers (corresponding to fixed boundary conditions at the roller bearings) that enclose all the measured frequencies. It was therefore concluded that the translation of the bearing mechanisms at the roller bearings must be fixed for such small amplitudes. Further, it was observed that the main factor affecting the first torsional frequency was the ballast stiffness and that, conversely, the soil stiffness was the parameter than more directly affected the first vertical bending frequency. This is consistent with the results shown in figure 4 where the torsional frequency is more affected by short periods of high temperatures. The ballast (on which the torsional frequency primarily depends) is more exposed to the environment that the soil and was expected to respond more rapidly to change in temperatures than the soil, which affects mainly the first vertical bending mode.

5.2. Modelling of the bridge

Assuming very small amplitudes of vibration, the steel and concrete was assumed to be linearly elastic. Effects of cracks in the concrete deck was ignored and attributed to the variability of the elastic modulus of the concrete. The mechanical properties of constructional steel are well known and the modulus of elasticity $E_{\text{steel}} = 210\,\text{GPa}$, the Poisson's ratio $\nu_{\text{steel}} = 0.3$ and density $\rho_{\text{steel}} = 7850\,\text{kg/m}^3$ was assumed.

Table 1: Comparison between static foundation stiffness coefficients for $E_{\text{soil}} = 50\,\text{MPa}$.

	k_x [GN/m]	k_y [GN/m]	k_z [GN/m]	k_{rx} [GNm/rad]	k_{ry} [GNm/rad]	k_{rz} [GNm/rad]
Handbook [26]	0.694	0.668	0.832	13.7	6.47	15.3
FE-model	0.774	0.731	1.292	15.0	7.97	16.3
ratio FE/handbook	1.12	1.09	1.55	1.09	1.23	1.07

As shown in figure 7, all relevant structural details were included in the model. The plates were modelled using quadratic shell elements and the cross-bracings were modelled using Timoshenko beam elements. The concrete deck as well as the edge beams were modelled with quadratic shell elements. Hence, it was assumed that the edge beams contribute not only with their mass, but also with their stiffness. The ballast was modelled using quadratic solid elements. The track was modelled with Timoshenko beam elements, which were perfectly coupled with the ballast by means of constraint equations.

A number of more complicated constraints were defined in order to capture the effects of the eccentricities at the supports of the main beams. The support points on the main beams were coupled to "bearing points" in order to define appropriate models of the bearing mechanisms. The bearing points were then rigidly connected with a point at the center of the bearings at each support to enable the introduction of the foundation stiffness there, see figure 8. The support points at support 1 were defined so that all the translations there were fixed while the rotations over the y-axis were free, while the support points at support 2 were defined with an elastic constraint in the longitudinal direction. This elastic constraint was then used to simulate free or fixed rolling of those two bearings by assigning either a very low or a very high value to it.

The track ends were connected to fix points with longitudinal spring elements to model the continuity of the track. The stiffness of these spring elements was modelled as a bar, resting on a longitudinal Winkler bed, stretching towards infinity in one direction

$$k = \sqrt{cEA} \tag{10}$$

where c is the longitudinal stiffness of the Winkler bed and E and A are the modulus of elasticity and cross-sectional area of the bar, i.e. the two rails (UIC60). Furthermore, the ballast ends were connected to a longitudinal spring to model the stiffness of the embankment. The stiffness of this spring was computed from the model of the abutments described in section 5.3.

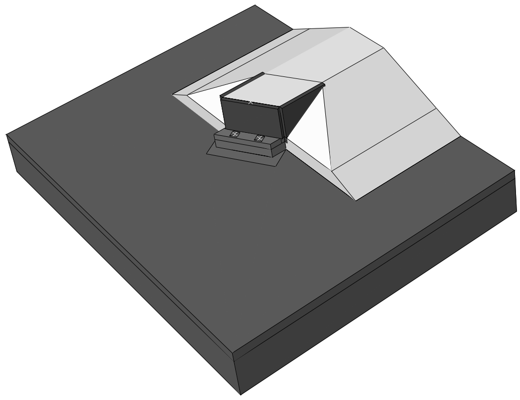

Figure 9: View of the finite element model of one of the abutments

5.3. Modelling of the foundations/abutments

It is well known that the dynamic stiffness of shallow foundations, for small soil strains in a linearly elastic homogeneous material, are dependent on the frequency of vibration. However, in the present context, where the elastic modulus of the soil is treated as a stochastic variable and only a limited range of low frequencies are of interest, the variation in the foundation stiffness due to its frequency dependency is likely to drown in the uncertainty of the elastic modulus of the soil. Therefore, in modelling the foundation stiffness, the relation between the stiffness coefficients are of greater concern than the absolute value of the soil material parameters. In order to obtain a reasonable approximation of this relation, a further assumption was introduced, namely that the embankment material had the same elastic properties as the subsoil. Then, a model of the entire abutment could be defined (see figure 9), from which the static stiffness matrix of the support points could be approximated, assuming also that the soil-structure interface is perfectly coupled. The use of only one soil elastic modulus simplifies the analysis much since then, as a consequence of assuming the soil to be linearly elastic, the stiffness coefficients can be scaled with the soil elastic modulus in a straightforward manner. Thus we performed only one evaluation of the abutment model using a reference value of 50 MPa for the soil modulus of elasticity.

It should also be mentioned that there is a coupling between the various degrees of freedom of the abutment (seen as a rigid body, since the concrete structure is much stiffer than the surrounding soil), but it is typically one order smaller than the diagonal components and is therefore neglected.

The FE model of the abutments was meshed with linear tetrahedrons. The bottom surface was constrained in all translations while the sides were constrained so that only the translations perpendicular to each side was constrained. A twice as large model was used to verify that a sufficient volume of the surrounding soil was included. The assumption that the static stiffness coefficients would suffice simplified this analysis greatly in that we did not need to fulfill the radiation condition, i.e. the propagation of elastic waves away from the source (the abutment).

Table 1 shows a comparison between the stiffness coefficients thus obtained and those determined from handbook [26] formulas. Naturally, the static stiffness of all degrees of freedom are increased by introducing the abutment and the embankment.

5.4. The meta model

Having determined a suitable numerical model for describing the free vibrations of the bridge at amplitudes of vibration less than 0.02m/s^2, a meta model was calculated in order to apply the MCMC updating scheme in an efficient manner. The meta model was created based on the computation of the eigenfrequencies and eigenmodes of the model using 5000 randomly chosen parameter combinations. The elastic modulus of the ballast and the soil were chosen from exponential distributions, i.e. a cumulative distribution function of the form

$$P(x, \lambda) = (1 - e^{-\lambda x})H(x) \tag{11}$$

Table 2: Parameters of the updated distribution functions. The subscripts b, s and c on the elastic moduli E correspond to ballast, soil and concrete, respectively.

		warm		cold	
		μ	$\frac{\sigma}{\mu}$	μ	$\frac{\sigma}{\mu}$
E_b	[MPa]	177.0	14.4	1450	0.22
E_s	[MPa]	74.7	3.80	107.6	17.7
E_c	[GPa]	37.6	2.50	38.1	3.20

with a 1 % probability of exceeding 5 GPa and 9 GPa, respectively. In equation (11), $H(x)$ is Heaviside's function. This corresponds to the parameters $\lambda_\text{ballast} = 9.1 \cdot 10^{-10}$ and $\lambda_\text{soil} = 5.1 \cdot 10^{-10}$. The longitudinal track stiffness c at the transition zones between the bridge and the embankments was also chosen from an exponential distribution with 1 % probability of exceeding $500\,\text{MN/m}^2$. The modulus of elasticity of the concrete was chosen from a uniform distribution with values in the range of 28–48 GPa and finally, the mechanism of the roller bearings was chosen from a uniform distribution of the integers 0 (free) and 1 (fixed).

The distinction between different mode shapes was made by studying the modal participation factors. For some parameter combinations, a transversal bending mode appeared in between the first vertical bending mode and the first torsional mode.

The data obtained from the FE simulations was divided into a training set and a validation set. The meta model was created by fitting a Gaussian Process to the input-output pairs (matching stiffness parameters to eigenfrequencies) from the training set. This was achieved with the algorithms described and implemented in [27]. The meta model was validated by comparing its output with the output of the FE model in the validation set.

6. Result

Figure 10 shows the marginal distributions functions computed in the warm state for each of the most influential parameters (panels in the diagonal subplots), i.e. E_ballast, E_soil and E_concrete, together with the pairwise relations between them, shown in scatter plots in the non diagonal subplots. The corresponding data for the cold state is plotted in figure 11. In the warm state, three distinct unconnected groups of parameter combinations can

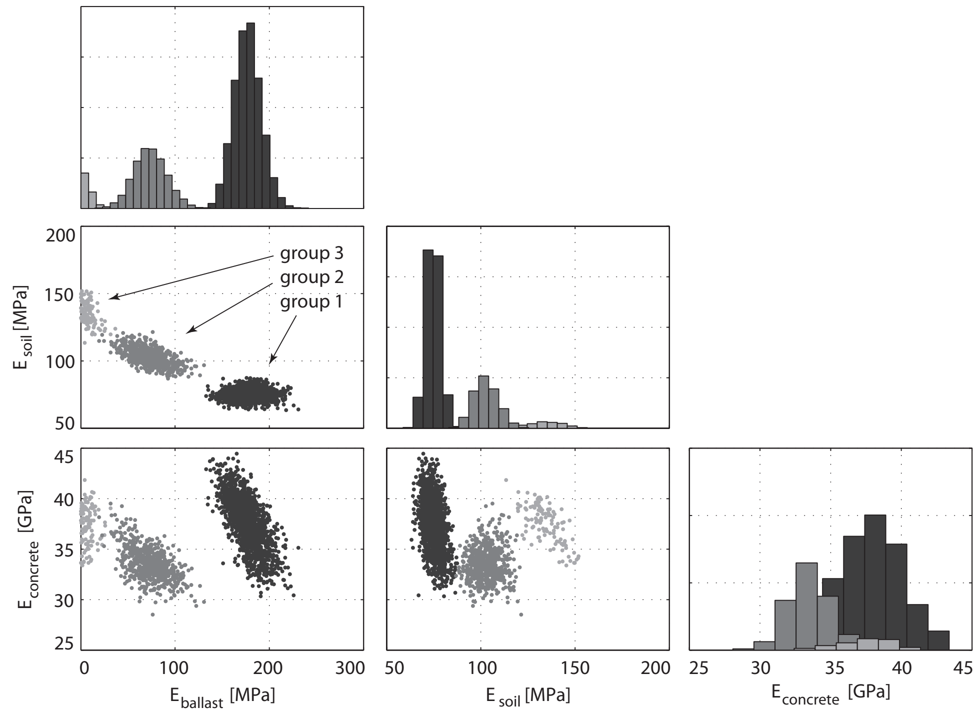

Figure 10: Plots of the updated variables in the warm condition.

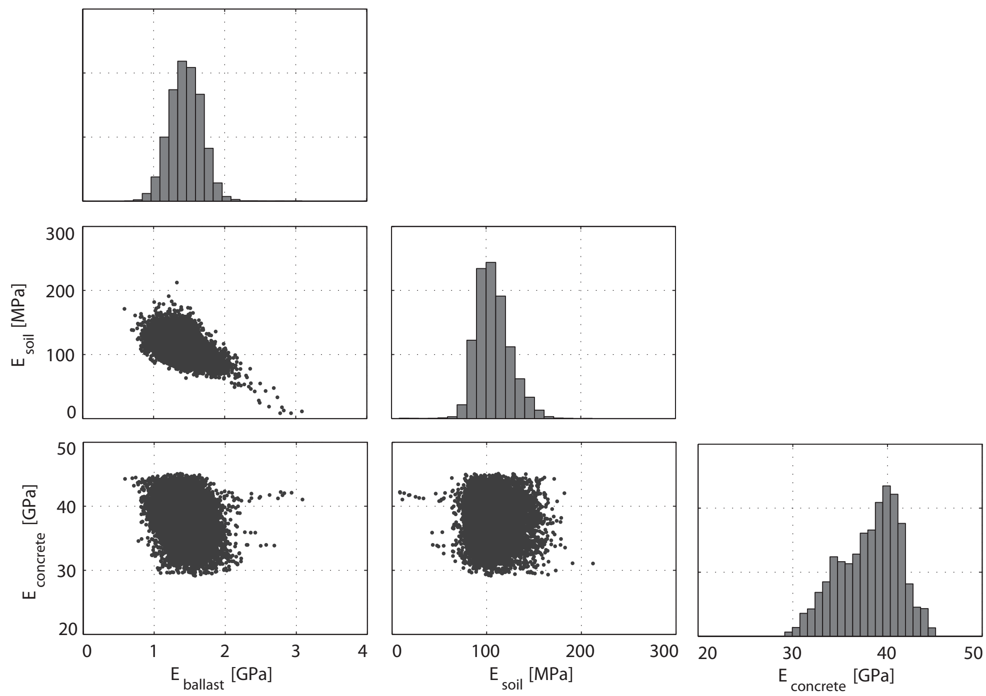

Figure 11: Plots of the updated variables in the cold condition.

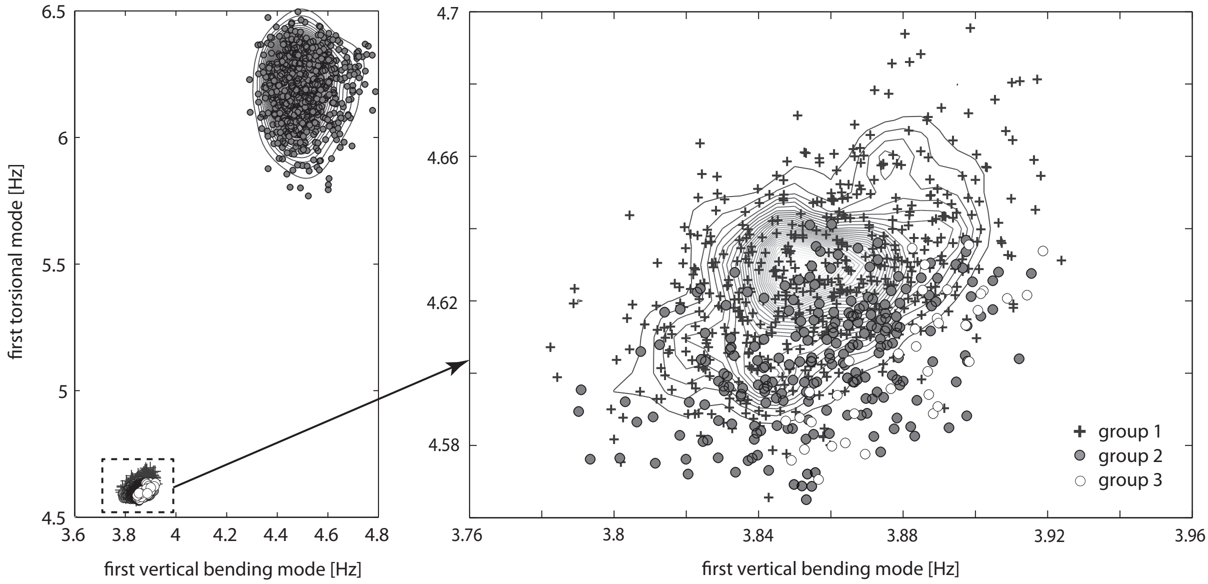

Figure 12: Comparison between the updated model and the measured frequencies in both the cold and the warm state (left) and a zoom (right) on the warm state, where the three different groups of theoretical parameter combinations are more clearly shown. The measured eigenfrequencies are shown as contours, computed using kernel density estimation.

be seen. In figure 10, they have been marked with different shades of grey, where the darkest shade represents the group which, in the authors opinion, appears to describe the real physical bridge, while the others seems to be artifacts of the method. The groups are ordered in ascending numbers so that the most realistic group is given the number 1 and so on. There are several arguments that indicate that group 1 is the one really describing the structure. Firstly it is the one with highest likelihood. Further, group 1 clearly covers the entire range of measured frequencies, as shown in figure 12 (where the measured frequencies have been plotted as contours using kernel density estimation) while the other groups only cover it partially. Another reason to believe that group 1 is the correct is that there, the distribution describing the stiffness of the concrete is practically the same as that obtained in the cold conditions, and the concrete stiffness can be expected to vary relatively little with temperature. Furthermore the mean values for soil and ballast stiffness are closer to what previous experiences indicate. In the cold state, the updating algorithm resulted in a more straight-forward distribution of the parameters, although the shape of the bar plot for the modulus of elasticity of the concrete is rather jagged. Clearly, higher values are obtained for the soil materials. The modulus of elasticity of the ballast increased with one order of magnitude and the modulus of elasticity of the soil increased by a factor 1.4. The modulus of elasticity of the concrete increased slightly as compared to that of group 1 in the warm state.

7. Conclusions

A study of the seasonal effects on the stiffness properties of a ballasted railway bridge has been performed. The resulting distribution of the studied stiffness parameters for the cold and warm season was determined using Bayesian model updating.

Based on our findings, and those of the references given in section 2, we conclude that the observed variations in the stiffness of the structure are likely to have been caused by the frost in the ground and the development of ice within the track superstructure.

During the cold period of the year, the natural frequencies of the bridge increase by 15 % and

35 % for the first vertical bending and first torsional modes, respectively.

The first vertical bending mode is more sensitive to variations in the elastic modulus of the soil while the first torsional mode is more sensitive to variations in the elastic modulus of the ballast.

The torsional mode is more sensitive to variations in temperature than the bending mode.

Negligence in considering the above stated conclusions for bridges in this type of climate will lead to erroneous decisions for example when calculating the resonance speeds for high-speed railway bridges or to SHM systems which would then give false positives.

The variation in the modal damping ratios due to the seasonal effects must be studied in order to give a more complete picture of the structural behavior. It has been concluded herein that an analysis using frequencies from the cold season lead to overestimated critical train speeds. If the damping ratios also increase during the cold period, such data could be highly misleading. A study of the modal damping ratios is currently being prepared by the authors.

8. Acknowledgements

This work is partly funded by the European Commission, Marie Curie 7th Framework Programme Project "Long Life Bridges", funded under the Industry and Academia Partnerships and Pathways call, Grant Agreement No. 286276, the Railway Group at KTH, Royal Institute of Technology and Tyréns AB. This work was done with the invaluable assistance of Claes Kullberg and Steffan Trillkot.

9. References

[1] L. Frybá. Dynamics of Railway Bridges, Telford, London, 1996.
[2] L. Frybá. A rough assessment of railway bridges for high speed trains, Engineering Structures 23 (2001) 548–556.
[3] CEN, Eurocode 1: Actions on structures - Part 2: Traffic loads on bridges, CEN, European Comittee for Standardization, 2008.
[4] Friswell, M., & Mottershead, J. E. (1995). Finite element model updating in structural dynamics (Vol. 38). Springer.
[5] Brownjohn, J. M. W., Moyo, P., Omenzetter, P., & Lu, Y. (2003). Assessment of highway bridge upgrading by dynamic testing and finite-element model updating. Journal of Bridge Engineering, 8(3), 162-172.
[6] Peeters, B., Maeck, J. and De Roeck, G.. Vibration-based damage detection in civil engineering: excitation sources and temperature effects, Smart Materials and Structures 10 (2001) 518–527.
[7] M. Ülker-Kaustell, R. Karoumi, Application of the continuous wavelet transform on the free vibrations of a steel-concrete composite railway bridge, Engineering Structures 33 (2011) 911–919.
[8] E. Simonsen, V. C. Janoo and U. Isacsson. Resilient Properties of Unbound Road Materials during Seasonal Frost Conditions, Journal of Cold Regions Engineering 16(1), 2002.
[9] J. C. Li, G. Y. Baladi and O. B. Andersland. Cyclic triaxial tests on frozen sand, Engineering Geology, 13, 1979.
[10] Xia, Y., Chen, B., Weng, S., Ni, Y.Q., Xu, Y.L. (2012). Temperature effect on vibration properties of civil structures: a literature review and case studies. Journal of Civil Health Monitoring 2(1), 29-46. DOI: 10.1007/s13349-011-0015-7
[11] Z. J. Yang, U. Dutta, D. Zhu, E. Marx and N. Biswas. Seasonal frost effects on the soil-foundation-structure interaction system, Journal of Cold Regions Engineering, 21(4), 2007.
[12] Alampalli, S.. Influence of in-service environment on modal parameters, Proc. of IMAC 16 (Santa Barbara, CA, February 1998), 111–116.
[13] P. V. Hobbs (1974). Ice Physics, Oxford.
[14] Indraratna, B. and Salim W.. Mechanics of Ballasted Rail Tracks – A Geotechnical Perspective, Taylor and Francis/Balkema, 2005.
[15] Teenakoon, N., Indraratna, B., Rujikiatkamjorn, C, Nimbalkar, S and Neville T.. The role of ballast fouling characteristics on the drainage capacity of rail substructure, Geotechnical Testing Journal, 35(4), 2012.
[16] Johnston, G. H. (Ed.). Permafrost: Engineering Design and Construction, Wiley and Sons, 1981.
[17] Andersland, O. B. and Ladanyi, B.. Frozen Ground Engineering, Wiley and Sons, 2004.
[18] Goldstein M., Wooff D. (2007). Bayes linear statisticstheory and methods. Wiley Series in probability and statistics. Chichester, John Wiley & Sons.
[19] Ntzoufras, I. (2009). Bayesian modeling using WinBUGS. John Wiley & Sons.
[20] Gamerman, D., Lopes, H.F. (2006). Markov chain Monte Carlo: stochastic simulation for Bayesian inference. Boca Raton (FL), Chapman & Hall.
[21] Metropolis, N., Rosenbluth, A., Rosenblith, M., Teller, A., Teller, E. (1953). Equation of state calculations by fast computing machines. Journal of chemical Physics 21(6), 1087-1092.
[22] Hasting, W. (1970). Monte Carlo sampling methods using Markov chains and their application. Biometrika, 57(1), 97-109.
[23] Tarantola, A. (2005). Inverse problem theory and methods for model parameter estimation. Society for Industrial and Applied Mathematics (SIAM).
[24] El Adlouni, S., Favre, A., Bobee, B. (2006). Comparison of methodologies to assess the convergence of Markov chain Monte Carlo methods. Computational statistics and data analysis, 50(10), 2685-2701.
[25] Box, G. E. P., Hunter, J. S. and Hunter, W. G.. Statistics for experimenters, 2:nd edition, Wiley and Sons, 2005.
[26] H. Fang (Ed.), Foundation Engineering Handbook, 2nd Edition, Van Nostrand Reinhold, New York, 1991.
[27] Rasmussen, C.E., Williams, C. (2006). Gaussian Processes for Machine Learning. The MIT Press, Boston. ISBN 0-262-18253-X.

Paper IV

Influence of rate-independent hysteresis on the dynamic response of a railway bridge

To appear in the International Journal of Rail Transportation.

International Journal of Rail Transportation, 2013
Vol. 1, No. 4, 237–257, http://dx.doi.org/10.1080/23248378.2013.835129

Influence of rate-independent hysteresis on the dynamic response of a railway bridge

M. Ülker-Kaustell* and R. Karoumi

The Royal Institute of Technology, KTH, Brinellvägen 23, SE-100 44 Stockholm, Sweden

(*Received 18 June 2013; final version received 24 July 2013*)

It is well known that the dynamic properties of civil engineering structures have a more or less pronounced amplitude dependency. However, it is rather difficult to quantify this both experimentally and theoretically. This paper describes an attempt to identify the sources of the amplitude dependent variation of the natural frequency and the modal damping ratio of the first vertical bending mode of a simply supported, ballasted steel-concrete composite railway bridge. It is proposed that the most likely sources to the non-linear properties of this mode of vibration are the ballasted track, the foundations and the roller bearings used mainly to relive constraint forces due to changes in temperature. The non-linear influence of the suggested sources were modelled in a 2D finite element model using the classical univariate Bouc–Wen model which was implemented as a user-defined element in ABAQUS. The results suggest that the roller bearings alone can give account for the variation in the dynamic properties observed in experimental data from the bridge and that the combination with a simple model of the track superstructure gives the most realistic result. A tremendous increase in the dissipation of energy was found as the amplitude of vibration was increased beyond that available in the experimental data, thus motivating further research within this field.

Keywords: railway bridges; non-linear dynamics; soil–structure interaction; ballast; roller bearing; Bouc–Wen models

1. Introduction

In a previous publication [1], the authors have shown that the dynamic properties, i.e. the natural frequency and the modal damping ratio of a particular simply supported steel-concrete composite bridge have a certain amplitude dependency. The natural frequencies of the first vertical bending and the first torsional mode were found to decrease with increasing amplitude of vibration, while the corresponding damping ratios were found to increase. These results were obtained by analyzing the free vibrations of the bridge after a train passage by means of the continuous wavelet transform (CWT). Clearly, the reduction of the eigenfrequency may lead to non-conservative conclusions in terms of critical train speeds for high-speed railway bridges. However, the increasing damping ratio may very well compensate for this effect.

A simplified analysis based on a single degree-of-freedom system of the bridge was later performed [2] which confirmed the above stated suggestions. However, the nature of these non-linear effects is still unknown, although it was suggested that they may originate in soil–structure interaction since it is a well-established fact that soil materials have a similar qualitative behaviour. Other sources are also possible, such as the hysteretic

*Corresponding author. Email: mahir.ulker@byv.kth.se

behaviour of the roller bearings, the non-linear material properties of the concrete bridge deck and the interface between steel and concrete. However, in the author's opinion, the three most likely sources of the observed non-linear effects are

(1) Foundations
(2) Track superstructure
(3) Roller bearings

These all fall in the category of rate-independent hysteretic systems, as will be discussed in subsequent sections.

The present study aims at determining the extent to which the above listed phenomena contribute to the observed non-linear behaviour during the free vibrations of the bridge after a train passage. A 2D finite element (FE) approach incorporating macro-elements based on the Bouc–Wen (BW) model was used to study the first vertical bending mode of the bridge. Thus, a phenomenological approach to the modelling of the hysteretic components was used, which is essential considering the level of complexity that a continuum approach would comprise. Experimental data available in the literature was used, as far as possible, to choose appropriate backbone curves for the hysteretic components. The results indicate that the main contribution to the observed non-linearity originates from the roller bearings and that the track superstructure has a significant but much smaller influence.

The main scientific contribution of this paper consists in the quantification of the influence of different hysteretic components of a typical railway bridge. The use of the BW-model in the context of roller bearings and the track superstructure is, as will be shown, a natural extension of previous work based on this theory.

Section 2 gives a short description of the modelling of rate-independent hysteresis by BW-models. In Section 3.1, the bridge is shortly described and the main findings of [1] is summarised for reference. The hysteretic nature of shallow foundations, the track superstructure and the roller bearings is described in Sections 3.2, 3.2 and 3.4, respectively. Finally, the results of our analysis are presented in Section 4 and the conclusions drawn from them are discussed in Section 5, followed by some suggestions regarding the continued work in this field in Section 6.

2. BW-model for rate-independent hysteresis

In a univariate (single degree of freedom) system, rate-independent hysteresis is characterised by a backbone curve and a set of rules which define how the system behaves at load reversals. There are many different approaches to modelling hysteresis in discrete systems. One way is to use Maxwell (bi-linear, ideally elasto-plastic) elements with varying stiffness and plastic limit in parallel [3]. Thereby, a piece-wise linear approximation to any backbone curve can be modelled. Another approach lies in the so called Preisach type models (see for example [4]), where a memory stack is used to keep track on all the reversals in the hysteretic element and the classical theory of plasticity could also be used. Here, the univariate BW-model was used to model the hysteretic behaviour. In structural mechanics, this class of models relate the force and relative displacement between two points.

The classical BW-model was first introduced by Bouc [5] and later refined by Wen [6]. It consists of an elastic spring and a hysteretic element in parallel (see Figure 1). The force F in the BW-element can be written in the following way:

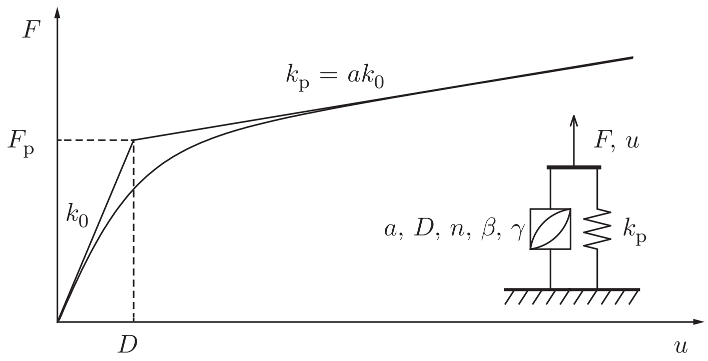

Figure 1. The classical BW-model.

$$F(t) = ak_0u(t) + (1 - a)Dk_0z(t) \tag{1}$$

with a, a model parameter relating the initial stiffness k_0 to the stiffness in the fully plasticised system $k_p = ak_0$, $D > 0$ is referred to as the plastic limit and the so called hysteretic variable, $z(t)$, an internal variable, governed by the non-linear differential equation

$$\dot{z} = \frac{\dot{u}}{D}[1 - (\beta + sgn(\dot{u}z)\gamma)|z|^n] \tag{2}$$

where $\beta + \gamma \neq 0$ and $n > 0$ are model parameters. The sign function sgn(x) is defined as

$$\mathrm{sgn(x)} = \begin{cases} -1 & \mathrm{x} < 0 \\ 0 & \mathrm{x} = 0 \\ 1 & \mathrm{x} > 0 \end{cases} \tag{3}$$

The plastic limit displacement D and the exponent n determine the shape of the backbone curves of the BW-model while β and γ determine the shape of the hysteresis loops. The basic loop shapes and the corresponding relations between β and γ are shown in Figure 2. If $\gamma = \beta = 1/2$, the force/displacement relation will follow a straight line on unloading. As long as $\gamma \geq \beta$, the loops will be rounded whilst if $\gamma < \beta$ they will be s-shaped.

The mathematical formulation of the classical BW-model described above has been thoroughly examined by Ikhouane and Rodellar [7]. A very useful analysis of the BW-

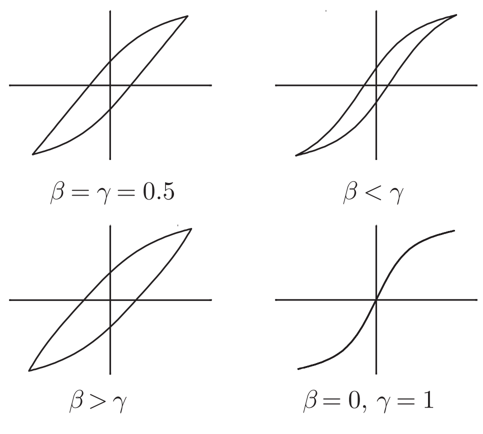

Figure 2. Loop shapes of the classical BW-model.

model, from a computational point of view but also in terms of comprehension, was given by Charalampakis and Koumousis [8]. They provided analytical solutions to the differential equation (2) for $n = 1,2$ and a scheme for the numerical evaluation of Equation (2) for arbitrary values of n. However, the BW-model in its classical form does fall short in a few aspects; if the BW-model is subjected to short unloading–reloading cycles, it exhibits displacement drift, force relaxation and unloading–reloading paths which are not properly closed. These shortcomings of the BW-model do not directly affect the analysis presented herein, but deserves mentioning as it limits the applicability of the BW-model in the more general context where simulations of passing trains are performed, a situation where short unloading–reloading paths cannot be ruled out. In a later publication [9], Charalampakis and Koumousis used their analytical solution to define a modified version of the BW-model, where the above-mentioned shortcomings are remedied.

In its classical form, the BW-model has been used in many civil engineering applications. Here we mention a few interesting examples. In the present context, the macro-element developed by Gerolymos and Gazetas [10,11] is a highly relevant, although much more complex example. Gerolymos and Gazetas created a macro-element for caisson foundations, which includes both contact conditions and soil plasticity. Hence it can be used to study foundations subjected to large displacements, such as those arising during an earthquake. The hysteretic behaviour of piles were studied by Soneji and Rangid [12], Assimaki [13] and others. Guggenberger and Grundmann [14] defined a beam element based on BW-hysteresis for an application in stochastic response analysis of space frames. Foliente [15] used BW-elements to study the influence of wood joint hysteresis on the structural response of wood frames.

2.1. *Implementation in ABAQUS*

A six degree of freedom FE for small displacements, i.e. no geometric nonlinear behaviour, with uncoupled univariate BW-elements, was implemented as a user-defined element in the commercial FEM code ABAQUS[1] which was used for the FE-analyses throughout this study. A linear viscous dashpot was added in order to obtain a general spring/dashpot element with the possibility of activating the hysteretic behaviour. Thus, the FE has three translational degrees of freedom, three rotational degrees of freedom and six internal variables, one for each degree of freedom. The increments of the internal variables are solved for using Newton–Raphson's method.

2.2. *Evaluation of the results*

A much more efficient alternative to the wavelet-based analysis used in [1] is provided by the Hilbert transform (see for example Huang et al. [16]) which gives the amplitude $A(t)$ and phase $\phi(t)$ as functions of time in a straightforward manner for the class of signals analysed here. The instantaneous frequency is then given by the time derivative of the phase

$$\omega(t) = \dot{\phi}(t). \tag{4}$$

In [1], the authors used the notion of an equivalent viscous damping ratio ξ_{eq} in order to quantify the variation in the modal damping ratio during free vibrations, caused by the non-linear behaviour of the structure. The developments in the current study enables an increase in the amplitude of vibration, which was not available in the measured free vibrations. The frictional nature of the hysteretic models studied here leads to a very important remark regarding this equivalent viscous damping ratio. Now, the idea behind ξ_{eq} was the assumption that the instantaneous decay of the signal can be represented by a linearly viscous damper. The equivalent instantaneous viscous damping ratio was then defined as

$$\xi_{eq}(t) = -\frac{\dot{A}(t)}{\omega(t)A(t)} \tag{5}$$

where $A(t)$ is the amplitude envelope and $\omega(t)$ is the instantaneous circular frequency of the mode of vibration in question. The problem with this choice of measure for the dissipation of energy in a given mode of vibration is that if the mechanisms which dissipates the energy are frictional, the exponential decay will not provide accurate results for all amplitudes of vibration. Consider the logarithmic decrement for a weakly damped system

$$\delta = \ln\frac{A_i}{A_{i+1}} \tag{6}$$

For a freely vibrating system with purely frictional damping, the amplitude is given by

$$A = A_0 - \frac{\Delta A}{T}t \tag{7}$$

where A_0 is the initial amplitude, t is time and ΔA is the constant decay during one period T. The logarithmic decrement can then be written

$$\delta = \ln\frac{A_0 - i\Delta A}{A_0 - i\Delta A - \Delta A} \tag{8}$$

which clearly tends towards infinity when $A_0 - i\Delta A \rightarrow \Delta A$. Furthermore, during the last cycle, the denominator in the logarithmic decrement is zero, so the equivalent viscous damping ratio is infinite there.

To illustrate this effect, a single-degree-of-freedom BW-model with similar properties as the bridge was studied using both a simulated forced excitation test and a free vibration test. The forced excitation test consisted in varying the frequency between 2 and 5 Hz in suitable steps with the force amplitudes 15, 30, 45 and 60 kN. In the forced vibration test, the damping ratio was computed using the definition

$$\xi = \frac{E_{\mathrm{h}}}{4\pi E_{\mathrm{el}}} \tag{9}$$

where E_{h} is the energy dissipated during one cycle, i.e. the area of the hysteresis loop, and $E_{\mathrm{el}} = F_{\max} \cdot u_{\max}/2$ is the maximum elastic energy stored during the cycle. The result is shown in Figure 3, which clearly shows that the equivalent viscous damping ratio overestimates the damping in an intermediate range of amplitudes. In the comparative study presented here, the errors in the equivalent instantaneous damping ratio do not impose any serious harm as the same procedure is used in both cases.

3. Modelling of the bridge

3.1. *Description of the studied bridge*

The studied bridge is situated in the northern parts of Sweden and has its longitudinal axis in the north-south direction. A photo of the bridge is shown in Figure 4(a), and the natural

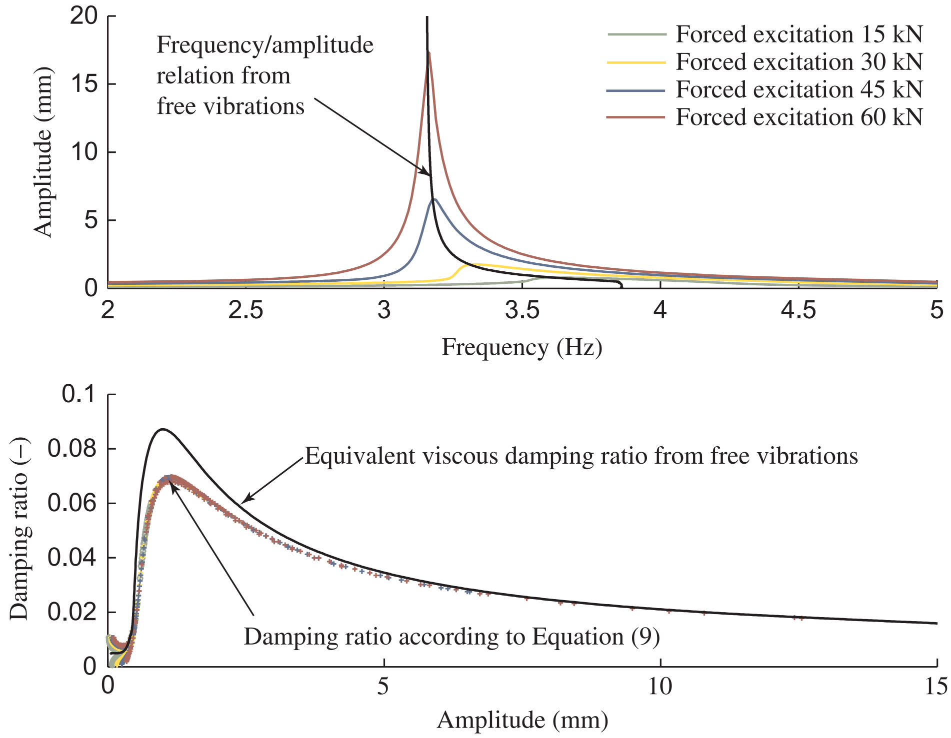

Figure 3. Comparison between natural frequency (top) and damping ratio (bottom) as estimated from simulations of free vibration and forced vibration tests on a single-degree-of-freedom BW-system.

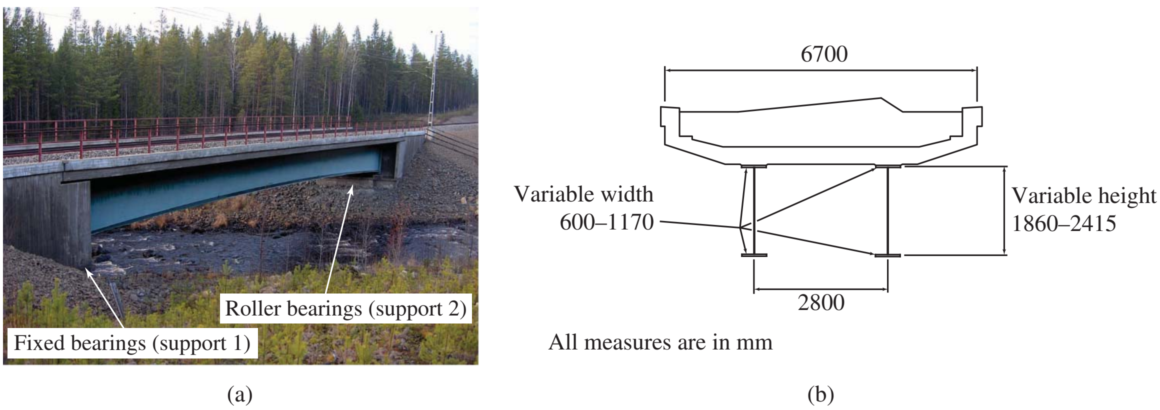

Figure 4. A photograph of the bridge at Skidträsk (a) and a sketch of its cross section (b).

frequency and equivalent viscous damping ratio, as estimated from measurements of free vibrations [1], are shown in Figure 5. The bridge has a horizontal skew of 30°, a span length of 36 m and carries one ballasted track. The thickness of the reinforced concrete deck varies between 320–350 mm and its total width is 6.7 m. The cross section of the two main steel beams varies along the bridge, see Figure 4(b). The main beams are connected with transverse braces at four sections along the beam as well as at the beam ends. One of the supports is fixed, but free to rotate over the transversal axis and the other end is supported on roller bearings to relieve constraints essentially caused by temperature variations. The bridge is founded on shallow foundations on an approximately 5 m thick layer of silty moraine. The geotechnical survey estimated the modulus of elasticity of the subsoil to be approximately 30 MPa and its density was determined as 1700 and

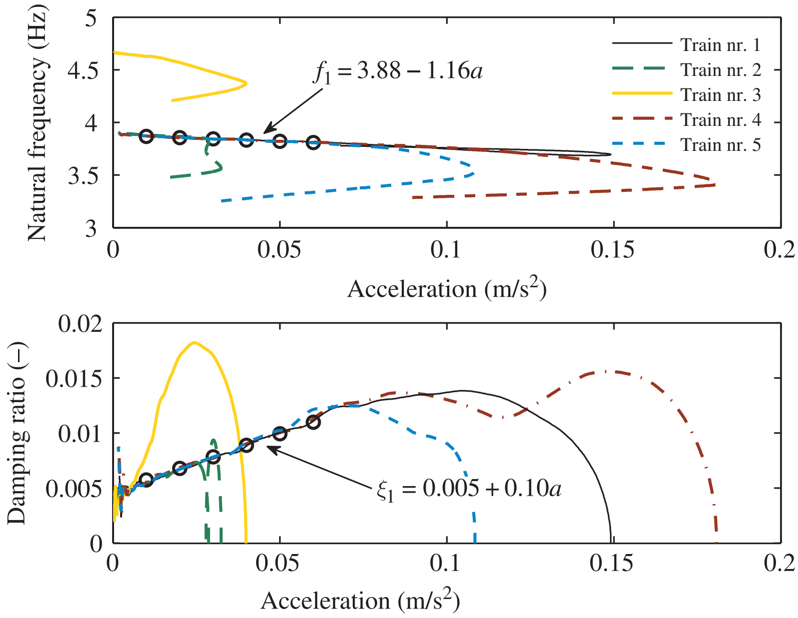

Figure 5. The estimated [1] natural frequency and modal damping ratio of the first vertical bending mode of the bridge at Skidträsk (train nr. 3 excited the first torsional mode).

2000 kg/m^3 for the drained and undrained state, respectively. The estimate of the elastic modulus of the subsoil is a lower bound characteristic value, intended for calculations of long-term settlements. The foundation plates have the width $W = 9.2$ m and the length $B = 5.8$ m and are placed with a skew of 30° with respect to the bridge centre line.

3.2. *Modelling of the foundations*

Shallow foundations resting on, or embedded in a linearly elastic, isotropic, homogeneous half space or infinite disc are quite well understood. They are typically characterised by a dynamic stiffness function, which is a complex function of frequency where the real part corresponds to the stiffness and the imaginary part corresponds to an equivalent viscous damping. This equivalent viscous damping, which should not be confused with that described in Section 2.2, consists of two parts: radiation damping caused by elastic waves propagating away from the foundation and soil material damping. In general, soil materials have an essentially rate-independent hysteretic nature, see for example [17,18]. The rate-independent non-linear soil material behaviour is expected to lead to a certain amount of hysteresis in such foundations [19–22]. However, these effects should only be relevant for loads approaching the bearing capacity of the foundation. This was concluded in both [20] and [21] in the context of machine foundations, but similar arguments should hold true also for bridge supports. Otherwise, excessive settlements would result from the serviceability limit state loads. The behaviour of shallow foundations subjected to large loads has been much studied in the field of earthquake engineering. Especially interesting, in the present context, is the development of various forms of macro-elements. Chatzigogos et al. [23] provided a nice literature review of the developments in that field.

Early developments in the field of macro-elements for shallow foundations provided by Nova and Montrasio [24] indicate that a model function suitable for the backbone curve for the vertical degree of freedom of a shallow foundation is available in an exponential function of the form

$$\frac{F_V}{F_{V,\mathrm{u}}} = 1 - \exp\left(-\frac{k_V u}{F_{V,\mathrm{u}}}\right) \tag{10}$$

where F_V is the vertical force, $F_{V,\mathrm{u}}$ is the ultimate vertical load, k_V is the initial vertical stiffness and u is the vertical displacement.

The initial vertical stiffness can be approximated by means of handbook formulas [25]. The initial vertical stiffness was assumed to vary between 1–3 GN/m. A lower bound of 15 MN for the ultimate load was provided by the design calculations. A family of conceivable backbone curves for the vertical foundation stiffness is shown in Figure 6. Previous experience with soil–structure interaction problems of this kind indicate that the vertical displacements of the foundations are ~1/10 of the vertical displacement at mid span, which reaches ~10 mm during the passage of the heaviest trains on the Skidträsk bridge. Thus, one can conclude that none of the backbone curves shown in Figure 6 would give any substantial hysteretic effects. In the proceeding, it will therefore be assumed that the foundations behave in a linearly elastic manner and that their only contribution to the damping of the structure is in the form of radiation damping. The parameters used in the analysis are given in Table 1. The frequency dependency of the foundation stiffness was ignored.

3.3. *Modelling of the track*

Typically, the track is included in numerical models of railway bridges when train-bridge interaction is considered, see for example Zhai et al. [26]. However, the longitudinal

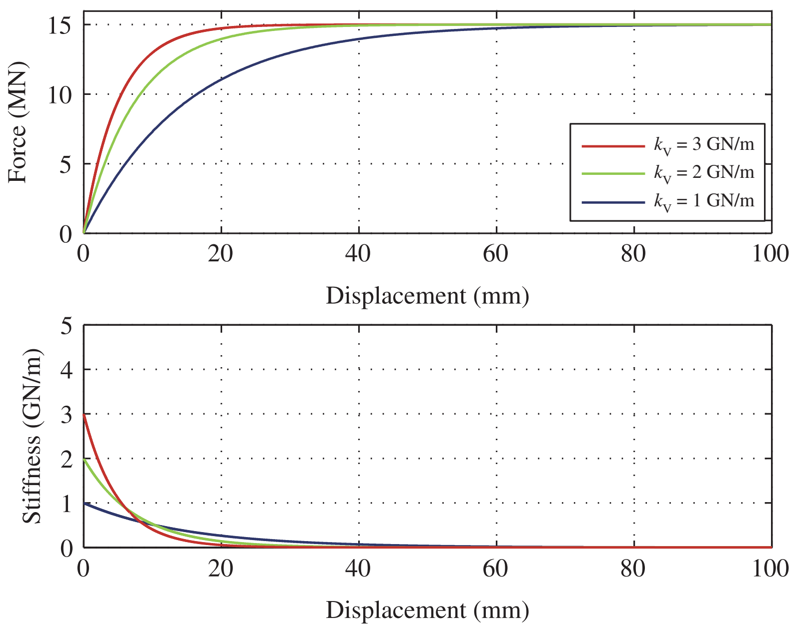

Figure 6. A family of approximated backbone curves according to Equation (10) for the vertical stiffness of the shallow foundations.

Table 1. Parameter values for foundation spring and dash-pot elements used in the FE model.

	k (GN/m)	c (MNs/m)
Foundation (horizontal)	1.55	1.00
Foundation (vertical)	2.58	1.50

track-bridge interaction is very important for so called continuously welded rails (CWR), where large constraint forces can appear between the rail and the underlying structure. Naturally, these effects are most pronounced for temperature loads and trains braking or accelerating, causing longitudinal forces in the track/bridge system, see for example the study by Ruge and Birk [27] or the textbook by Esveld [28]. For that purpose, a bi-linear, ideally plastic model of the longitudinal track resistance has been developed [29], based on tests performed by the European Rail Research Institute (ERRI) in research programme D202. Several tests were performed by various railway institutes in Europe and two of them studied the longitudinal track resistances, namely TU Delft [30] and MAV[2] [31].

Figure 7 shows one of the models recommended by UIC (ballasted, unloaded track) together with typical outcomes of the experiments by TU Delft and MAV. The higher resistance of the UIC model, together with its non-smooth transition to the plastic regime at a relative displacement of 2 mm, makes it more conservative than the experimental force–displacement relationships, in the quasi-static analysis involving temperature loads and train traction. In the present context however, the bi-linear model is not satisfactory as very large relative displacements between the rails and the bridge deck are needed in order to leave the linear regime of the model.

MAV performed their tests on an old track, which had been replaced whereas TU Delft performed their tests in a laboratory environment. Only MAV performed cyclic tests on the track. A typical outcome of such results is shown in Figure 8, which clearly shows the hysteretic nature of the longitudinal track resistance. One can also see that some stiffness degradation occurs when the displacement exceeds approximately 2 mm. Thus, a classical BW-model should be able to represent this type of hysteresis well for the small displacements (<1 mm) expected during a train passage over the Skidträsk bridge. It was decided to use the test results from TU Delft in the current analysis as the ballast grading used in those tests seemed to better match the Swedish requirements in operating tracks.

The vertical stiffness of the track was taken as 0.2 GN/m, based on the results presented in [32,33]. The longitudinal track model parameters used in the study are summarised in Table 3 and the backbone curve is shown in Figure 9.

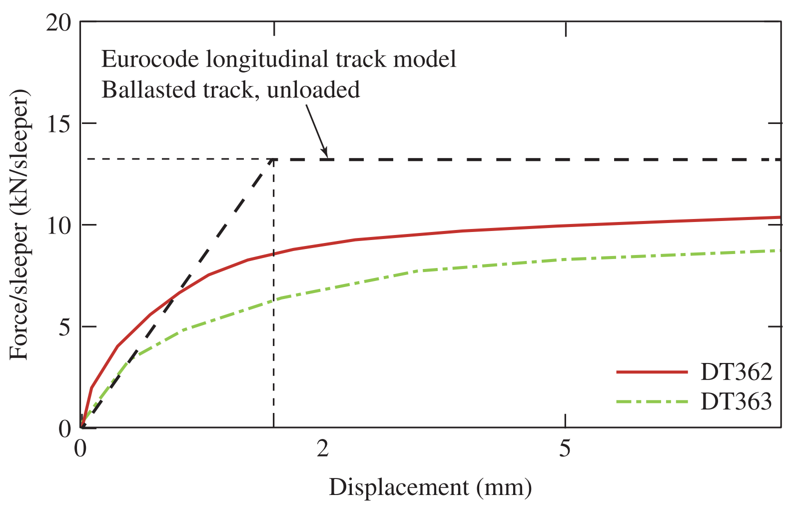

Figure 7. Longitudinal track resistance as measured by TU Delft [30] (solid line) and MAV [31] (dash-dotted line), compared with the Eurocode/UIC model. Note that the measured track resistances are given in force per sleeper and the Eurocode/UIC model has been recalculated to comply with the measurements assuming a sleeper distance of 650 mm.

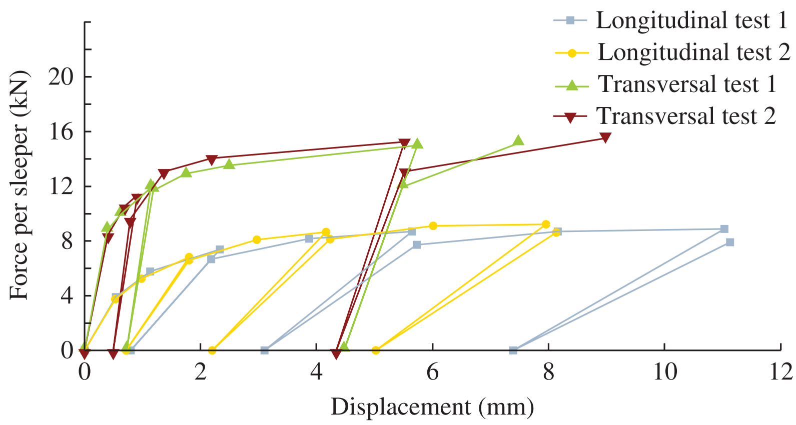

Figure 8. Cyclic longitudinal track resistance tests by MAV [31].

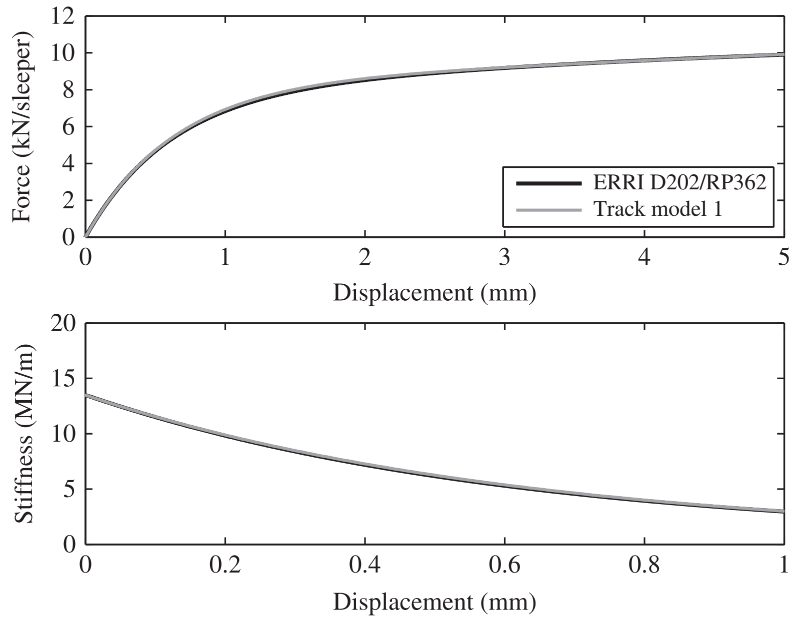

Figure 9. The backbone curve of the track longitudinal stiffness model used in the analysis.

3.4. *Modelling of the roller bearings*

In the mechanical engineering sciences, much effort has been made to understand the behaviour of rolling contacts, mainly with the aim of designing roller and ball bearings and in studies of the wheel–rail contact for railways. These historical developments are well described in textbooks such as [34,35], and will not be further elucidated here. However, in later years, an interest for the so called micro-slip and pre-rolling resistance has been given some attention. The basic concepts of sliding friction based on the distinction between static and kinematic friction are well known. The transition between static and kinematic friction, is governed by micro-slip, which is basically the result of tangential deformations of the highest asperities in the contact region and slip on the lowest asperities [36,37]. This phenomenon results in a hysteretic behaviour with a smooth backbone curve. In rolling contacts, a similar behaviour arises in the transition between static and dynamic equilibrium, and this is referred to as pre-rolling resistance. The hysteretic nature of the pre-rolling resistance of various rolling contacts has been well described by Al-Bender and Symens [38]. The pre-rolling resistance is very similar to micro-slip in that it produces a hysteretic behaviour and it is related to the case where the applied force does not overcome the initial resistance to rolling. However, the mechanism is somewhat more complicated as it involves the rolling resistance and not only the contact of two flat surfaces. Al-Bender and De Moerlooze [39] presented a numerical technique to model the pre-rolling behaviour of balls in various configurations. In reference [40] the same authors provide an experimental validation of their modelling, which shows that an exponential curve of the same form as Equation (10) can be fitted to their experimental hysteresis loops. Although their analysis was limited to a ball rolling in a V-grooved track, it has been assumed that the exponential backbone curve should give a reasonable first approximation for our purposes.

The bearing geometry is shown in Figure 10. On the Skidträsk bridge, the rollers are steel cylinders of length 600 mm and radius 146 mm. Each roller is guided by two rulers, one on each side and a groove and notch along the centres of the rollers. In the initial configuration, ideally, the guiding devices are not in contact with their counterparts, but in a general case, such contacts must be expected. It is beyond the scope of the present study to include such effects, which would combine pre-rolling with sliding friction. Instead, the purpose of this section is to choose an approximate backbone curve for a BW bearing model, which can illustrate the effects of the bearings on the global bridge behaviour. Based on the above reasoning, a model for the bearing rolling resistance was chosen as

$$\frac{F(x)}{F_\tau} = 1 - \exp\left(-\frac{k_0 x}{F_\tau}\right) \tag{11}$$

with F_τ and k_0 being the rolling resistance and the initial stiffness, respectively, and x is the longitudinal displacement over the bearing.

The rolling resistance F_τ depends primarily on the distribution of tractive (shear) stress in the contact although several other phenomena may influence the rolling resistance of a given contact pair. Especially if large loads are applied, so that plastic deformations occur in the contact patch. However, here we only consider elastic deformations. The elastic contact patch can be divided in two regions, referred to as the “stick” and “slip” regions. In the stick region, the traction does not overcome the friction and no sliding occurs whereas in the slip region, the contacting surfaces slide against each other.

When the rolling surface passes through the contact patch, it is compressed so that both the normal and the tangential strain there is compressive. The compressive tangential strain gives rise to a phenomenon referred to as creepage, which in this case causes the roller to move a slightly shorter distance than that represented by its undeformed

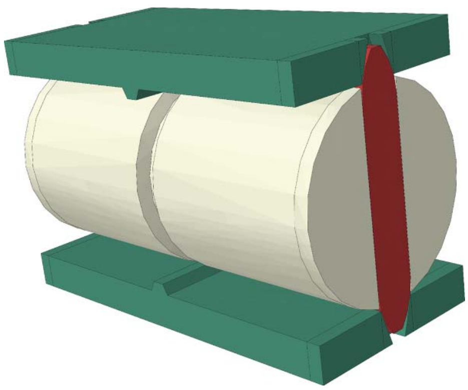

Figure 10. 3D view of the roller bearing geometry.

circumference. For a cylinder on a flat plate one can define the creep ratio ξ_x, i.e. the ratio of the relative velocity between the contact surfaces and the velocity of the cylinder $\dot{x}$, as

$$\xi_x = \frac{\dot{x} - \omega R}{\dot{x}} \tag{12}$$

where ω is the angular velocity of the cylinder and R is its radius.

To estimate the rolling resistance at steady rolling F_τ we used the relation [35]

$$F_\tau = -\mu L F_\mathrm{n} \left[1 - \left(1 - \frac{R\xi_x}{\mu a} \right)^2 \right] \tag{13}$$

where μ is the coefficient of friction, $L = 600$ mm is the length of cylinder, a is half the length of the Hertzian contact area

$$a = \sqrt{\frac{4F_\mathrm{n}R}{\pi E^*}} \tag{14}$$

and $E^* = E/(2(1-\nu^2))$, i.e. the contact surfaces have the same material properties with the modulus of elasticity E and the Poisson ratio ν. The creep ratio was assumed to be $\xi_x = 0.0005$, a value appropriate as an approximation for the wheel–rail contact, [41] the Hertzian contact length was found to be $a = 2$ mm and the normal force F_n was taken as one-quarter of the dead weight of the bridge, i.e. 1.5 MN. With these values, a rolling resistance of 104 kN was calculated, neglecting all influences of the guiding devices.

The paper by Spiegelberg et al. [42] provides an estimate of the initial stiffness

$$k_0 = 2Lak_t \tag{15}$$

where k_t is given by

$$k_t = 0.85\frac{E^*}{a}. \tag{16}$$

A family of backbone curves with different values of the parameter n in the BW-model is shown in Figure 11.

3.5. *The FE-model*

Given the non-linearity of the problem and the uncertainties involved, a study such as the current one should be performed in a very simple FE model. The computational time should not be prohibiting and the accuracy of the model should be adapted to the available experimental data. Since we basically only have empirical knowledge about the first vertical bending mode, the numerical model only needs to represent that mode in a satisfactory way. Thus, a 2D model is sufficient and has been devised as described in this section.

The FE models used in this study were based on a 2D Euler–Bernoulli beam with elastic supports and are illustrated in Figures 12 and 13. To obtain the correct constraints at the beam ends, rigid links were used to define the distance between the neutral axis of the beam

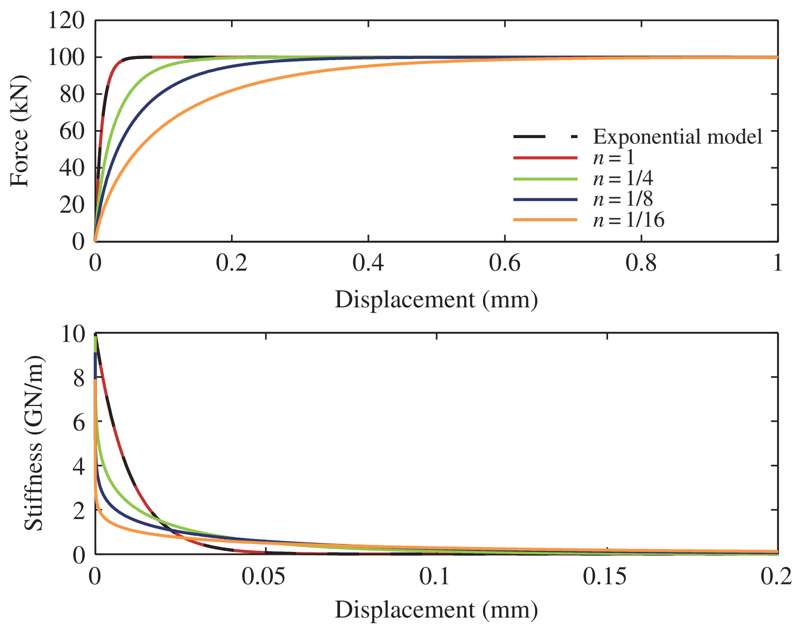

Figure 11. Backbone curves for the exponential rolling resistance model (top) and stiffness (bottom) with $k_0 = 10$ GN/m, $a = 1 \cdot 10^{-12}$, $D = 1 \cdot 10^{-5}$ and different values of n.

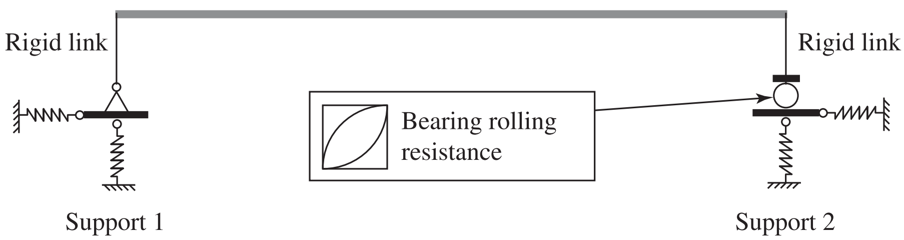

Figure 12. Sketch of model 1.

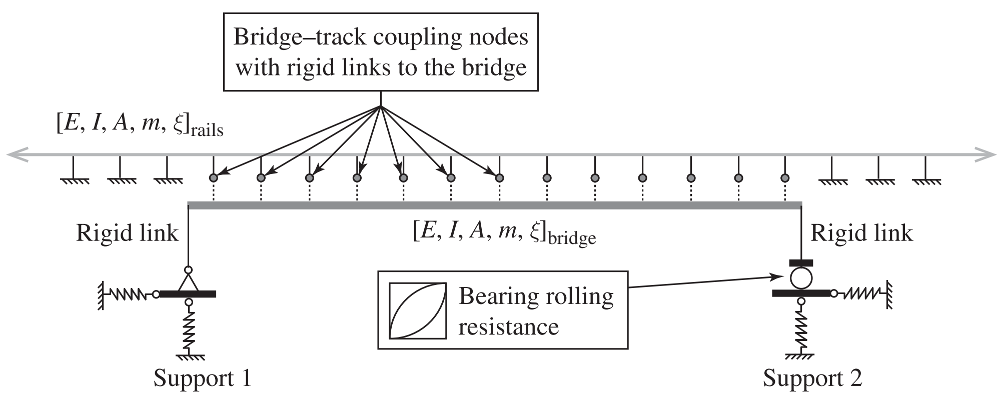

Figure 13. Sketch of models 2 and 3. The BW-element was used to model the longitudinal track resistance in model 3.

and the support points. The elastic supports were modelled using linear springs and dashpots as described in Section 3.2. Three different model alternatives were used in the study:

(1) Model 1: No track
(2) Model 2: Linear track
(3) Model 3: Non-linear track

Table 2. Parameter values for beam elements used in the FE model. The beam section properties are an equivalent steel section, including the concrete.

	A (m^2)	I (m^4)	E (GPa)	ρ (kg/m^3)	Rayleigh damping coefficients α_R (–)	β_R (–)
Beam						
Model 1	0.8	0.51	210	13500	0.038	$3.8 \cdot 10^{-4}$
Models 2 & 3	0.8	0.51	210	7850	0.038	$3.8 \cdot 10^{-4}$
Rails	0.015	$6.08 \cdot 10^{-5}$	210	7850	0.038	$3.8 \cdot 10^{-4}$

Table 3. Parameter values for Bouc–Wen elements used in the FE models.

	a (–)	k_0 (GN/m)	D (m)	β (–)	γ (–)	n (–)
Bearing model 1	$1 \cdot 10^{-12}$	60	$1.0 \cdot 10^{-6}$	0.5	0.5	1/16
Bearing model 2	$1 \cdot 10^{-12}$	60	$7.5 \cdot 10^{-7}$	0.5	0.5	1/16
Track	$2.4 \cdot 10^{-2}$	0.014	$6.3 \cdot 10^{-4}$	0.5	0.5	1

The mass of the ballast was weighted into the mass of the beam in model 1 and placed at the bridge–track coupling nodes in models 2 and 3 (see Figure 13). Thus, the only difference in mass between the models was the additional mass of the rails in models 2 and 3, which is essentially negligible. The support points were given some inertia to represent the soil mass on top of the foundation plates and the mass of the abutments (162,000 kg on each foundation) and a small rotatory inertia for numerical stability. In the real structure, the cross section varies along its length, but in the model used here, this was neglected and a mean value of the cross-sectional properties was used to determine an equivalent constant cross section. Timoshenko beam elements were used to model the rails (UIC60). The rails were connected to the bridge beam by means of linear spring elements (model 2) and BW elements (model 3). These elements were connected to the bridge with rigid links in order to correctly model the eccentricity between the top of the bridge deck and the neutral axis of the bridge beam, see Figure 13. Structural damping was included using Rayleigh damping. All parameter values used in modelling the bridge and the foundations are summarised in Tables 1 and 2 whereas the Bouc–Wen model parameters are summarised in Table 3. The trapezoidal rule was used to integrate the equations of motion with no additional numerical damping. Typically, the time steps required varied between 10^{-5}–10^{-3} s, depending on the degree of non-linearity introduced by the hysteretic mechanisms. Generally, the smaller time steps dominated at very small amplitudes of vibration, where the roller bearing is constantly trying to overcome the rolling resistance.

4. Computational results

4.1. *General results*

In this section, we present some general results from the simulations. In Figure 14, the acceleration and displacement of the bridge beam at mid-span are shown for the BW-model parameters in Table 3. Clearly, the free vibrations can be divided into two parts. In the beginning of the free vibrations, the amplitude function is linear, signifying that the damping is dominated by friction-like forces and in the end a completely different

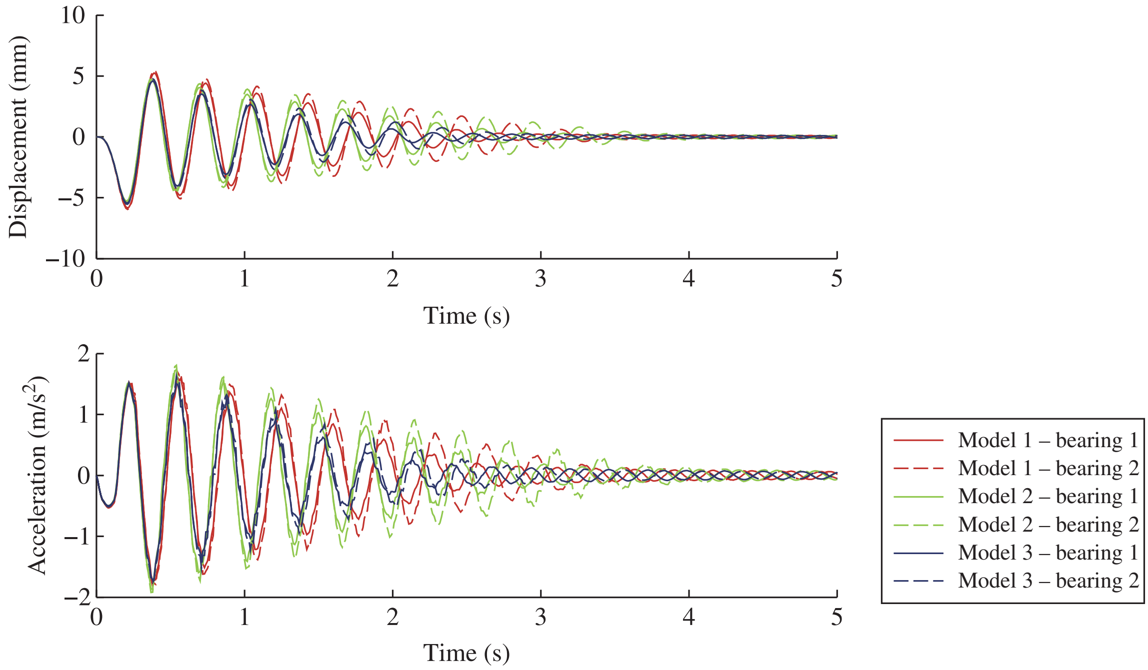

Figure 14. Vertical displacement and acceleration at mid-span.

slope is seen, which is dominated by viscous damping forces. The transition between the two parts of the free vibrations occurs at approximately 2.5 s. The cause of the significantly different characteristics of them is well illustrated by Figure 15, in which the reaction forces at the supports are shown for model 3 and bearing model 2. Clearly, at around 2.5 s the horizontal force over the bearing no longer overcomes the pre-rolling resistance and the horizontal translation there begins to be significantly more restrained. The friction-like component of the overall damping becomes less dominating and the viscous damping sources dominate. The vertical bridge deck acceleration in this part of the free vibrations is bounded by approximately 0.5 m/s^2.

This behaviour is also reflected by the horizontal displacements at the support points, as shown in Figure 16. The horizontal displacements at the foundations are always bounded by ~0.1 mm, whilst the displacement at the top plate of the roller bearing is

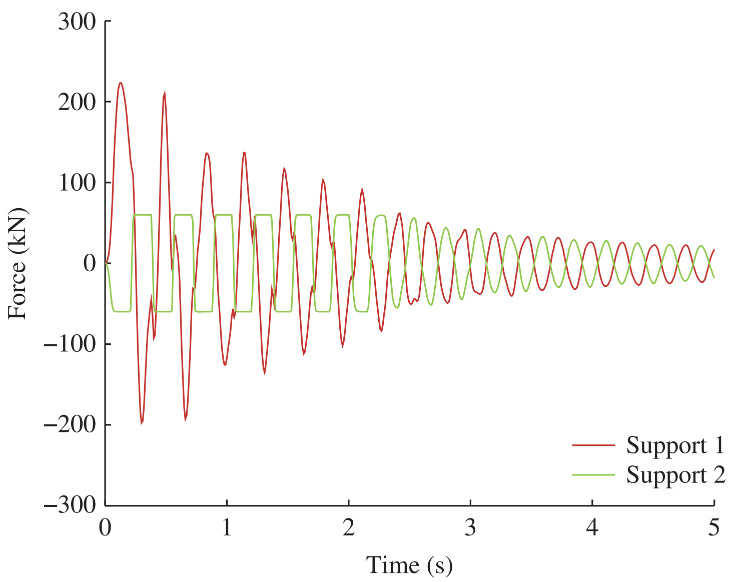

Figure 15. The horizontal reaction forces computed for model 3 with bearing model 2.

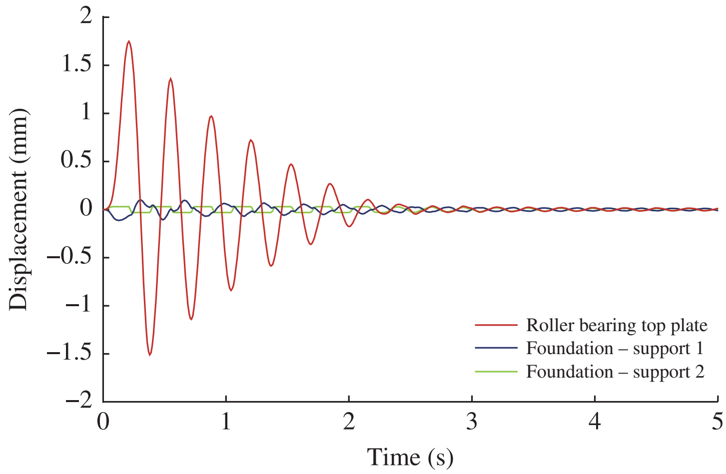

Figure 16. The horizontal displacements of the foundations and the top plate of the roller bearings for model 3 with bearing model 2.

one order of magnitude larger in the first part of the free vibrations and then similar to the displacement of the foundations in the end.

The hysteresis loops of the bearing response are shown in Figure 17, which again reflects the two different mechanisms (rolling and fixed) represented by the bearing. In the first part, the loops essentially follow the backbone curve of the bearing and towards the end, the loops are affected by the interaction with the foundation.

4.2. *Roller bearing hysteresis*

The plastic limit D and the shape parameter n of the roller bearing model were found to have the largest influence on the bridge response. Figures 18 and 19 show the backbone curves and the result of a family of roller bearing models, based on the parameters shown in Table 3 and described in Section 3.4.

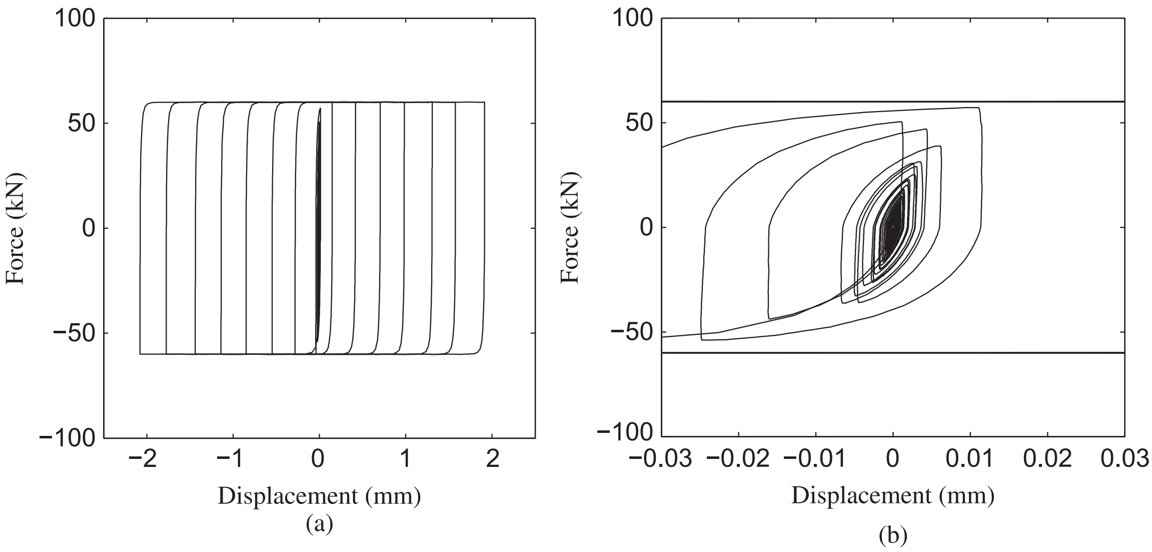

Figure 17. The bearing hysteresis loops for the whole free vibration period (a) and the end of the free vibration period (b) for model 3 with bearing model 2.

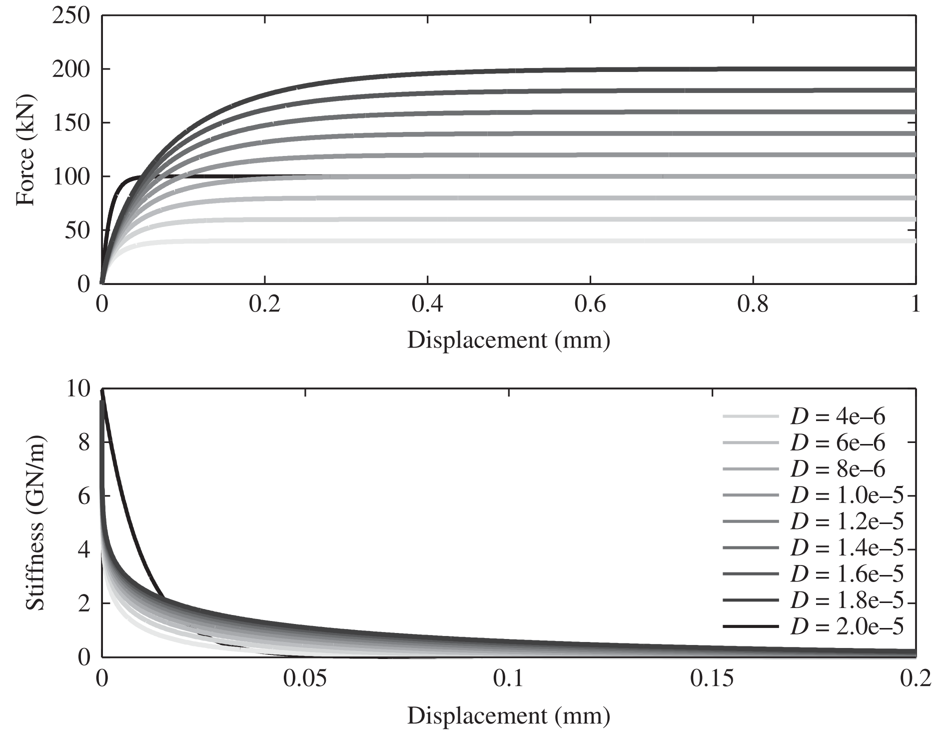

Figure 18. Roller bearing backbone curves with $k_0 = 10$ GN/m, $a = 1 \cdot 10^{-12}$, $n = 1/6$, $\beta = \gamma = 0.5$ and different values of the plastic limit D. The thick black line is the initial bearing model defined in Section 3.4.

These results show that the roller bearing has two major influences on the dynamic properties of the structure: (1) it introduces a mechanism which makes the bearing behave as a fixed bearing for very small amplitudes of vibration and as a roller bearing for larger amplitudes of vibration; (2) it introduces a significant amount of friction damping in the

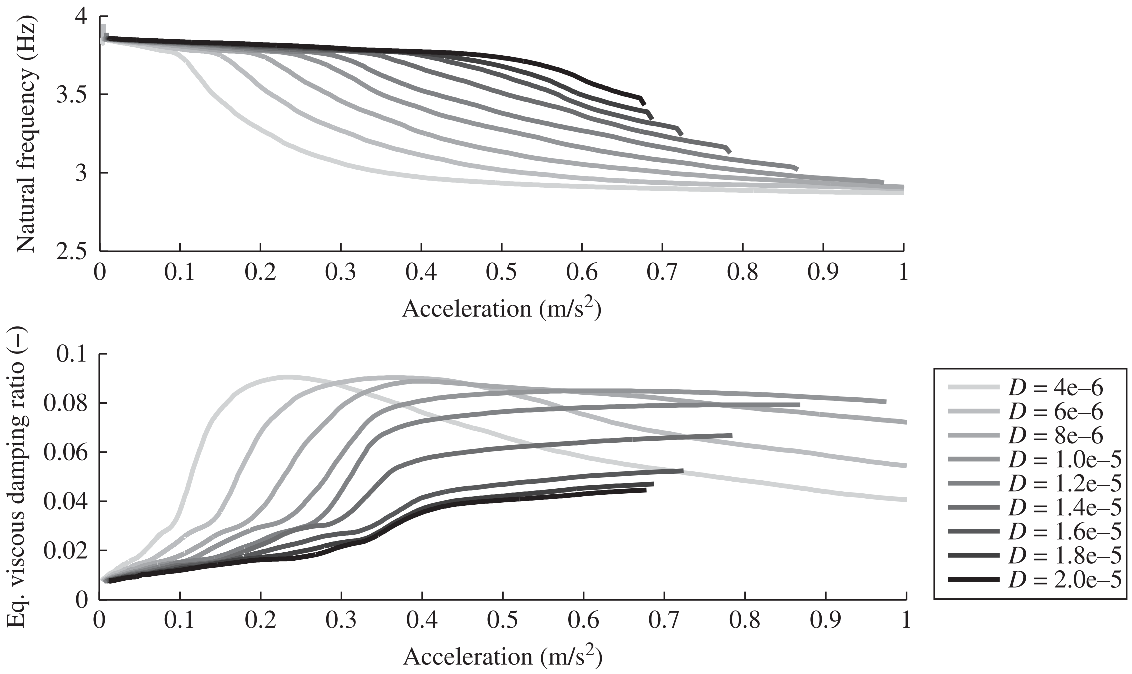

Figure 19. Frequency and equivalent viscous damping calculated using the bridge mid-point acceleration with the roller bearing backbone curves shown in Figure 18.

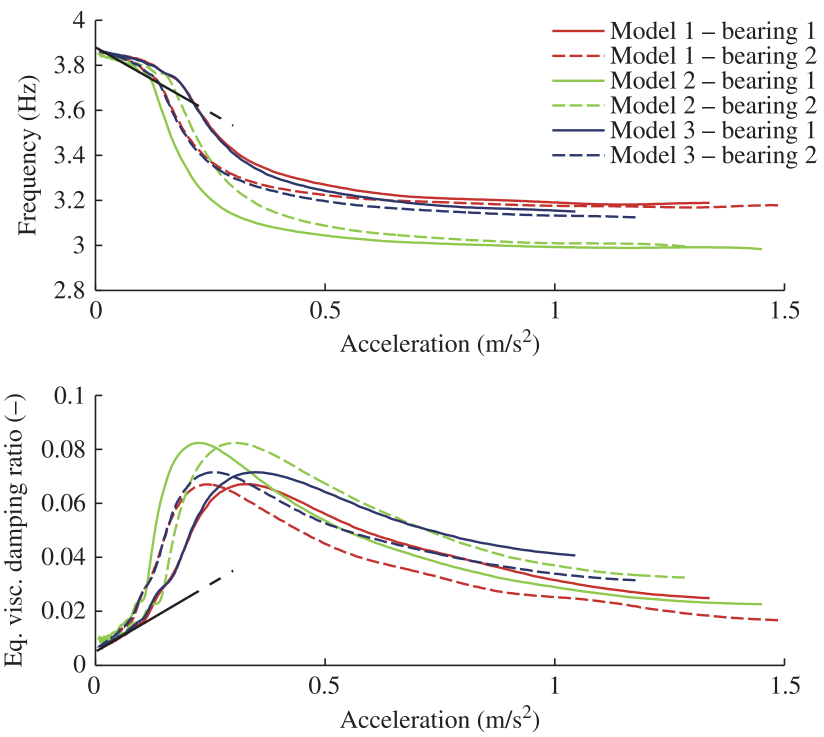

Figure 20. Frequency and equivalent viscous damping calculated using the bridge mid-point acceleration for models 1–3 with the two different bearing models given in Table 3. The results from [1] are shown with black, broken lines (see also Figure 5).

system. This friction damping has a peak value at a certain amplitude of vibration and then decreases towards some asymptotic value at larger amplitudes of vibration.

It should be noted that the initial model defined in Section 3.4 had to be adjusted somewhat in order to obtain a correct behaviour in a qualitative sense. These adjustments consisted mainly in varying the parameter n. Clearly, one should have to determine the shape of the bearing backbone curve from experiments on an isolated bearing in order to remove this uncertainty from the analysis.

4.3. *The combination of the roller bearing and track hysteresis*

Figure 20 shows the natural frequency and equivalent viscous damping ratio of models 1, 2 and 3 with the two bearing models, together with the results from [1] which are shown as black broken lines (see also Figure 5). Clearly, model 1 gives a lower frequency than the two other models when the bearing is fully rolling. The “bump” in the damping ratio is also higher for model 1 than for the two other models. The linear track model appears to reduce the hysteretic effects of the bearing by the constraints it imposes at the beam ends. The non-linear track model hardly has any influence at all on the stiffness, but does provide a small contribution to the overall damping. The variation in frequency and damping is obviously dominated by the bearing mechanism and by neglecting the track superstructure, these effects are overestimated.

5. Discussion and conclusion

The qualitative agreement between the presented theoretical model and experimental data has led to the conclusion that the non-linear effects observed in the free vibrations of the first vertical bending mode of this bridge are mainly caused by the hysteretic effects induced by the rolling resistance of its roller bearings. However, as experimental data for the backbone curve of the bearing was not available, a mismatch between the theoretical results and measured reality remains. It is clear that the observed non-linear behaviour is affected by the interaction of at least two different sources, i.e. the track and the bearings, and the modelling of them is afflicted with some degree of uncertainty. Therefore, further attempt to remove the remaining mismatch was judged unnecessary as it could still not be validated for accelerations beyond those available from the measurements of free vibrations.

The damping ratios obtained in this study are very high compared to those specified by the Eurocode [43] for design calculations. For this bridge, the design value would be 0.5% in all modes of vibration whilst the presented results indicate that in a state of resonance dominated by the first vertical bending mode of vibration, a conservative choice would be in the range of 2–4%, judging by the asymptotic behaviour of the damping ratio as the amplitude of vibration increases. The Eurocode recommendations are essentially lower bounds of the results presented in the report by ERRI [44], which includes numerous estimates of damping ratios from existing bridges, determined mainly from free vibrations.

6. Further research

In the author's opinion, the continued work in this field has two major concerns:

(1) The amplitude dependency should be studied using forced excitation tests at different environmental conditions. This would enable a validation of the work done so far, but more importantly, a robust identification and analysis of other modes of vibration than the first vertical bending mode.
(2) A range of bridges need to be tested in order to draw general conclusions regarding the amplitude dependency of railway bridges.

In the Swedish common practice today, roller bearings of this type are quite uncommon and typically, sliding bearings are used instead. Hence, in addition to studying the backbone curves of the roller bearings in laboratory conditions, some common types and dimensions of sliding bearings should also be studied. By reducing the uncertainty in the modelling of the bearings, more detailed bridge models can be motivated and thereby, studies of train–bridge resonance.

There are some numerical issues associated with the BW-models used in this study. The displacement over the bearing at the onset of rolling is very small, in the order of $<10^{-5}$ m, and this led to very small time steps ($\sim 10^{-4}$ s and even less). This made the computations very time consuming and this can probably be much improved.

A generalisation of the Bouc–Wen model to simulate the dependency of the rolling resistance on the normal force could be implemented with little effort, but again, input for such a development in terms of laboratory tests on the bearing type is needed. The same generalisation could also be used to improve the accuracy of the track model for use in simulations of passing trains.

Acknowledgements

This research was funded by the Railway Group at KTH, Royal Institute of Technology and Tyréns AB. The authors wish to thank Claes Kullberg and Stefan Trillkot for providing the experimental data.

Notes

1. http://www.3ds.com/products/simulia
2. The Hungarian railway administration.

References

[1] Ülker-Kaustell M, Karoumi R. Application of the continuous wavelet transform on the free vibrations of a steel-concrete composite railway bridge. Eng Struct. 2011;33:911–919.
[2] Ülker-Kaustell M, Karoumi R. Inuence of non-linear stiffness and damping on the train-bridge resonance of a simply supported railway bridge. Eng Struct. 2012;34:350–355.
[3] Goldfarb M, Celanovic N. A lumped parameter electromechanical model for describing the nonlinear behavior of piezoelectric actuators. J Dyn Syst-T ASME. 1997;119:478–485.
[4] Mayergoyz I. Mathematical models of hysteresis. New York, NY: Springer-Verlag; 1991.
[5] Bouc R. Forced vibration of mechanical systems with hysteresis. In: Proceedings of the Fourth International Conference on Nonlinear Oscillations, Prague; Sept 5–9; 1967.
[6] Wen YK. Method for random vibration of hysteretic systems. J Eng Mech Div ASCE. 1976;102(2):249–243.
[7] Ikhouane F, Rodellar J. Systems with hysteresis. Chichester: John Wiley and Sons; 2007.
[8] Charalampakis AE, Koumousis VK. On the response and dissipated energy of Bouc-Wen hysteretic model. J Sound Vib. 2008;309:887–895.
[9] Charalampakis AE, Koumousis VK. A Bouc-Wen model compatible with plasticity postulates. J Sound Vib. 2009;322:954–968.
[10] Gerolymos N, Gazetas G. Development of Winkler model for static and dynamic response of caisson foundations with soil and interface nonlinearities. Soil Dyn Earthq Eng. 2006;26: 363–376.
[11] Gerolymos N, Gazetas G. Static and dynamic response of massive caisson foundations with soil and interface nonlinearities–validation and results. Soil Dyn Earthq Eng. 2006;26:377–394.
[12] Soneji BB, Jangid RS. Inuence of soil–structure interaction on the response of seismically isolated cable-stayed bridge. Soil Dyn Earthq Eng. 2008;28:245–257.
[13] Assimaki VD. A generalized hysteresis model for biaxial response of pile foundations in sands. Soil Dyn Earthq Eng. 2012;32:56–70.
[14] Guggenberger J, Grundmann H. Stochastic response of large FEM models with hysteretic behaviour in beam elements. Comput Method Appl M. 2005;194:1739–1756.
[15] Foliente GC. Hysteresis modelling of wood joints and structural systems. J Struct Eng ASCE. 1995;121(6):1013–1022.
[16] Huang NE, Shen Z, Long SR, Wu MC, Shih HH, Zheng Q, Yen N-C, Tung CC, Liu HH. The empirical mode decomposition and the Hilbert spectrum for nonlinear and non-stationary time series analysis. P R Soc A. 1998;454:903–995.
[17] Hardin BO, Drnevich VP. Shear modulus and damping in soils: measurement and parameter effects. J Soil Mech Found Eng Div ASCE. 1972a;98(SM6):603–624.
[18] Hardin BO, Drnevich VP. Shear modulus and damping in soils: design equations and curves. J Soil Mech Found Eng Div ASCE. 1972b;98(SM7):667–692.
[19] Novak M. The vibrations of massive foundations on soil. IABSE Publications. 1960;20:263–281.
[20] Funston NE, Hall WJ. Footing vibration with nonlinear subgrade support. J Soil Mech Found Div ASCE. 1967;SM5:191–211.
[21] Richart FE Jr, Whitman RV. Comparison of footing vibration tests with theory. J Soil Mech Found Div ASCE. 1967;SM6:143–168.
[22] Novak M. Prediction of footing vibrations. J Soil Mech Found Div ASCE. 1970;SM3:837–861.
[23] Chatzigogos CT, Pecker A, Salençon J. Macroelement modelling of shallow foundations. Soil Dyn Earthq Eng. 2009;29:765–781.
[24] Nova R, Montrasio L. Settlements of shallow foundations on sand. Gotechnique. 1991;41 (2):243–256.
[25] Fang H. Foundation engineering handbook. 2nd ed. New York, NY: Van Nostrand Reinhold; 1991.

[26] Zhai WM, Xia H, Cai CB, Gao MM, Li XZ, Guo XR, Zhang N, Wang KY. High-speed traintrack-bridge dynamic interactions – Part I: theoretical model and numerical simulation. Int J Rail Transportation. 2013;1(1–2):3–24.
[27] Ruge P, Birk C. Longitudinal forces in continuously welded rails on bridge decks due to nonlinear track-bridge interaction. Comp Struct. 2007;85:458–475.
[28] Esveld C. Modern railway track. 2nd ed. Zaltbommel: MRT-Productions; 2001.
[29] UIC 774-3R. Track/bridge interaction – Recommendations for calculations. Paris: International Union of Railways; 2001.
[30] ERRI D 202 DT362. Ballast resistance under three-dimensional loading. Utrecht: European Rail Research Institute; 1997.
[31] ERRI D 202 DT363. Volume 2 – Determination of lateral and longitudinal ballast resistance of a railway track by experimental tests. Utrecht: European Rail Research Institute; 1997.
[32] Grassie SL, Gregory RW, Harrison D, Johnson KL. The dynamic response of railway track to high frequency vertical excitation. J Mech Eng Sci. 1982;24(2):77–90.
[33] Zhai WM, Wang KY, Lin JH. Modelling and experiment of railway ballast vibrations. J Sound Vib. 2004;270:673–683.
[34] Kalker JJ. Three dimensional elastic bodies in rolling contact. Dordrecht: Kluwer Academic Publishers; 1990.
[35] Johnson KL. Contact mechanics. Cambridge: Cambridge University Press; 1992.
[36] Olofsson U, Hagman L. A model for micro-slip between at surfaces based on deformation of ellipsoidal elastic bodies. Trib Int. 1997;30(8):599–603.
[37] Hagman L, Olofsson U. A model for micro-slip between at surfaces based on deformation of ellipsoidal elastic asperities–parametric study and experimental investigation. Trib Int. 1998;31 (4):209–217.
[38] Al-Bender F, Symens W. Dynamic characterization of hysteresis elements in mechanical systems. 1. Theoretical analysis. Chaos. 2005;15. doi:10.1063/1.1844991
[39] Al-Bender F, De Moerlooze K. A model of the transient behavior of tractive rolling contacts. Adv Trib. 2008. doi:10.1155/2008/214894
[40] De Moerlooze K, Al-Bender F. Experimental investigation into the tractive prerolling behavior of balls in V-grooved tracks. Adv Trib. 2008. doi:10.1155/2008/561280
[41] Kalker JJ. Wheel-rail rolling contact theory. Wear. 1991;144:243–261.
[42] Spiegelberg C, Björklund S, Andersson S. Simulation of transient friction of a cylinder between two planes. Wear. 2003;254:1170–1179.
[43] Eurocode 1: Actions on structures – Part 2: Traffic loads on bridges. Brussels: CEN, European Committee for Standardization; 2008.
[44] ERRI D 214 RP3. Rail Bridges for Speeds >200 km/h – Recommendations for calculating damping in rail bridge decks. European Rail Research Institute; 2000.

List of Bulletins from the Department of Structural Engineering, The Royal Institute of Technology, Stockholm

TRITA-BKN. Bulletin

Pacoste, C., On the Application of Catastrophe Theory to Stability Analyses of Elastic Structures.
Doctoral Thesis, 1993. Bulletin 1.

Stenmark, A-K., Dämpning av 13 m lång stålbalk – "Ullevibalken". Utprovning av dämpmassor och fastsättning av motbalk samt experimentell bestämning av modformer och förlustfaktorer. Vibration tests of full-scale steel girder to determine optimum passive control.
Licentiatavhandling, 1993. Bulletin 2.

Silfwerbrand, J., Renovering av asfaltgolv med cementbundna plastmodifierade avjämningsmassor.
1993. Bulletin 3.

Norlin, B., Two-Layered Composite Beams with Nonlinear Connectors and Geometry – Tests and Theory.
Doctoral Thesis, 1993. Bulletin 4.

Habtezion, T., On the Behaviour of Equilibrium Near Critical States.
Licentiate Thesis, 1993. Bulletin 5.

Krus, J., Hållfasthet hos frostnedbruten betong.
Licentiatavhandling, 1993. Bulletin 6.

Wiberg, U., Material Characterization and Defect Detection by Quantitative Ultrasonics.
Doctoral Thesis, 1993. Bulletin 7.

Lidström, T., Finite Element Modelling Supported by Object Oriented Methods.
Licentiate Thesis, 1993. Bulletin 8.

Hallgren, M., Flexural and Shear Capacity of Reinforced High Strength Concrete Beams without Stirrups.
Licentiate Thesis, 1994. Bulletin 9.

Krus, J., Betongbalkars lastkapacitet efter miljöbelastning.
1994. Bulletin 10.

Sandahl, P., Analysis Sensitivity for Wind-related Fatigue in Lattice Structures.
Licentiate Thesis, 1994. Bulletin 11.

Sanne, L., Information Transfer Analysis and Modelling of the Structural Steel Construction Process.
Licentiate Thesis, 1994. Bulletin 12.

Zhitao, H., Influence of Web Buckling on Fatigue Life of Thin-Walled Columns.
Doctoral Thesis, 1994. Bulletin 13.

Kjörling, M., Dynamic response of railway track components. Measurements during train passage and dynamic laboratory loading.
Licentiate Thesis, 1995. Bulletin 14.

Yang, L., On Analysis Methods for Reinforced Concrete Structures.
Doctoral Thesis, 1995. Bulletin 15.

Petersson, Ö., Svensk metod för dimensionering av betongvägar.
Licentiatavhandling, 1996. Bulletin 16.

Lidström, T., Computational Methods for Finite Element Instability Analyses.
Doctoral Thesis, 1996. Bulletin 17.

Krus, J., Environment- and Function-induced Degradation of Concrete Structures.
Doctoral Thesis, 1996. Bulletin 18.

Editor, Silfwerbrand, J., Structural Loadings in the 21st Century.
Sven Sahlin Workshop, June 1996. Proceedings. Bulletin 19.

Ansell, A., Frequency Dependent Matrices for Dynamic Analysis of Frame Type Structures.
Licentiate Thesis, 1996. Bulletin 20.

Troive, S., Optimering av åtgärder för ökad livslängd hos infrastrukturkonstruktioner.
Licentiatavhandling, 1996. Bulletin 21.

Karoumi, R., Dynamic Response of Cable-Stayed Bridges Subjected to Moving Vehicles.
Licentiate Thesis, 1996. Bulletin 22.

Hallgren, M., Punching Shear Capacity of Reinforced High Strength Concrete Slabs.
Doctoral Thesis, 1996. Bulletin 23.

Hellgren, M., Strength of Bolt-Channel and Screw-Groove Joints in Aluminium Extrusions.
Licentiate Thesis, 1996. Bulletin 24.

Yagi, T., Wind-induced Instabilities of Structures.
Doctoral Thesis, 1997. Bulletin 25.

Eriksson, A., and Sandberg, G., (editors), Engineering Structures and Extreme Events – proceedings from a symposium, May 1997. Bulletin 26.

Paulsson, J., Effects of Repairs on the Remaining Life of Concrete Bridge Decks.
Licentiate Thesis, 1997. Bulletin 27.

Olsson, A., Object-oriented finite element algorithms.
Licentiate Thesis, 1997. Bulletin 28.

Yunhua, L., On Shear Locking in Finite Elements.
Licentiate Thesis, 1997. Bulletin 29.

Ekman, M., Sprickor i betongkonstruktioner och dess inverkan på beständigheten.
Licentiate Thesis, 1997. Bulletin 30.

Karawajczyk, E., Finite Element Approach to the Mechanics of Track-Deck Systems.
Licentiate Thesis, 1997. Bulletin 31.

Fransson, H., Rotation Capacity of Reinforced High Strength Concrete Beams.
Licentiate Thesis, 1997. Bulletin 32.

Edlund, S., Arbitrary Thin-Walled Cross Sections. Theory and Computer Implementation.
Licentiate Thesis, 1997. Bulletin 33.

Forsell, K., Dynamic analyses of static instability phenomena.
Licentiate Thesis, 1997. Bulletin 34.

Ikäheimonen, J., Construction Loads on Shores and Stability of Horizontal Formworks.
Doctoral Thesis, 1997. Bulletin 35.

Racutanu, G., Konstbyggnaders reella livslängd.
Licentiatavhandling, 1997. Bulletin 36.

Appelqvist, I., Sammanbyggnad. Datastrukturer och utveckling av ett IT-stöd för byggprocessen.
Licentiatavhandling, 1997. Bulletin 37.

Alavizadeh-Farhang, A., Plain and Steel Fibre Reinforced Concrete Beams Subjected to Combined Mechanical and Thermal Loading.
Licentiate Thesis, 1998. Bulletin 38.

Eriksson, A. and Pacoste, C., (editors), Proceedings of the NSCM-11: Nordic Seminar on Computational Mechanics, October 1998. Bulletin 39.

Luo, Y., On some Finite Element Formulations in Structural Mechanics.
Doctoral Thesis, 1998. Bulletin 40.

Troive, S., Structural LCC Design of Concrete Bridges.
Doctoral Thesis, 1998. Bulletin 41.

Tärno, I., Effects of Contour Ellipticity upon Structural Behaviour of Hyparform Suspended Roofs.
Licentiate Thesis, 1998. Bulletin 42.

Hassanzadeh, G., Betongplattor på pelare. Förstärkningsmetoder och dimensioneringsmetoder för plattor med icke vidhäftande spännarmering.
Licentiatavhandling, 1998. Bulletin 43.

Karoumi, R., Response of Cable-Stayed and Suspension Bridges to Moving Vehicles. Analysis methods and practical modeling techniques.
Doctoral Thesis, 1998. Bulletin 44.

Johnson, R., Progression of the Dynamic Properties of Large Suspension Bridges during Construction – A Case Study of the Höga Kusten Bridge.
Licentiate Thesis, 1999. Bulletin 45.

Tibert, G., Numerical Analyses of Cable Roof Structures.
Licentiate Thesis, 1999. Bulletin 46.

Ahlenius, E., Explosionslaster och infrastrukturkonstruktioner - Risker, värderingar och kostnader.
Licentiatavhandling, 1999. Bulletin 47.

Battini, J-M., Plastic instability of plane frames using a co-rotational approach.
Licentiate Thesis, 1999. Bulletin 48.

Ay, L., Using Steel Fiber Reinforced High Performance Concrete in the Industrialization of Bridge Structures.
Licentiate Thesis, 1999. Bulletin 49.

Paulsson-Tralla, J., Service Life of Repaired Concrete Bridge Decks.
Doctoral Thesis, 1999. Bulletin 50.

Billberg, P., Some rheology aspects on fine mortar part of concrete.
Licentiate Thesis, 1999. Bulletin 51.

Ansell, A., Dynamically Loaded Rock Reinforcement.
Doctoral Thesis, 1999. Bulletin 52.

Forsell, K., Instability analyses of structures under dynamic loads.
Doctoral Thesis, 2000. Bulletin 53.

Edlund, S., Buckling of T-Section Beam-Columns in Aluminium with or without Transverse Welds.
Doctoral Thesis, 2000. Bulletin 54.

Löfsjögård, M., Functional Properties of Concrete Roads − General Interrelationships and Studies on Pavement Brightness and Sawcutting Times for Joints.
Licentiate Thesis, 2000. Bulletin 55.

Nilsson, U., Load bearing capacity of steel fibre reinforced shotcrete linings.
Licentiate Thesis, 2000. Bulletin 56.

Silfwerbrand, J. and Hassanzadeh, G., (editors), International Workshop on Punching Shear Capacity of RC Slabs − Proceedings. Dedicated to Professor Sven Kinnunen. Stockholm June 7-9, 2000. Bulletin 57.

Wiberg, A., Strengthening and repair of structural concrete with advanced, cementitious composites.
Licentiate Thesis, 2000. Bulletin 58.

Racutanu, G., The Real Service Life of Swedish Road Bridges - A case study.
Doctoral Thesis, 2000. Bulletin 59.

Alavizadeh-Farhang, A., Concrete Structures Subjected to Combined Mechanical and Thermal Loading.
Doctoral Thesis, 2000. Bulletin 60.

Wäppling, M., Behaviour of Concrete Block Pavements - Field Tests and Surveys.
Licentiate Thesis, 2000. Bulletin 61.

Getachew, A., Trafiklaster på broar. Analys av insamlade och Monte Carlo genererade fordonsdata.
Licentiatavhandling, 2000. Bulletin 62.

James, G., Raising Allowable Axle Loads on Railway Bridges using Simulation and Field Data.
Licentiate Thesis, 2001. Bulletin 63.

Karawajczyk, E., Finite Elements Simulations of Integral Bridge Behaviour.
Doctoral Thesis, 2001. Bulletin 64.

Thöyrä, T., Strength of Slotted Steel Studs.
Licentiate Thesis, 2001. Bulletin 65.

Tranvik, P., Dynamic Behaviour under Wind Loading of a 90 m Steel Chimney.
Licentiate Thesis, 2001. Bulletin 66.

Ullman, R., Buckling of Aluminium Girders with Corrugated Webs.
Licentiate Thesis, 2002. Bulletin 67.

Getachew, A., Traffic Load Effects on Bridges. Statistical Analysis of Collected and Monte Carlo Simulated Vehicle Data.
Doctoral Thesis, 2003. Bulletin 68.

Quilligan, M., Bridge Weigh-in-Motion. Development of a 2-D Multi-Vehicle Algorithm.
Licentiate Thesis, 2003. Bulletin 69.

James, G., Analysis of Traffic Load Effects on Railway Bridges.
Doctoral Thesis 2003. Bulletin 70.

Nilsson, U., Structural behaviour of fibre reinforced sprayed concrete anchored in rock.
Doctoral Thesis 2003. Bulletin 71.

Wiberg, A., Strengthening of Concrete Beams Using Cementitious Carbon Fibre Composites.
Doctoral Thesis 2003. Bulletin 72.

Löfsjögård, M., Functional Properties of Concrete Roads – Development of an Optimisation Model and Studies on Road Lighting Design and Joint Performance.
Doctoral Thesis 2003. Bulletin 73.

Bayoglu-Flener, E., Soil-Structure Interaction for Integral Bridges and Culverts.
Licentiate Thesis 2004. Bulletin 74.

Lutfi, A., Steel Fibrous Cement Based Composites. Part one: Material and mechanical properties.
Part two: Behaviour in the anchorage zones of prestressed bridges.
Doctoral Thesis 2004. Bulletin 75.

Johansson, U., Fatigue Tests and Analysis of Reinforced Concrete Bridge Deck Models.
Licentiate Thesis 2004. Bulletin 76.

Roth, T., Langzeitverhalten von Spannstählen in Betonkonstruktionen.
Licentitate Thesis 2004. Bulletin 77.

Hedebratt, J., Integrerad projektering och produktion av industrigolv – Metoder för att förbättra kvaliteten.
Licentiatavhandling, 2004. Bulletin 78.

Österberg, E., Revealing of age-related deterioration of prestressed reinforced concrete containments in nuclear power plants – Requirements and NDT methods.
Licentiate Thesis 2004. Bulletin 79.

Broms, C.E., Concrete flat slabs and footings New design method for punching and detailing for ductility.
Doctoral Thesis 2005. Bulletin 80.

Wiberg, J., Bridge Monitoring to Allow for Reliable Dynamic FE Modelling - A Case Study of the New Årsta Railway Bridge.
Licentiate Thesis 2006. Bulletin 81.

Mattsson, H-Å., Funktionsentreprenad Brounderhåll – En pilotstudie i Uppsala län.
Licentiate Thesis 2006. Bulletin 82.

Masanja, D. P, Foam concrete as a structural material.
Doctoral Thesis 2006. Bulletin 83.

Johansson, A., Impregnation of Concrete Structures – Transportation and Fixation of Moisture in Water Repellent Treated Concrete.
Licentiate Thesis 2006. Bulletin 84.

Billberg, P., Form Pressure Generated by Self-Compacting Concrete – Influence of Thixotropy and Structural Behaviour at Rest.
Doctoral Thesis 2006. Bulletin 85.

Enckell, M., Structural Health Monitoring using Modern Sensor Technology – Long-term Monitoring of the New Årsta Railway Bridge.
Licentiate Thesis 2006. Bulletin 86.

Söderqvist, J., Design of Concrete Pavements – Design Criteria for Plain and Lean Concrete.
Licentiate Thesis 2006. Bulletin 87.

Malm, R., Shear cracks in concrete structures subjected to in-plane stresses.
Licentiate Thesis 2006. Bulletin 88.

Skoglund, P., Chloride Transport and Reinforcement Corrosion in the Vicinity of the Transition Zone between Substrate and Repair Concrete.
Licentiate Thesis 2006. Bulletin 89.

Liljencrantz, A., Monitoring railway traffic loads using Bridge Weight-in-Motion.
Licentiate Thesis 2007. Bulletin 90.

Stenbeck, T., Promoting Innovation in Transportation Infrastructure Maintenance – Incentives, Contracting and Performance-Based Specifications.
Doctoral Thesis 2007. Bulletin 91

Magnusson, J., Structural Concrete Elements Subjected to Air Blast Loading.
Licentiate Thesis 2007. Bulletin 92.

Pettersson, L., G., Full Scale Tests and Structural Evaluation of Soil Steel Flexible Culverts with low Height of Cover.
Doctoral Thesis 2007. Bulletin 93

Westerberg, B., Time-dependent effects in the analysis and design of slender concrete compression members.
Doctoral Thesis 2008. Bulletin 94

Mattsson, H-Å, Integrated Bridge Maintenance. Evaluation of a pilot project and future perspectives.
Doctoral Thesis 2008. Bulletin 95

Andersson, A., Utmattningsanalys av järnvägsbroar. En fallstudie av stålbroarna mellan Stockholm Central och Söder Mälarstrand, baserat på teoretiska analyser och töjningsmätningar.
Licentiate Thesis 2009. Bulletin 96

Malm, R., Predicting shear type crack initiation and growth in concrete with non-linear finite element method.
Doctoral Thesis 2009. Bulletin 97

Bayoglu Flener, E., Static and dynamic behavior of soil-steel composite bridges obtained by field testing.
Doctoral Thesis 2009. Bulletin 98

Gram, A., Numerical Modelling of Self-Compacting Concrete Flow
Licentiate Thesis 2009. Bulletin 99

Wiberg, J., Railway bridge response to passing trains. Measurements and FE model updating.
Doctoral Thesis 2009. Bulletin 100

Athuman M.K. Ngoma, Characterisation and Consolidation of Historical Lime Mortars in Cultural Heritage Buildings and Associated Structures in East Africa.
Doctoral Thesis 2009. Bulletin 101

Ülker-Kaustell, M., Some aspects of the dynamic soil-structure interaction of a portal frame railway bridge.
Licentiate Thesis 2009. Bulletin 102

Vogt, C., Ultrafine particles in concrete
Doctoral Thesis 2010. Bulletin 103

Selander, A., Hydrophobic Impregnation of Concrete Structures
Doctoral Thesis 2010. Bulletin 104

Ilina, E., Understanding the application of knowledge management to safety critical facilities
Doctoral Thesis 2010. Bulletin 105

Leander, J., Improving a bridge fatigue life prediction by monitoring
Licentiate Thesis 2010. Bulletin 106

Andersson, A., Capacity assessment of arch bridges with backfill – Case of the old Årsta railway bridge
Doctoral Thesis 2011. Bulletin 107

Enckell, M., Lessons Learned in Structural Health Monitoring of Bridges Using Advanced Sensor Technology
Doctoral Thesis 2011. Bulletin 108

Hansson, H., Warhead penetration in concrete protective structures
Licentiate Thesis 2011. Bulletin 109

Gonzalez Silva, I., Study and Application of Modern Bridge Monitoring Techniques
Licentiate Thesis 2011. Bulletin 110

Safi, M., LCC Applications for Bridges and Integration with BMS
Licentiate Thesis 2012. Bulletin 111

Guangli, D., Towards sustainable construction, life cycle assessment of railway bridges
Licentiate Thesis 2012. Bulletin 112

Hedebratt, J., Industrial Fibre Concrete Slabs – Experiences and Tests on Pile-Supported Slab
Doctoral Thesis 2012. Bulletin 113

Ahmed, L., Models for analysis of shotcrete on rock exposed to blasting
Licentiate Thesis 2012. Bulletin 114

Le, T., N., Corotational formulation for nonlinear dynamic analysis of flexible beam structures
Licentiate Thesis 2012. Bulletin 115

Johansson, C., Simplified dynamic analysis of railway bridges under high-speed trains
Licentiate Thesis 2013. Bulletin 116

Jansson, R., Fire Spalling of Concrete – Theoretical and Experimental Studies
Doctoral Thesis 2013. Bulletin 117

Leander, J., Refining the fatigue assessment procedure of existing steel bridges
Doctoral Thesis 2013. Bulletin 118

Le, T., N., Nonlinear dynamics of flexible structures using corotational beam elements
Doctoral Thesis 2013. Bulletin 119

The bulletins enumerated above, with the exception for those which are out of print, may be purchased from the Department of Civil and Architectural Engineering, The Royal Institute of Technology, SE-100 44 Stockholm, Sweden.

The department also publishes other series. For full information see our homepage http://www.byv.kth.se